

## Inorganic perovskite photocatalysts for solar energy utilization

Guan Zhang,<sup>ab</sup> Gang Liu,<sup>\*c</sup> Lianzhou Wang<sup>\*d</sup> and John T. S. Irvine<sup>\*b</sup>

Received 00th January 20xx,  
Accepted 00th January 20xx

DOI: 10.1039/x0xx00000x  
[www.rsc.org/](http://www.rsc.org/)

The development and utilization of solar energy in environmental remediation and water splitting is being intensively studied worldwide. During the past few decades, tremendous efforts have been devoted to developing non-toxic, low-cost, efficient and stable photocatalysts for water splitting and environmental remediation. To date, several hundreds photocatalysts mainly based on metal oxides, sulfides and (oxy)nitrates with different structures and compositions are reported. Among them, perovskite oxides and their derivatives (layered perovskite oxides) comprise of a large family of semiconductor photocatalysts because of their structural simplicity and flexibility. This review specifically focuses on the general background of perovskite and its related materials, summarizes the recent development of perovskite photocatalysts and their applications in water splitting and environmental remediation, discusses the theoretical modelling and calculation of perovskite photocatalysts and presents the key challenges and perspective on the research of perovskite photocatalysts.

### 1. Introduction

Solar energy is the ultimate source of renewable energy for addressing the energy crisis and global warming challenge. The utilization of solar energy in environmental remediation and solar chemical conversion are being intensively studied worldwide.<sup>1,2</sup> Among a variety of solar conversion technologies, semiconductor photocatalysis driven water splitting and CO<sub>2</sub> reduction (or artificial photosynthesis) have been demonstrated as promising ways for converting solar energy into chemical fuels.<sup>3-5</sup> Using the same concept, semiconductor photocatalysis has also been extensively investigated for potential applications in environmental remediation including degradation and removal of organic pollutants in aqueous/air phase,<sup>6,7</sup> reduction of heavy metal ions,<sup>8-10</sup> bacterial inactivation,<sup>11-13</sup> etc.. During the past few decades, tremendous efforts have been devoted to developing efficient, low-cost and stable photocatalysts, especially those that can work under visible light such as In<sub>1-x</sub>Ni<sub>x</sub>TaO<sub>4</sub>,<sup>14</sup> (Ga<sub>1-x</sub>Zn<sub>x</sub>)(N<sub>1-x</sub>O<sub>x</sub>),<sup>15</sup> CaBi<sub>2</sub>O<sub>4</sub>,<sup>16</sup> Ag/AgCl,<sup>17</sup> AgPO<sub>4</sub>,<sup>18</sup> hydrogenated TiO<sub>2</sub>,<sup>19</sup> and metal-free photocatalysts including graphitic carbon nitride (C<sub>3</sub>N<sub>4</sub>),<sup>20</sup> boron carbide,<sup>21</sup> elemental  $\alpha$ -sulfur,<sup>22</sup> rhombohedral boron,<sup>23</sup> P-doped graphene,<sup>24</sup> nanoporous carbon,<sup>25</sup> carbon dots imbedded C<sub>3</sub>N<sub>4</sub><sup>26</sup> and organic polymer photocatalysts.<sup>27-29</sup> Although water splitting in suspension system is considered as not practically feasible as that in photoelectrochemical system in terms of separation of generated H<sub>2</sub>

and O<sub>2</sub> for inhibition of back recombination,<sup>30-33</sup> this drawback could be overcome by constructing an Z-scheme system<sup>34</sup> or selectively loading H<sub>2</sub> and O<sub>2</sub> evolution co-catalysts on different sites in a single particulate catalyst.<sup>35</sup> In addition, the particulate semiconductor photocatalyst has the following interesting features that distinguish itself from the photoelectrochemical system: (1) Electrolyte is not needed; (2) Each photocatalyst works as a microphotoelectrode; (3) They possess large surface areas (10<sup>4</sup> to 10<sup>6</sup> cm<sup>2</sup>g<sup>-1</sup>), and the flux of the photogenerated carriers per unit surface is very small, compared with that of the bulk electrode; (4) It is much simpler for large scale application, which does not require applying external bias and manufacturing nanostructured photoelectrodes. To date, a few hundred photocatalysts mainly including metal oxides, metal sulfides and metal (oxy)nitrates have been reported. However, the reported external quantum yield at a given visible light wavelength for pure water splitting in a particulate system is still far below the solar to hydrogen conversion efficiency goal of 10 % for practical applications.<sup>36</sup> Considering the huge potential of "solar + water  $\rightarrow$  clean fuel", photocatalysis has been considered as one of the Holy Grails of chemistry and material fields, it is highly desirable to develop new photocatalysts to boost the solar conversion efficiency. This has also led to decades-long intensive research effort on the search for new-photocatalysts, especially for those that can harvest full range of visible light photons.

Among a large library of photocatalyst materials, perovskite oxides and their derivatives (layered perovskite oxides) comprise of a large family of promising semiconductor photocatalysts because of their structural simplicity and flexibility, good stability and efficient photocatalytic performance. The ideal perovskite has a cubic structure with general formula of ABO<sub>3</sub>. The A and B sites can accommodate most of the metal elements in periodic table into the crystal structure, which thus extends the family of perovskite oxides by rationally combining different metal ions at A and B sites.<sup>37</sup> Apart

<sup>a</sup> School of Civil and Environmental Engineering, Harbin Institute of Technology (Shenzhen), Shenzhen 518055, China.

<sup>b</sup> School of Chemistry, University of St Andrews, St Andrews KY16 9ST, UK. Email: [jtsi@st-andrews.ac.uk](mailto:jtsi@st-andrews.ac.uk).

<sup>c</sup> Institute of Metal Research, Chinese Academy of Sciences, Shenyang 110016, China. Email: [gangliu@imr.ac.cn](mailto:gangliu@imr.ac.cn).

<sup>d</sup> School of Chemical Engineering, The University of Queensland, Brisbane St Lucia QLD 4072, Australia. Email: [l.wang@uq.edu.au](mailto:l.wang@uq.edu.au).

from the ideal cubic perovskite, structural distortion can be induced by multiple metal cation substitutions. Such structural distortion can inevitably change the physical, electronic and photocatalytic properties of pristine materials. In addition, a series of layered perovskites consist of infinite 2D slabs of the  $ABO_3$  structure which are separated by embedded blocks (metal oxides). The possibility of preparing multicomponent perovskites by either partial substitution of metal cations in A or B sites or inserting metal oxides into layered structure allows researchers to explore and modulate the crystal structures and the related physicochemical and catalytic properties of the perovskite oxides. To date, more than two hundred perovskites or perovskites-related photocatalysts have been reported, and more importantly some of the perovskite-based materials have been recorded with “benchmark” performance for photocatalytic application. Thus, the perovskites materials have shown great potential for future applications on the basis of putting more efforts on them.

Although a number of excellent review articles targeted at semiconductor photocatalysts have been published recently,<sup>38-41</sup> only a few of them paid attention to inorganic perovskite (mainly  $ABO_3$ -based) photocatalysts.<sup>42-44</sup> A comprehensive classification and full coverage of this material family, for instance, the layered perovskite photocatalysts is still lacking. The aim of this review is to summarize the recent development of perovskite photocatalysts for water splitting and environmental remediation, discuss recent findings and advances on perovskite photocatalysts and give a perspective on the future research of perovskites. After a brief introduction of general structure of perovskite materials, the reported perovskite photocatalysts are summarized, classified and discussed based on photocatalyst preparation, optical properties including band-gap and band edge position, morphologies as well as the photocatalytic activities of the materials. In order to develop more efficient perovskite photocatalysts, theoretical modelling is a powerful tool to give a comprehensive understanding of the bands structure configuration of semiconductors and to predict new semiconductor photocatalysts with promising performance. Some typical examples on the theoretical calculation of perovskite photocatalysts will be illustrated. Finally, a summary will be given to comment on the recent progress and development of the perovskite photocatalysts for solar energy utilization. The potential applications, current challenges and the research direction in future will be addressed in the last part. However, the fundamentals on semiconductor photocatalysis and processes in photocatalytic water splitting and environmental remediation will not be covered in this review, since these aspects are already well addressed in the literature.<sup>38-41</sup>

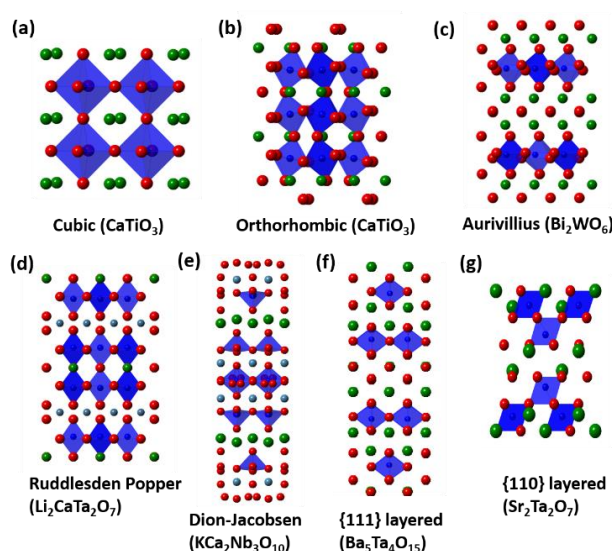


**Fig. 1** Crystal structures of perovskites and layered perovskites compounds (red spheres: oxygen; dark blue spheres: B-site element; green and light blue spheres: A-site element)

## 2. Fundamentals of perovskite materials

### 2.1 Perovskite structures

The general formula of perovskite-type oxides can be described as  $ABO_3$ , where the A cation (normally much larger than B) is 12-fold coordinated and the B cation is 6-fold coordinated to the oxygen anions. Fig. 1a depicts the representative coordinated skeleton of the  $ABO_3$  structure, which is composed of a three-dimensional framework of corner sharing  $BO_6$  octahedra and an A cation at the centre. In the  $ABO_3$  structure, the A cation is normally an alkali or alkaline earth metal or rare earth element, while the B cation is typically a metallic transition metal element. An ideal  $ABO_3$  perovskite has a cubic crystal structure with tolerance factor ( $t$ ) = 1, which is defined as  $t = (r_A + r_O) / \sqrt{2} (r_B + r_O)$ , where  $r_A$ ,  $r_B$  and  $r_O$  are the ionic radii of A, B and oxygen elements, respectively.<sup>37</sup> For composing a stable perovskite, it is normally accepted that the  $t$  should lie between 0.75 - 1.0. A lower  $t$  value ( $< 1$ ) produces slightly distorted perovskite structure with orthorhombic (Fig. 1b) or rhombohedral symmetry. The ideal cubic perovskite structure only exists in limited cases where  $t$  is very close to 1 and often at high temperatures. Although the  $t$ , determined by the ionic size, is an important index for the stability of perovskite structures, the octahedral factor ( $u$ )  $u = r_B / r_O$  and the contribution of the chemical nature of A and B atoms, such as the coordinating number of the constituent elements, need also to be considered.<sup>45</sup> Taking into account those influencing factors and the electroneutrality, the  $ABO_3$  perovskite can accommodate a wide range of pairs of A and B with the same or different valences and ionic radius. Furthermore, either A or B cation can be partially substituted by the other dopants, to extend the  $ABO_3$  perovskite into a broad family of  $A_xA'_{1-x}B_yB'_{1-y}O_{3\pm\delta}$ . The substitution of multiple cations into the A- or B-sites can alter the symmetry of the pristine structure and hence the physicochemical and catalytic properties. In

particular, the change of electronic and optical properties has a great influence on the photocatalytic process.

## 2.2 Layered perovskite related structures

In addition to the general  $ABO_3$  structure, other typical polymorphs of the perovskite structure are Brownmillerite ( $A_2B_2O_5$ ) and  $K_2NiF_4$  structures. Brownmillerite is a kind of oxygen deficient perovskite, in which the unit cell is composed by ordered  $BO_6$  and  $BO_4$  units. Due to the oxygen deficiency, the coordination number of A-site cations decreases to eight. The structure of oxygen deficient perovskite will be discussed in the next paragraph.  $K_2NiF_4$  structure is a combination of oxygen defects and ordered B sites, which is well studied as superconducting materials. The  $K_2NiF_4$  structure consists of the  $KNiF_3$  perovskite unit and the KF rock salt unit. Because the rock salt unit is embedded into the c-axis direction, the  $K_2NiF_4$  materials exhibit layered properties. Based on the intergrowth of the different numbers of  $KNiF_3$  and KF units, there are many structures that can be classified as {100}, {110} and {111} layered perovskites according to the layered orientation relative to the principle axis of an ideal cubic perovskite. The general formula for most well-known layered perovskite oxides are described as  $(Bi_2O_2)(A_{n-1}B_nO_{3n+1})$  (Aurivillius phase),  $A_{n+1}B_nO_{3n+1}$  or  $A'_2A_{n-1}B_nO_{3n+1}$  (Ruddlesden-Popper phase) and  $A'[A_{n-1}B_nO_{3n+1}]$  (Dion-Jacobson phase) for {100} series,  $(A_nB_nO_{3n+2})$  for {110} series and  $(A_{n+1}B_nO_{3n+3})$  for {111} series. In these structures,  $n$  represents the number of  $BO_6$  octahedra that span a layer, which defines the thickness of the layer. The representative examples of these layered structures are shown in Fig. 1c - 1g. For Aurivillius phases, their structures are built by alternating layers of  $[Bi_2O_2]^{2+}$  and pseudo-perovskite blocks.  $Bi_2WO_6$  and  $BiMoO_6$  ( $n = 1$ ), found as the first ferroelectric Aurivillius compounds, recently have been intensively studied as visible light photocatalysts. For Ruddlesden-Popper phases, their structures result from intergrowth of perovskite  $ABO_3$  and  $A'O$  as intermediate spacing layer. These compounds possess interesting properties in magnetoresistance, superconductivity, ferroelectricity and catalytic activity.  $Sr_2SnO_4$  and  $Li_2CaTa_2O_7$  are the examples of simple Ruddlesden-Popper type photocatalysts. The Dion-Jacobson phases with general formula of  $A'[A_{n-1}B_nO_{3n+1}]$  ( $n > 1$ ), where  $A'$  separates the perovskite-like blocks and is typically a univalent alkali cation. The representative Dion-Jacobson type photocatalysts are  $RbLnTa_2O_7$  ( $n = 2$ ) and  $KCa_2Nb_3O_{10}$  ( $n = 3$ ). Members of the  $A_nB_nO_{3n+2}$  and  $A_{n+1}B_nO_{3n+3}$  structural series with different layered orientations have also been identified in a number of photocatalysts such as  $Sr_2Ta_2O_7$  and  $Sr_5Ta_4O_{15}$  ( $n = 4$ ).

## 2.3 Defects in perovskites

Perovskite ( $ABO_3$ ) materials have three different ionic species, making for diverse and potentially useful defect chemistry. In addition to the partial substitution of A and B ions is allowed while preserving the perovskite structure, deficiencies of cations at the A-site or of oxygen anions are frequent. By substitution of parent cations with similar-sized cations of different valence, defects can be introduced into the structure. The defect concentrations of perovskites can be controlled and tailored by doping. Oxygen ion vacancies or interstitials can be generated by substitution of B-site

ions with cations of lower or higher valence, respectively, producing compounds of  $AB_{(1-x)}B'_xO_{3\pm\delta}$ . A common oxygen deficient perovskite structure is Brownmillerite ( $A_2B_2O_5$ ), in which one sixth of oxygen atoms are removed. A-site vacancies can be introduced by substitution of A-site ions with cations of higher valence, giving compounds of stoichiometry of  $A_{1-x}A'_xB_3$ . Substitution of A-site ions with lower-valence cations results in oxygen vacancy formation giving compounds of  $A_{(1-x)}A'_xB_3$ . B-site vacancies in perovskite oxides are not as common as they are not thermodynamically favoured because of the large charge and the small size of the B cations. A-site vacancies are more observed because the  $BO_3$  array in the perovskite structure forms a stable network, the large A cations at 12 coordinated sites can be partially missing. Recently, introducing appropriate defects onto the surface of metal oxides semiconductors has been intensively studied as a means of altering the electronic structures and optical absorption properties of the parent materials. For example, hydrogenated  $TiO_2$  (black  $TiO_2$ ) has been reported as an efficient photocatalyst that can split water under UV or visible light irradiation.<sup>23</sup> From this point of view, perovskite materials provide a huge platform for defect engineering to change the photocatalytic properties of perovskite photocatalysts.

## 3. Perovskite materials for photocatalysis

A wide range of perovskite photocatalysts have been developed for water splitting and organic pollutants degradation under UV or visible light irradiation during the past few decades. These representative examples and brief experimental results on them are summarized according to their structures, which can be classified into five groups. Specifically,  $ABO_3$ -type perovskites,  $AA'BO_3$ ,  $ABB'O_3$  and  $AB(ON)_3$ -type perovskites, and  $AA'BB'O_3$ -type perovskites are listed in Table 1, Table 2 and Table 3, respectively.

### 3.1 $ABO_3$ type

#### 3.1.1 Tantalates

$NaTaO_3$  has long been recognized as an efficient UV-light photocatalyst for overall water splitting.<sup>46-57</sup> It has a band gap of 4.0 eV and can be synthesized by solid-state,<sup>46-48,53,56</sup> hydrothermal,<sup>49,52,54,55</sup> sol-gel<sup>50,51</sup> and molten salt methods.<sup>57</sup> As a first example, Kato and Kudo reported highly efficient splitting of pure water into  $H_2$  and  $O_2$  over  $NaTaO_3$  photocatalyst. The quantum yield of  $NaTaO_3$  (0.05 wt% NiO as co-catalyst) photocatalyst prepared by solid-state reaction method was 28% for water splitting at 270 nm.<sup>46-48</sup> In order to increase surface area of  $NaTaO_3$  bulk particles, many researchers attempted to use other synthetic routes to prepare nano-sized particles as an extension of the study on  $NaTaO_3$  photocatalyst. Kondo et al. synthesized a colloidal array of  $NaTaO_3$  nanoparticles using three-dimensional mesoporous carbon as template, which was replicated by the colloidal array of silica nanospheres. After burning out the mesoporous carbon matrix, a colloidal array of  $NaTaO_3$  nanoparticles with size of 20 nm and surface area of  $34\text{ m}^2\text{g}^{-1}$  was obtained. Compared to non-nanostructured bulk  $NaTaO_3$  particles, the nanostructured  $NaTaO_3$

exhibited more than 3 times higher photocatalytic activity for overall water splitting.<sup>54</sup> Shortly afterwards, Shi and Li *et al.* developed a fast and facile method for the preparation of NaTaO<sub>3</sub> nanocrystals via microwave-assisted hydrothermal process.<sup>55</sup> An indirect transformation route from Ta<sub>2</sub>O<sub>5</sub> to Na<sub>2</sub>Ta<sub>2</sub>O<sub>6</sub> and to NaTaO<sub>3</sub> was proposed as the main reason for that pure NaTaO<sub>3</sub> could be synthesized in a rather short time (less than 3 h) under mild conditions. The water splitting efficiency of NaTaO<sub>3</sub> nanocrystals prepared by this approach was more than two times higher than that prepared from conventional hydrothermal synthesis. Recently, the nano-sized NaTaO<sub>3</sub>, prepared by an exo-template method with crystallite size of about 25 nm, showed an 18 times higher hydrogen evolution rate than the NaTaO<sub>3</sub> synthesized by the solid-state reaction method (Fig. 2).<sup>56</sup> The hydrogen production activity of NaTaO<sub>3</sub> obtained from the exo-template synthesis could be further improved about 30–40 times by mixing with reduced graphene oxide and using Au as a co-catalyst. However, it did not show the improvement of activity for NaTaO<sub>3</sub> prepared from solid-state reaction under the identical condition.

In addition to the nanostructure engineering of the NaTaO<sub>3</sub>, much effort has been made to achieve a higher activity of NaTaO<sub>3</sub> by doping with lanthanide<sup>58–66</sup> or alkaline-earth cations.<sup>67</sup> Kudo *et al.* found that the photocatalytic activity of NiO-loaded NaTaO<sub>3</sub>:La was 9 times higher than that of non-doped sample.<sup>58,59</sup> The maximum apparent quantum yield of the NiO/NaTaO<sub>3</sub>:La photocatalyst reached to 56% at 270 nm (highest record). It was explained that La doping reduced the particle size of NaTaO<sub>3</sub> from 2–3 μm to 0.1–0.7 μm and created ordered surface nanostructure with many characteristic steps, which accounts for the enhancement of photocatalytic activity. The bulk recombination of photogenerated electrons and holes was less in smaller particles with high crystallinity. In addition, the back recombination of H<sub>2</sub> and O<sub>2</sub> was inhibited because of the effective separation of the reaction sites for H<sub>2</sub> and O<sub>2</sub> evolution. Afterwards, La-doped NaTaO<sub>3</sub> powders with high surface area and good crystallinity were made by microwave irradiation method<sup>61</sup> and H<sub>2</sub>O<sub>2</sub> assisted sol-gel route.<sup>65</sup> The highest H<sub>2</sub> production rate of 2.86 mmol/h/g was obtained for a 2.0 mol% La-doped sample from a 10% methanol solution.<sup>65</sup> In addition to the La-doping, Kudo *et al.* also systematically investigated the effect of alkaline earth metal ion dopants (Ca, Sr and Ba) on water splitting with NaTaO<sub>3</sub> powder.<sup>67</sup> Interestingly, doping of Ca, Sr and Ba can also create surface nanostep structures on doped NaTaO<sub>3</sub> when the amount of dopants were larger than 0.5 mol%. The formation of nanostep structure could dramatically enhance water splitting efficiency. However, both positive and negative effects existed for Sr-doping as proved by photoluminescence measurements. A small amount of Sr dopant enhanced charge separation, whereas a large amount of Sr dopant created a significant amount of defects as recombination centers. These studies demonstrated that doping of La and alkaline earth metals is a useful approach for suppressing electron-hole pair recombination by reducing particle size of NaTaO<sub>3</sub> as well as forming surface nanostep structure, however the concentration of dopants needs to be considered for maximizing the photocatalytic performance.

Recently, a major research topic on NaTaO<sub>3</sub> is trying to extend the absorption spectrum of NaTaO<sub>3</sub> into visible light by doping of metals such as Ta<sup>4+</sup>,<sup>68</sup> Cr,<sup>69</sup> Eu,<sup>70</sup> Bi,<sup>71–73</sup> Mn and Fe,<sup>74</sup> and non-metals such as N,<sup>75</sup> C,<sup>76</sup> or co-doping of La/Cr,<sup>77,78</sup> La/N<sup>79</sup> and N/F.<sup>80</sup> The doping mechanism on band gap narrowing of NaTaO<sub>3</sub> are generally accepted that *d* orbitals of metal elements and *s* or *p* orbitals of non-metal elements contribute some intermittent energy levels within the band gap of NaTaO<sub>3</sub>, which are mainly determined by Ta 5*d* and O 2*p* orbitals.<sup>74</sup> For example, Chen *et al.* prepared 5% Bi-doped NaTaO<sub>3</sub> powders by solid-state reaction with varying the ratio of Na/Ta in starting materials.<sup>71,72</sup> They have found that the Na/Ta molar ratio strongly influenced doping sites of Bi in the lattice of NaTaO<sub>3</sub> and optical and photocatalytic properties. The visible light absorption of Bi-doped NaTaO<sub>3</sub> prepared under mild Na-rich conditions was extended up to 550 nm, because Bi dopants were located both at Na and Ta sites. As a result, this sample was the most active one for degradation of methylene blue under visible light irradiation compared to others prepared under Na-deficient or strongly Na-rich conditions. Although doping of metal or non-metal elements into NaTaO<sub>3</sub> (likewise doping of TiO<sub>2</sub>) can be realized by various synthetic methods, it is worth mentioning that Cao and Hu *et al.* developed self-doped (Ta<sup>4+</sup>) NaTaO<sub>3</sub> nanoclusters by a facile one-pot low-temperature solvothermal method.<sup>68</sup> Compared to the foreign element doping, self-doping method benefits from a more homogeneous feature. Furthermore, low-temperature synthesis avoids the increase of particle size and aggregation during prolonged high temperature synthesis. Doping of Ta<sup>4+</sup> greatly reduced the band gap of NaTaO<sub>3</sub> from 3.94 eV to 1.70 eV as indicated by the reddish colour of doped NaTaO<sub>3</sub> sample. In addition, Zhou and Li *et al.* theoretically calculated the band structures of Mn and Fe-doped NaTaO<sub>3</sub> and they found that Mn-doped NaTaO<sub>3</sub>, with a band gap of 2.82 eV, was only active for photo-oxidation of water. The Fe-doped NaTaO<sub>3</sub> (2.03 eV) was capable for overall water splitting.<sup>74</sup>

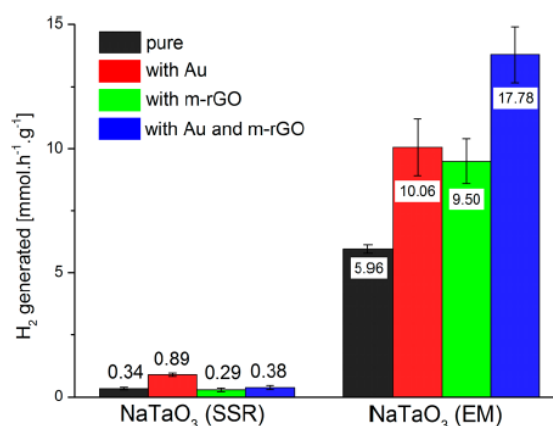


**Fig. 2** Comparison of hydrogen generation rates from NaTaO<sub>3</sub> prepared by solid-state reaction (SSR) and exo-template method (EM) with loading gold or/and reduced graphene oxide. Reprinted with permission from ref. 56. Copyright © 2014, American Chemical Society.

Following the early studies on NaTaO<sub>3</sub>, other tantalate photocatalysts including ATaO<sub>3</sub> (A = Li and K) and AgTaO<sub>3</sub> were also reported. Kudo *et al.* compared the alkali tantalate ATaO<sub>3</sub> (A = Li, Na

and K) photocatalysts for water splitting under UV-light irradiation.<sup>47</sup> The ilmenite  $\text{LiTaO}_3$  photocatalyst showed higher activity than the  $\text{NaTaO}_3$  and  $\text{KTaO}_3$ , when no co-catalyst was employed. However, in the presence of NiO co-catalyst, the  $\text{NaTaO}_3$  exhibited the highest activity and the activity of the NiO/ $\text{NaTaO}_3$  was enhanced by 1 order of magnitude compared to the pure  $\text{NaTaO}_3$ . Furthermore, the activity of  $\text{KTaO}_3$  could be enhanced by Zr-doping as an acceptor. The Zr dopant plays the roles of reducing the charge density in the sample and increasing the lifetime of photoexcited charges.<sup>81</sup> Shortly afterwards, they also found that  $\text{AgTaO}_3$  (3.4 eV) can split water with or without co-catalyst under UV-light irradiation.<sup>82</sup>

The tantalate-based perovskite oxides are considered as a group of promising UV-light photocatalysts with wide band gaps. The band structures are mainly determined by Ta  $5d$  and O  $2p$  orbitals, whereas the A site cations (A = Li, Na, K and Ag) have little effect. Through the nanostructure engineering and doping modification, the photocatalytic performance of parent tantalates could be dramatically enhanced, as demonstrated by the fact that the apparent quantum yield of La-doped  $\text{NaTaO}_3$  (with NiO co-catalyst) reached to 56% at 270 nm.<sup>58,59</sup> In addition, doping of tantalates with appropriate metals or non-metals makes them active under visible light.<sup>68-80</sup>

### 3.1.2 Titanates

$\text{SrTiO}_3$ , one of the earliest studied perovskite photocatalysts, has a band gap of 3.2 eV and suitable band levels for water splitting. A  $\text{SrTiO}_3$  single crystal was found to generate  $\text{H}_2$  from highly alkaline condition ( $[\text{NaOH}] > 5\text{M}$ ) under UV-light illumination.<sup>83,84</sup> The hydroxide ions at or near the photocatalyst surface were suggested as facile hole acceptors to increase the lifetime of electrons for protons reduction. Reduced  $\text{Ti}^{3+}$  surface species were found on the illuminated crystal surface, which might be involved in the production of  $\text{H}_2$  under UV-light illumination. Almost simultaneously, Domen *et al.* also reported photocatalytic splitting of water vapor on a NiO (1.7 wt%) loaded  $\text{SrTiO}_3$ .<sup>85</sup> Later on, they found that liquid water splitting was 3 times faster than water vapor splitting with the NiO/ $\text{SrTiO}_3$  photocatalyst.<sup>86</sup> The NiO loading was crucial for the significant enhancement (100 times) of the water splitting performance. Through further study on the structure of the NiO co-catalyst,<sup>87</sup> it was revealed that a core/shell structure was formed on the surface of  $\text{SrTiO}_3$  during the pre-treatment process (Fig. 3). The NiO on the surface of  $\text{SrTiO}_3$  has undergone a reduction and re-oxidation process, with forming Ni/NiO core/shell structure. The Ni metal in contact with  $\text{SrTiO}_3$  was important for the photocatalytic activity. On the other hand, the NiO in the outer-layer was partly changed to  $\text{Ni}(\text{OH})_2$  during the reaction with water under irradiation. This work reminds us that the co-catalyst engineering (e.g. structure, morphology, distribution and composition tuning) is also vitally important to enhance the photocatalyst performance.

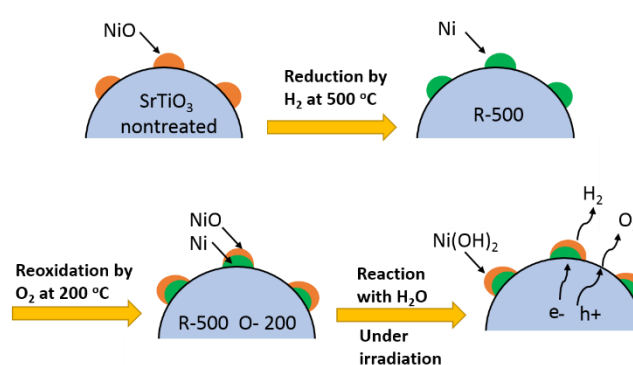


**Fig. 3** Schematic illustration of the core/shell structure of NiO on  $\text{SrTiO}_3$  catalyst. Adapted with permission from ref. 87. Copyright © 1986, American Chemical Society.

These early works have demonstrated that  $\text{SrTiO}_3$  is an excellent material for water splitting under UV-light irradiation. Recently, various nano-structured  $\text{SrTiO}_3$  particles with high surface area were prepared by hydrothermal<sup>88-91</sup> or sol-gel<sup>92</sup> methods to improve the performance. For example, single-crystal-like porous  $\text{SrTiO}_3$  nanocube assemblies were prepared via a facile hydrothermal reaction at 150 °C using layered protonated titanate hierarchical spheres of sub-micrometer size as a precursor template.<sup>90</sup> The hierarchical 3D assemblies were formed by oriented stacking of  $\text{SrTiO}_3$  nanocube of 60-80 nm, as a result of topographic transformation in crystallography between the layered titanate and perovskite structure as well as Ostwald-ripening assisted oriented attachment. Similarly, single-crystal-like mesoporous  $\text{SrTiO}_3$  sub-micrometer spheres with a wormlike structure were synthesized by a hydrothermal method using polyvinyl alcohol as an additive.<sup>89</sup> Despite the well-documented roles in nanoscale engineering of solid photocatalysts, Osterloh *et al.* have observed the activity for overall water splitting of  $\text{SrTiO}_3$  decreases from 28  $\mu\text{mol H}_2/\text{g/h}$  (bulk  $\text{SrTiO}_3$ ) to 19.4  $\mu\text{mol H}_2/\text{g/h}$  (30 nm  $\text{SrTiO}_3$ ), and 3.0  $\mu\text{mol H}_2/\text{g/h}$  (6.5 nm  $\text{SrTiO}_3$ ).<sup>93</sup> The reasons for this decrease were ascribed to an increase of water oxidation overpotential for the smaller particles and reduced light absorption due to a quantum size effect. They suggested that the catalyst particles based on  $\text{SrTiO}_3$  should be larger than 30 nm for overall water splitting under UV-light irradiation. The controversial results on the nanoscale engineering of solid photocatalysts should be considered in future studies.

Recent studies on  $\text{SrTiO}_3$  are concentrated on doping  $\text{SrTiO}_3$  for achieving visible light activity. Doping of single metal elements such as Cr,<sup>94,95</sup> Fe,<sup>96</sup> Mn,<sup>97</sup> Ir,<sup>97</sup> Ru,<sup>97</sup> Rh,<sup>97</sup> Er,<sup>98</sup> Zn<sup>99</sup> and Ti (III),<sup>100,101</sup> and non-metal elements such as N<sup>102</sup> and F<sup>103</sup> as well as co-doping of Cr/Sb,<sup>104</sup> Cr/ N,<sup>105</sup> Cr/Ta,<sup>106</sup> Cr/La<sup>107</sup>, La/Ni,<sup>108</sup> S and C,<sup>109</sup> N/La,<sup>110</sup> Ni/Ta<sup>111</sup> and La/Rh<sup>112</sup> have been intensively investigated for showing photocatalytic activities under visible light irradiation. Among the different noble metal ions, Rh ion was the best one than the others like Ru and Ir. The donor level located at *ca.* 1.0 eV above valence band was formed by the  $\text{Rh}^{3+}$  doping, which behaved as visible light absorption centre and surface reaction centre for oxidation of methanol (hole scavenger).<sup>97</sup> Later on, Cr-doped  $\text{SrTiO}_3$  was also evaluated for photocatalytic hydrogen production under visible light

irradiation. The  $\text{Sr}_{0.95}\text{Cr}_{0.05}\text{TiO}_3$  sample prepared by hydrothermal method extended its visible light absorption up to 540 nm and exhibited 3 times higher activity than that synthesized by solid-state reaction due to the increased surface area.<sup>95</sup> Note that the  $\text{Cr}^{3+}$  substitution of  $\text{Ti}^{4+}$  sites in  $\text{SrTiO}_3$  would create oxygen defects and/or generate  $\text{Cr}^{6+}$  ions to keep the charge balance, which may increase the recombination between photogenerated electrons and holes. The positive doping effect for  $\text{Cr}^{3+}$  was suggested only for substitution of  $\text{Sr}^{2+}$  sites in  $\text{SrTiO}_3$ . Recently, La and Rh co-doped  $\text{SrTiO}_3$  and Mo-doped  $\text{BiVO}_4$  powders embedded into a gold layer in a Z-scheme system was developed for water splitting with a solar-to-hydrogen energy conversion efficiency of over 1% and an apparent quantum yield of over 30% at 419 nm was achieved. Another important feature is that the photocatalyst sheet is scalable by screen-printing an ink containing the mixed photocatalysts.<sup>112</sup> In addition to the foreign element doping, self-doped  $\text{SrTiO}_{3-x}$  was prepared through a one-step combustion method followed by annealing at high temperatures under Ar atmosphere.<sup>100</sup> The oxygen vacancy played dual roles: enhancing visible light absorption and chemical adsorption of  $\text{CO}_2$  onto catalyst, which improved the artificial photosynthesis to produce hydrocarbon fuels from  $\text{CO}_2$  and  $\text{H}_2\text{O}$  as a result of the synergetic effect. However, as observed from Sun's group, oxygen vacancy on the surface of  $\text{SrTiO}_3$  induced by chemical reduction can only improve the UV-light photocatalytic activity due to the enhancement of charge separation, but it had little effect on the visible light activity.<sup>101</sup> In the case of doping of non-metal elements, mesoporous N-doped  $\text{SrTiO}_3$  was prepared using glycine as both nitrogen source and mesopore creator.<sup>102</sup> The doped sample has a higher specific surface area ( $52.3 \text{ m}^2\text{g}^{-1}$ ) with a lower band gap of 2.9 eV, and exhibits excellent activity in photodegradation of dyes.

In contrast to forming donor/acceptor levels within the band gaps through doping of metal or non-metal ions, a series of upconversion luminescent materials (e.g.  $\text{Er}^{3+}$ ) doped  $\text{SrTiO}_3$  photocatalysts have been demonstrated to be active for visible light driven water splitting with sacrificial agents.<sup>98</sup> The upconversion luminescent agents (e.g. rare earth elements) such as  $\text{Eu}^{3+}$ ,  $\text{Nd}^{3+}$  and  $\text{Er}^{3+}$  can emit high-energy photons by absorbing two or more low-energy photons. By this approach, visible light photons can be firstly up-converted into UV-light photons so as to excite the large band-gap semiconductors if the upconversion material is properly trapped into the large band gap semiconductor host as shown in Fig. 4.

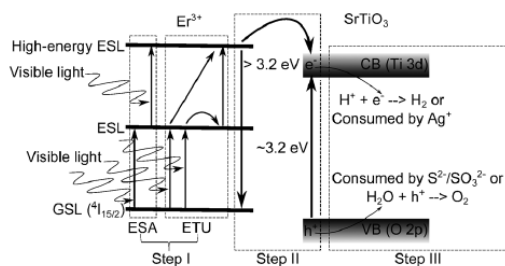


**Fig. 4** Schematic illustration of the main processes of the photocatalytic reaction on  $\text{Er}^{3+}$  doped  $\text{SrTiO}_3$  sample. Reprinted with permission from ref. 98. Copyright © 2012, Wiely-VCH Verlag GmbH & Co. KGaA, Weinheim.

Other titanates including  $\text{BaTiO}_3$ ,<sup>113-115</sup> Rh or Fe-doped  $\text{BaTiO}_3$ ,<sup>116,117</sup>  $\text{CaTiO}_3$ ,<sup>118,119</sup> and Cu,<sup>120</sup> Rh,<sup>121</sup> Ag and La-doped  $\text{CaTiO}_3$ ,<sup>122</sup> and  $\text{PbTiO}_3$ ,<sup>123,124</sup> were also reported as UV or visible light photocatalysts. It was interestingly found that Pt loaded  $\text{CaTiO}_3$  photocatalyst exhibited an enhanced production rate of hydrogen from a mixture of water vapor and methane due to the simultaneous photocatalytic steam reforming of methane and water decomposition.<sup>119</sup> The activated methane species or reaction intermediates would accelerate the water splitting or suppress the reverse reaction. This result implies that the renewable sources such as methane from biogas can be utilized for producing  $\text{H}_2$  by photocatalytic steam reforming.  $\text{BaTiO}_3$ , an n-type semiconductor with a band gap of 3.0 eV, was studied by doping Rh species in order to generate a new absorption band in visible light region. Rh-doped  $\text{BaTiO}_3$  powder prepared by the polymerized complex method was examined for water reduction with sacrificial agent under visible light irradiation.<sup>116</sup> Interestingly, Rh-doped  $\text{BaTiO}_3$  or  $\text{SrTiO}_3$  electrode<sup>125</sup> generated a stable cathodic photocurrent, in contrast to the anodic photocurrent generated from the un-doped  $\text{BaTiO}_3$  electrode under UV light irradiation. Thus, Rh-doped  $\text{BaTiO}_3$  is regarded as a p-type semiconductor, which is rarely observed for doped metal oxides. Similar to the reported Rh-doped  $\text{SrTiO}_3$ , substitution of  $\text{Ti}^{4+}$  sites with a  $\text{Rh}^{3+}$  ions without forming oxygen vacancies yields positive holes due to the charge compensation and thus changes the semiconducting property from n-type to p-type. However, it should be noted that doping Rh into n-type oxide semiconductors does not always produce p-type character.

Titanate photocatalysts, represented by  $\text{SrTiO}_3$  as a prototype perovskite, are attractive in the research field of photo(electro)catalysis. In a similar manner as that employed in tantalates photocatalysts, nanostructure engineering and doping modification are two of the most commonly adopted strategies to improve the photocatalytic performance of titanates. However, the smaller particle size of solid photocatalyst can't guarantee higher water splitting efficiency due to the quantum size effect. On the other hand,  $\text{SrTiO}_3$  is a good candidate of investigating the surface defects related to visible light activity and adsorption property due to the flexible conversion between  $\text{Ti}^{3+}$  and  $\text{Ti}^{4+}$ .

### 3.1.3 Niobates

Alkaline niobates such as  $\text{KNbO}_3$  and  $\text{NaNbO}_3$  have been widely investigated as UV-light photocatalysts. The bulk  $\text{KNbO}_3$  with a band gap of 3.12 eV was synthesized by hydrothermal reaction under supercritical water conditions in an earlier report.<sup>126</sup> By heating at 400 °C, a single phase of  $\text{K}_4\text{Nb}_6\text{O}_{17}$  was gradually transformed into a single phase of  $\text{KNbO}_3$  in 24 h. However, the mixed phases of  $\text{K}_4\text{Nb}_6\text{O}_{17}$  and  $\text{KNbO}_3$  were found more photoactive for water splitting than pure  $\text{K}_4\text{Nb}_6\text{O}_{17}$  and  $\text{KNbO}_3$  under UV-light irradiation. Nano-structured  $\text{KNbO}_3$  with different morphologies of nanowires, nanorods, nanocubes, nanocrystals and microcubes can be prepared by hydrothermal synthesis,<sup>127-133</sup> which basically involves the hydrothermal treatment of mixed aqueous solution of  $\text{KOH}$  and  $\text{Nb}_2\text{O}_5$  at about 180 - 200 °C in an autoclave for several hours. The

variation of hydrothermal parameters such as temperature, reaction time, pH of solution and concentration of precursors changes the morphologies. For example, cubic, orthorhombic and tetragonal  $\text{KNbO}_3$  microcubes were prepared by varying the ratio of KOH and  $\text{Nb}_2\text{O}_5$  in precursor solution.<sup>129,130</sup> The cubic  $\text{KNbO}_3$ , with relatively larger BET surface area and band gap compared to the tetragonal and orthorhombic samples, exhibited the highest  $\text{H}_2$  production rate. At the same time, Yi *et al.* proposed a dissolution-recrystallization mechanism to explain the formation of the corresponding nanostructures.<sup>131</sup> In addition, gold nanoparticles deposited  $\text{KNbO}_3$  microcubes were prepared for utilizing visible light induced surface plasmon resonance effect on gold nanoparticles.<sup>132</sup> N-doped  $\text{KNbO}_3$  nanocubes with a band gap of 2.76 eV were prepared and tested for water splitting with sacrificial agents under visible light.<sup>133</sup>

Compared to the  $\text{KNbO}_3$ ,  $\text{NaNbO}_3$  showed relatively lower photocatalytic activity probably because of its relative larger band gap.<sup>134,135</sup> However, an interesting phenomenon was found that the  $\text{KNbO}_3$  film exhibited photoinduced hydrophilicity under UV-light irradiation, even though the photocatalytic oxidation of dye by the  $\text{KNbO}_3$  film was negligible.<sup>136</sup> Normally, the photoinduced hydrophilicity was observed for  $\text{TiO}_2$  film because of the photocatalytic decomposition of organic compounds with regenerating a hydrophilic surface. These results confirm that photoinduced hydrophilicity was not caused solely by the photocatalytic oxidation. In addition, N-doped  $\text{NaNbO}_3$ <sup>137,138</sup> and Ru-doped  $\text{NaNbO}_3$  nanocubes and nanowires<sup>139</sup> were also reported for the photocatalytic decomposition of phenol and 2-propanol under visible light irradiation.

In contrast to the alkaline niobates,  $\text{AgNbO}_3$  has a smaller band gap about 2.8 eV and can be prepared by solid-state, sol-gel, solvothermal and molten-salt flux techniques.<sup>140-143</sup> For example, polyhedron-shaped  $\text{AgNbO}_3$  photocatalyst with surface nanosteps was prepared by a solvothermal method.<sup>142</sup> The well-defined edges and corners on the polyhedron-shaped  $\text{AgNbO}_3$  were found to be able to enhance its photocatalytic activity, in a similar manner to that observed on La-doped  $\text{NaTaO}_3$ . Likewise, the formation of 20-50 nm terraced surface microstructure was also observed on the  $\text{AgNbO}_3$  nanoparticles synthesized by molten-salt flux, whereas there was no well-defined morphology and microstructure for the sample prepared from solid-state synthesis.<sup>143</sup> In order to further enhance the photocatalytic activity of  $\text{AgNbO}_3$ , La-doped  $\text{AgNbO}_3$  was prepared by a solid-state reaction method.<sup>144</sup> The  $\text{Ag}_{0.88}\text{La}_{0.12}\text{NbO}_3$  sample showed 12-fold higher rate for photocatalytic decomposition of gaseous 2-propanol under visible light irradiation. The enhanced performance was assumed to several possible reasons such as the enlarged surface area, enhanced mobility of photo-generated electrons, deposition of metallic silver and A-site defects in perovskite structure.

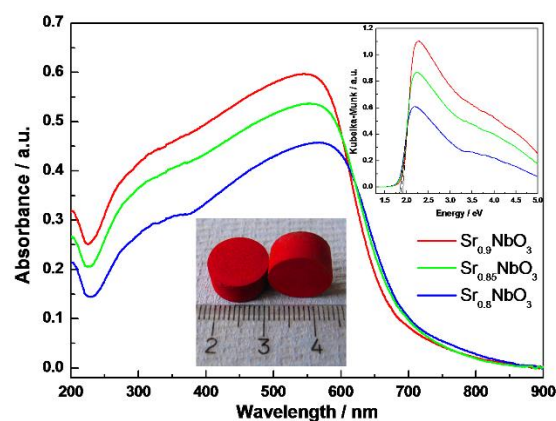


**Fig. 5** Ultraviolet-visible absorbance spectra for  $\text{Sr}_{1-x}\text{NbO}_3$ . Kubelka-Munk transformation of the absorption curves is shown in the top inset. The colour of sample pellet is shown in the bottom inset. Reprinted with permission from ref. 145. Copyright © 2012, Nature Publishing group.

Recently, a nonstoichiometric  $\text{Sr}_{1-x}\text{NbO}_3$  ( $x = 0.1 - 0.2$ ) was reported as a novel metallic visible light photocatalyst by Irvine *et al.*<sup>145,146</sup> A series of strongly coloured red materials with band gap energy of 1.9 eV were obtained by controlling the nonstoichiometry in the perovskite (Fig. 5). The band structures of metallic oxide conductors are assumed to be different from the semiconductor oxides, in which the valence and conduction bands are clearly distinguished. For the metallic  $\text{Sr}_{1-x}\text{NbO}_3$ , it was described that the band below conduction band as the highest fully occupied band ( $B_{-1}$ ) and that above it as the lowest unoccupied band ( $B_1$ ), respectively. Therefore, the photon excitation by visible light might be involved either from  $B_{-1}$  to conduction band or from conduction band to  $B_1$ . The high conductivity of the sample might allow the fast separation and mobility of charge carrier. As a result,  $\text{Sr}_{0.9}\text{NbO}_3$  showed the highest efficiency for  $\text{H}_2$  or  $\text{O}_2$  evolution from a sacrificial aqueous solution.

The niobate perovskite photocatalysts are less-studied than those tantalate and titanate-based photocatalysts, probably because of their relatively lower activities and stabilities. Most of the studies on the alkaline niobates photocatalysts are focused on the preparation of nano-structured niobates with different morphologies.<sup>127-133,140-143</sup> In an exceptional case, the nonstoichiometric  $\text{Sr}_{1-x}\text{NbO}_3$  ( $x = 0.1 - 0.2$ ) has been demonstrated as a novel metallic visible light photocatalyst,<sup>145,146</sup> which opens up a new research direction of searching visible light photocatalysts.

### 3.1.4 Ferrites

Magnetic  $\text{BiFeO}_3$ , known as the one of the multiferric material in magnetoelectric applications, was also studied as a visible light photocatalyst for water splitting and degradation of organic pollutants due to its small band gap (*ca.* 2.2 eV). Both  $\text{BiFeO}_3$  nanoparticle powders and films were prepared for evaluating their photo(electro)catalytic performance.<sup>147-156</sup> In an early report,  $\text{BiFeO}_3$  with band gap about 2.18 eV synthesized by a citric acid assisted sol-gel method has shown its visible light

photocatalytic activity by decomposition of methyl orange dye.<sup>147</sup> The following studies on the BiFeO<sub>3</sub> are mainly focused on the preparation of novel structured BiFeO<sub>3</sub> with different morphologies. For example, Lin and Nan *et al.* synthesized BiFeO<sub>3</sub> uniform microspheres and microcubes by a controlled hydrothermal method as shown in Fig. 6.<sup>150</sup> The band gaps of BiFeO<sub>3</sub> materials were estimated about 1.82 eV for BiFeO<sub>3</sub> microspheres, 2.12–2.27 eV for microcubes. The clear shift for the absorption edge among these samples was influenced by particle size, morphology and crystal-field strength. The microcubes sample exhibited the highest efficiency for the photocatalytic degradation of congo red dye under visible light irradiation because of the relative larger band gap. Later on, a facile aerosol-spraying approach was developed to prepare mesoporous BiFeO<sub>3</sub> hollow spheres with enhanced activity for removal of RhB dye and 4-chlorophenol, due to the enhanced light absorbance resulting from multiple light reflections in hollow chamber and higher surface area.<sup>148</sup>

In addition, a remarkably enhanced water oxidation activity on Au nanoparticles loaded BiFeO<sub>3</sub> nanowires under visible light irradiation was reported.<sup>154</sup> The Au-BiFeO<sub>3</sub> hybrid structure was induced by electrostatic interaction of positively charged BiFeO<sub>3</sub> nanowires and negatively charged Au nanoparticles at pH 6.0 according to their different isoelectric points. An enhanced absorbance between 500 and 600 nm was observed for the Au/BiFeO<sub>3</sub> samples due to the typical Au surface plasmon band in visible light region. The amount of O<sub>2</sub> produced from Au/BiFeO<sub>3</sub> nanowires with 1 wt% Au loading was 30 times higher than that from parent BiFeO<sub>3</sub> nanowires during the first 4 h reaction. More interestingly, a synergistic effect was found between the Au nanoparticles and the BiFeO<sub>3</sub> nanowires support, as the photocatalytic activity of self-assembled Au/BiFeO<sub>3</sub> nanowires was much higher than the composite of Au and BiFeO<sub>3</sub> nanowires. The photoluminescence study suggested the occurrence of efficient charge transfer from BiFeO<sub>3</sub> to Au, which explained the enhancement of the photocatalytic activity. In addition, Ba, Ca, Mn and Gd doped BiFeO<sub>3</sub> nanofibers and nanoparticles have shown obvious room temperature ferromagnetic behaviours and photocatalytic activity for decomposition of dyes.<sup>157–161</sup>

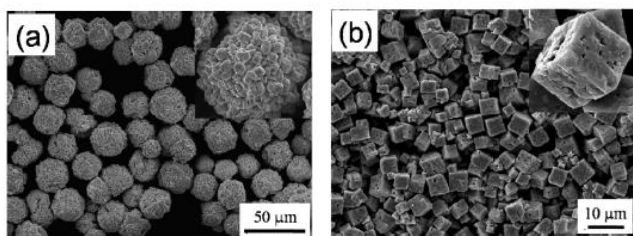


**Fig. 6** SEM images of BiFeO<sub>3</sub>: (a) Microspheres and (b) Microcubes. The magnified images are shown in the top insets. Reprinted with permission from ref. 150. Copyright © 2010, American Chemical Society.

Various nanostructured LaFeO<sub>3</sub> with different morphologies such

as nanoparticles, nanosheets, nanotubes, nanorods, and nanospheres have been also prepared as visible light photocatalysts for water splitting and degradation of organic dyes.<sup>162–170</sup> Other ferrites like PrFeO<sub>3</sub>,<sup>171</sup> SrFeO<sub>3</sub><sup>172,173</sup> and GaFeO<sub>3</sub><sup>174</sup> were reported as novel visible light photocatalysts. Particularly, GaFeO<sub>3</sub>, with a band-gap of 2.7 eV, exhibited attractive overall water splitting activity without any co-catalyst loading from pure water. The hydrogen and oxygen yields were about 10.0 and 5.0 μmol/g/h under visible light irradiation.

Considering the ferroelectric and magnetoelectric properties of ferrites materials, it is more attractive to develop multifunctional photocatalysts as demonstrated by the study of BiFeO<sub>3</sub> and LnFeO<sub>3</sub>, even though their photocatalytic activities are not as good as their counterparts such as titanate and tantalate perovskites. For example, the ferroelectric BiFeO<sub>3</sub> has recently been used in photovoltaic devices for coupling of light absorption with other functional properties.<sup>175,176</sup>

### 3.1.5 Others

Other perovskites such as BaZrO<sub>3</sub>,<sup>177–179</sup> Mg, Ta-doped BaZrO<sub>3</sub>,<sup>180,181</sup> MSnO<sub>3</sub> (M = Ca, Sr, Ba)<sup>182–186</sup> and BaCeO<sub>3</sub><sup>187</sup> were barely studied as UV-light photocatalysts with relative large band gaps of over 4.0 eV. Among them, SrSnO<sub>3</sub> nanorods prepared by hydrothermal method exhibited much higher photocatalytic water splitting performance.<sup>183</sup> The hydrogen and oxygen yields with Pt-loaded SrSnO<sub>3</sub> in the sacrificial systems were 8200 and 2500 μmol/g/h under UV-light irradiation, respectively. In addition, LaCoO<sub>3</sub>,<sup>188–190</sup> C, Fe-doped LaCoO<sub>3</sub><sup>191,192</sup> and LaNiO<sub>3</sub><sup>193,194</sup> are active for photocatalytic degradation of dyes and water splitting under visible light irradiation.

### 3.2 AA'BO<sub>3</sub> type

Substitution of A ion in ABO<sub>3</sub> by A' ion with a different valence state will alter the valence state of B metal ion or induce some defects and oxygen vacancies into the structure, which would significantly influence optical and photocatalytic activities. Thus, this strategy offers us more options to design new perovskite photocatalysts by rational combination of dual metal ions with consideration of the charge balance. For illustration, sodium bismuth titanate (Bi<sub>0.5</sub>Na<sub>0.5</sub>TiO<sub>3</sub>) has been widely used for piezoelectric, ferroelectric and pyroelectric devices. It was also studied as a UV-light photocatalyst with a band gap of *ca.* 3.0 eV.<sup>195–197</sup> Hierarchical micro/nanostructured Bi<sub>0.5</sub>Na<sub>0.5</sub>TiO<sub>3</sub> was synthesized by *in situ* self-assembly of Bi<sub>0.5</sub>Na<sub>0.5</sub>TiO<sub>3</sub> nanocrystal under a controlled hydrothermal condition, during which the growth mechanism was studied in detail.<sup>195</sup> It was proposed that the hierarchical nanostructure was built through a process of nucleating and growth and aggregation of nanoparticles and subsequent *in situ* dissolution-recrystallization of the microsphere nanoparticles with prolonged heating time and increased temperature or basic condition. The 3D hierarchical Bi<sub>0.5</sub>Na<sub>0.5</sub>TiO<sub>3</sub> exhibited much higher photocatalytic activity for removal of methyl orange dye due to the increased surface area and adsorption of dye molecules. The activities of Na<sub>0.5</sub>Bi<sub>0.5</sub>TiO<sub>3</sub> were also evaluated by photocatalytic production of H<sub>2</sub> from water and removal of nitric oxide in gas phase.<sup>196,197</sup> Another



example is that K-doping in  $\text{Na}_{1-x}\text{K}_x\text{TaO}_3$  photocatalyst transformed the distorted perovskite  $\text{NaTaO}_3$  to a pseudo-cubic phase, which significantly promoted photocatalytic water splitting activity.<sup>198</sup> In terms of the crystalline structure, approximately  $180^\circ$  (a value ideal for delocalization of the excited energy in tantalates) Ta-O-Ta bond linkage caused by K-doping, facilitates the separation of photogenerated charges as to enhance the photocatalytic activity.  $\text{La}_{0.7}\text{Sr}_{0.3}\text{MnO}_3$ , as a visible light photocatalyst, was investigated for solar photocatalytic degradation of methyl orange.<sup>199</sup> In addition,  $\text{La}_{0.5}\text{Ca}_{0.5}\text{NiO}_3$ ,<sup>200</sup>  $\text{La}_{0.5}\text{Ca}_{0.5}\text{CoO}_3$ ,<sup>201</sup> and  $\text{Sr}_{1-x}\text{Ba}_x\text{SnO}_3$  ( $x = 0 - 1$ )<sup>202</sup> nanoparticles were prepared for showing enhanced photocatalytic degradation of dyes.

### 3.3 ABB'O<sub>3</sub> type

In a similar manner to A-site substitution, B-site substitution by a different cation is another option for tuning physicochemical or photocatalytic properties of perovskites. A  $\text{KTaO}_3$  is well known as a good UV light photocatalyst for water splitting, Ishihara et al. systematically investigated the effect of doping a series of cations ( $\text{Zn}^{2+}$ ,  $\text{Y}^{3+}$ ,  $\text{Al}^{3+}$ ,  $\text{Ga}^{3+}$ ,  $\text{In}^{3+}$ ,  $\text{Ce}^{4+}$ ,  $\text{Ti}^{4+}$ ,  $\text{Zr}^{4+}$ ,  $\text{Hf}^{4+}$ ,  $\text{Si}^{4+}$ ,  $\text{Ge}^{4+}$ ,  $\text{Nb}^{5+}$ ,  $\text{Sb}^{5+}$  and  $\text{W}^{6+}$ ) to substitute Ta in  $\text{KTaO}_3$ .<sup>203</sup> It was found that 8% doping of  $\text{Zr}^{4+}$  exhibited the highest rate for water splitting under UV-light irradiation. The increased activity was proposed to the enhancement of the lifetime of photoexcited charge due to the decreased charge density. Later on, they further combined the  $\text{KTa}(\text{Zr})\text{O}_3$  with various organic dyes for water splitting in a Z-scheme system.<sup>204</sup> The cyanocobalamin sensitized  $\text{K}_{0.95}\text{Ta}_{0.92}\text{Zr}_{0.08}\text{O}_3$  exhibited the highest photocatalytic water splitting efficiency with formation rate of 575.0 and 280.4  $\mu\text{mol/g/h}$  for  $\text{H}_2$  and  $\text{O}_2$ , respectively. The enhanced charge transfer mechanism on the porphyrinoids modified  $\text{K}_{0.95}\text{Ta}_{0.92}\text{Zr}_{0.08}\text{O}_3$  was further studied by photoluminescence spectroscopy in detail as shown in Fig. 7.<sup>205</sup> Unlike dye sensitization, photo-excited electrons transferred from  $\text{K}_{0.95}\text{Ta}_{0.92}\text{Zr}_{0.08}\text{O}_3$  to dyes and Z-type excitation was successfully achieved. The photogenerated charges were spatially separated between  $\text{KTa}(\text{Zr})\text{O}_3$  and Cr-TPP dye as in a photosynthetic system. This work suggests promise for organic-inorganic hybrid Z-scheme systems for water splitting, compared to the all-solid-state Z-scheme systems.

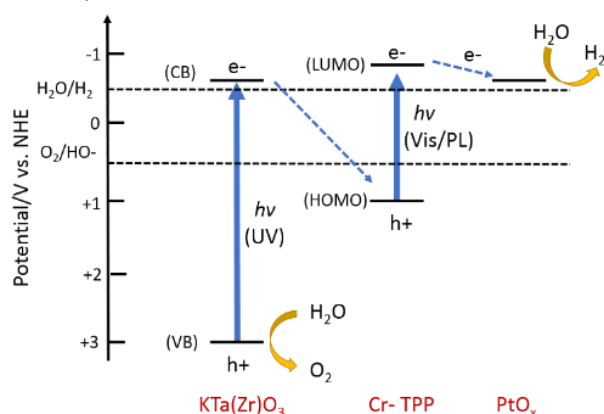


**Fig. 7** Schematic mechanism for the photocatalytic water splitting into  $\text{H}_2$  and  $\text{O}_2$  on dye (Cr-TPP) modified  $\text{KTa}(\text{Zr})\text{O}_3$  at pH 11. Reprinted with permission

from ref. 205. Copyright © 2009, Wiley-VCH Verlag GmbH & Co. KGaA, Weinheim.

Another series of  $\text{M}(\text{N}_x\text{Nb}_{1-x})\text{O}_3$ , ( $\text{M} = \text{Ca}, \text{Sr}$  and  $\text{Ba}$ ;  $\text{N} = \text{Co}, \text{In}$  and  $\text{Zn}$ ) solid solution samples were synthesized by solid state reaction and evaluated their performance for water splitting under UV-light irradiation.<sup>206-211</sup> Among these different compositions,  $\text{BaZn}_{1/3}\text{Nb}_{2/3}\text{O}_3$  seemed the most active photocatalyst for pure water splitting and generation of  $\text{H}_2$  from a methanol containing aqueous solution under UV-light irradiation. Raman spectra indicated that different binding modes of M-O-Nb may be the dominant factors in the migration of photogenerated charge carriers and affecting the photocatalytic activity. Furthermore, highly electronegative non-transition metal Pb or Sn ions were incorporated into the perovskite lattice of  $(\text{BaIn}_{1/3}\text{M}_{1/3}\text{M}'_{1/3})\text{O}_3$  ( $\text{M} = \text{Sn}, \text{Pb}$ ;  $\text{M}' = \text{Nb}, \text{Ta}$ ).<sup>212,213</sup> The Pb-containing quaternary metal oxides  $\text{Ba}(\text{In}_{1/3}\text{Pb}_{1/3}\text{M}_{1/3})\text{O}_3$  possess a much narrower band gap of ca. 1.50 eV when compared to those of the ternary oxides  $\text{Ba}(\text{In}_{1/2}\text{M}_{1/2})\text{O}_3$  (2.97-3.30 eV) and the Sn-containing  $\text{Ba}(\text{In}_{1/3}\text{Sn}_{1/3}\text{M}_{1/3})\text{O}_3$  derivatives (2.85-3.00 eV). These results provided a new method of developing efficient visible light photocatalysts by doping electronegative non-transition metal cations.<sup>212</sup> In addition, A-site strontium based perovskites such as  $\text{SrTi}_{(1-x)}\text{Fe}_x\text{O}_{3-\delta}$ ,  $\text{SrTi}_{0.1}\text{Fe}_{0.9}\text{O}_{3-\delta}$ ,  $\text{SrCo}_{1/2}\text{Fe}_{1/2}\text{O}_{3-\delta}$ ,  $\text{SrNb}_{1/2}\text{Fe}_{1/2}\text{O}_3$  compounds were synthesized through solid-state reaction and sol-gel methods, and investigated for degradation of dyes under visible light irradiation.<sup>214-218</sup> Another group of A-site Lanthanum based perovskites such as  $\text{LaNi}_{1-x}\text{Cu}_x\text{O}_3$  and  $\text{LaFe}_{1/2}\text{Ti}_{1/2}\text{O}_3$  were demonstrated as efficient visible light photocatalysts for generation of  $\text{H}_2$  from HCHO aqueous solution and degradation of p-chlorophenol under visible light irradiation.<sup>219-221</sup> The other ABB'O<sub>3</sub> type photocatalysts including  $\text{Ba}(\text{ZrSn})\text{O}_3$ ,<sup>222</sup>  $\text{Ca}(\text{TiZr})\text{O}_3$ ,<sup>223</sup>  $\text{Bi}(\text{MgFeTi})\text{O}_3$ ,<sup>224</sup>  $\text{Na}(\text{BiTa})\text{O}_3$ ,<sup>225</sup>  $\text{Na}(\text{TiCu})\text{O}_3$ ,<sup>226</sup>  $\text{Ag}(\text{TaNb})\text{O}_3$ <sup>227</sup> have also been reported.

Compared to the AA'BO<sub>3</sub> type perovskites, ABB'O<sub>3</sub> type structure provides more flexibility in composing the perovskites photocatalyst, because normally the B-site cations in ABO<sub>3</sub> mainly determine the level of conduction band, in addition to build the framework of perovskite structure with oxygen atoms. The band structures of photocatalysts can be finely tuned by rationally combining dual or ternary metal cations at B-site, or varying the ratio of the multiple cations, which has been well demonstrated by the examples given above. Further investigations on ABB'O<sub>3</sub> type photocatalysts are expected to explore their new exciting photocatalytic performance.

### 3.4 AB(ON)<sub>3</sub> type

In addition to the A- or B-site doping, nitridation of perovskite oxides to form oxynitride-type perovskite  $\text{AB}(\text{ON})_3$  is another effective approach to reduce the band gap of ABO<sub>3</sub> and enhance the photo(electro)catalytic performance under visible light. Since the N 2p orbitals can introduce new intermittent energy levels above the valence band edge constructed by O 2p orbitals, most of the  $\text{AB}(\text{ON})_3$  materials have strong visible light absorption up to 600-650 nm. The development of oxynitride photocatalysts successfully makes visible light driven water

splitting possible at irradiation wavelength of over 600 nm. For example, LaTiO<sub>2</sub>N developed by Domen and co-workers has been researched as a visible light photocatalyst for water splitting.<sup>228-234</sup> It has a band gap of 2.1 eV and exhibits both photocatalytic H<sub>2</sub> and O<sub>2</sub> evolution from a sacrificial aqueous system under visible light irradiation up to ca. 600 nm.<sup>229,230</sup> By loading LaTiO<sub>2</sub>N with CoO<sub>x</sub> co-catalyst, the O<sub>2</sub> evolution efficiency can be greatly enhanced.<sup>228,231</sup> However, it shows a relatively lower activity for H<sub>2</sub> evolution even with Pt co-catalyst. The infrared spectroscopic analysis suggests that photoexcited electrons in LaTiO<sub>2</sub>N cannot efficiently transfer to the Pt co-catalyst.<sup>232</sup> It was thought that LaTiO<sub>2</sub>N prepared by nitridation process may contain a lot of defects, especially in the surface region, which would prevent the charge transfer at the interfaces between the photocatalyst and co-catalyst. Recently, eliminating such surface defects layer on LaTiO<sub>2</sub>N with appropriate acid etching gave rise to significant improvements in photocatalytic activity for both the H<sub>2</sub> and O<sub>2</sub> evolution reactions.<sup>233</sup> Furthermore, the LaTiO<sub>2</sub>N powder can be fabricated into a photoanode for photoelectrochemical water splitting.<sup>235-240</sup> The LaTiO<sub>2</sub>N photoanode decorated with IrO<sub>2</sub> co-catalysts exhibited a markedly improved anodic photocurrent based on water oxidation.

Tantalum or Niobium oxynitride series (ABO<sub>2</sub>N, A: Ca, Sr and Ba; B: Ta and Nb) are another successful examples that can generate H<sub>2</sub> or O<sub>2</sub> from aqueous sacrificial solution under visible light irradiation up to ca. 600 nm. In the case of ATaO<sub>2</sub>N, the band gaps decrease with increasing the radius of alkaline-earth metals with 2.5, 2.1, 2.0 eV for A = Ca, Sr and Ba, respectively.<sup>241</sup> Only H<sub>2</sub> was produced from aqueous methanol solution with these photocatalysts, while no O<sub>2</sub> was evolved even from silver nitrate solution. Thus, ATaO<sub>2</sub>N is usually used as a H<sub>2</sub> production photocatalyst in a Z-Scheme water splitting system.<sup>242,243</sup> Recently, doping of pentavalent W-species into BaTaO<sub>2</sub>N significantly improved the activity for O<sub>2</sub> evolution from aqueous silver nitrate solution in the presence of IrO<sub>2</sub> co-catalyst.<sup>244</sup> The optimum ratio of W/Ta = 0.005 was found for the O<sub>2</sub> evolution. Since the W-doping didn't largely alter the band gap structure of BaTaO<sub>2</sub>N, a plausible explanation for the enhanced oxidation of water was proposed to the pronounced upward band-bending, because holes in valence band are able to migrate easily to the surface according to the upward band-bending. The BaTaO<sub>2</sub>N fabricated photoanode can achieve water splitting under visible light irradiation up to 660 nm wavelength. The IPCE value was estimated about ca. 10% at 1.2 V vs RHE under 600 nm, which is the highest record among the photoanodes excited beyond 600 nm for water oxidation.<sup>245</sup> Niobium-based oxynitrides generally have much smaller band-gaps than the corresponding tantalum analogues. The band-gaps of ANbO<sub>2</sub>N are 2.0, 1.8, 1.7 and 1.6 eV for A = Ca, Sr, Ba and La, respectively.<sup>246</sup> However, only CaNbO<sub>2</sub>N is photoactive for H<sub>2</sub> and O<sub>2</sub> evolution under sacrificial conditions. SrNbO<sub>2</sub>N powder showed weak photocatalytic O<sub>2</sub> evolution activity even in the presence of silver nitrate, but generated an anodic

photocurrent due to the water oxidation upon irradiation with visible light photons up to 700 nm, even without an externally applied potential.<sup>247</sup> Under visible light irradiation with an applied potential of 1.0-1.55 V vs. RHE, stoichiometric H<sub>2</sub> and O<sub>2</sub> evolution was achieved on SrNbO<sub>2</sub>N electrode decorated with colloidal IrO<sub>2</sub> co-catalyst.

The nitridation approach can efficiently narrow the band gap of ABO<sub>3</sub> oxide and increase the capability of visible light absorption, thus has been widely employed for developing new materials in both photochemical and photoelectrochemical systems. The development of nitridized materials is indeed a great success in extending visible light response of the photocatalysts and photoelectrodes. However, it is not faultless. The nitridized materials suffer from stability challenge during water oxidation process, as the nitrogen component would be easily oxidized to nitrogen gas instead of water oxidation.<sup>233</sup> Therefore, how to improve the stability of the nitridized materials is important and requires further investigations.

### 3.5 ABO<sub>3</sub>-A'B'O<sub>3</sub>(A'B'O<sub>2</sub>N) type

Because of the high capacity of accommodating a wide range of cations and valences at both A- and B-sites, ABO<sub>3</sub> type perovskite oxides are promising candidates for making solid-solution photocatalysts. In this case, both the A and B cations can be replaced by equivalent cations resulting in a perovskite with the formula of (ABO<sub>3</sub>)<sub>x</sub>(A'B'O<sub>3</sub>)<sub>1-x</sub>. Since most of reported visible light photocatalysts are not capable of generating H<sub>2</sub> and O<sub>2</sub> simultaneously due to the unsuitable band edge positions, it is thus expected that the band structures of solid solution materials can be tuned by combining a H<sub>2</sub> evolution photocatalyst and a O<sub>2</sub> evolution photocatalyst, in order to achieve the purpose of overall splitting of water on a single-phase material under visible light irradiation.

For instance, SrTiO<sub>3</sub> (3.2 eV) and AgNbO<sub>3</sub> (2.7 eV) have been respectively reported as H<sub>2</sub> and O<sub>2</sub> evolution photocatalysts, due to their different band gap energies and band edge potentials. Ye *et al.* developed a series of solid-solution samples (AgNbO<sub>3</sub>)<sub>1-x</sub>(SrTiO<sub>3</sub>)<sub>x</sub> (0 < x < 1), which have shown modulated band structures and enhanced visible light photocatalytic activity.<sup>248,249</sup> The rietveld refinement revealed that the perovskite-type solid solutions (AgNbO<sub>3</sub>)<sub>1-x</sub>(SrTiO<sub>3</sub>)<sub>x</sub> were crystallized in an orthorhombic phase (0 < x < 0.9) or a cubic phase (0.9 < x < 1). The (Ag<sub>0.75</sub>Sr<sub>0.25</sub>)(Nb<sub>0.75</sub>Ti<sub>0.25</sub>)O<sub>3</sub> exhibited the best visible light activities for O<sub>2</sub> evolution and decomposition of gaseous 2-propanol.

Another example is BaZrO<sub>3</sub>-BaTaO<sub>2</sub>N solid solution photocatalysts developed by Maeda and Domen *et al.*<sup>250-253</sup> The BaTaO<sub>2</sub>N with a band gap of 1.8-1.9 eV has been shown as a H<sub>2</sub> evolution photocatalyst over 600 nm irradiation. However, the apparent quantum yield is very low (< 0.1% at 420-440 nm) in a two-step water splitting process, when combined with Pt-loaded WO<sub>3</sub> as an O<sub>2</sub> evolution photocatalyst. By composing a solid solution with BaZrO<sub>3</sub> (4.8 eV), the BaZrO<sub>3</sub>-BaTaO<sub>2</sub>N solid solution (Zr/Ta = 0.05) exhibited much higher activity for H<sub>2</sub> evolution in aqueous NaI solution under visible light (> 420 nm) than BaTaO<sub>2</sub>N.<sup>250,251</sup> When Pt-WO<sub>3</sub> was employed as O<sub>2</sub> evolution catalyst in NaI solution,

stoichiometric water splitting into  $H_2$  and  $O_2$  was achieved under visible light. The apparent quantum yield was calculated about 0.6 % at 420–440 nm, which was at least six times higher than that obtained with the optimized Pt/BaTaO<sub>2</sub>N. Furthermore, the BaZrO<sub>3</sub>–BaTaO<sub>2</sub>N solid solution has been demonstrated to be active for both photocatalytic water reduction and oxidation under visible light irradiation.<sup>252,253</sup> The overall water splitting on the BaZrO<sub>3</sub>–BaTaO<sub>2</sub>N based material was also tested in a photoelectrochemical cell system. This is the first single photoanode material with a band gap smaller than 2.0 eV for overall water splitting. It should be mentioned that IrO<sub>2</sub>-loading is indispensable to achieve stable water oxidation over BaTaO<sub>2</sub>N-based photocatalysts owing to the self-oxidation. When colloidal IrO<sub>2</sub> was deposited on the solid solution anode, the anodic photocurrent was significantly improved. In addition, the onset potential was shifted to *ca.* -0.3 V vs. RHE, indicating that colloidal IrO<sub>2</sub> loaded onto BaTaO<sub>2</sub>N promoted water oxidation, which was consistent with the results of photocatalytic reactions. Recently, Pan and Domen *et al.* tried to solve the self-oxidation problem by double-coating a mixture of silica and titania layer (SiO<sub>x</sub>H/TiO<sub>x</sub>H) on a complex perovskite-type oxynitride, LaMg<sub>x</sub>Ta<sub>1-x</sub>O<sub>1+3x</sub>N<sub>2-3x</sub> ( $x \geq 1/3$ ), namely the solid solution of oxynitride LaTaON<sub>2</sub> and the complex oxide LaMg<sub>2/3</sub>Ta<sub>1/3</sub>O<sub>3</sub>.<sup>254</sup> The amorphous coating layer successfully prevented N<sub>2</sub> evolution due to the accumulated hole oxidation of nitrogen species. By employing RhCrO<sub>y</sub> as H<sub>2</sub> evolution co-catalyst as shown in Fig. 8, the TiO<sub>x</sub>H/SiO<sub>x</sub>H-deposited LaMg<sub>1/3</sub>Ta<sub>2/3</sub>O<sub>2</sub>N exhibited stable overall water splitting performance at wavelengths of up to 600 nm. However, the quantum efficiency of overall water splitting is still low (*ca.* 0.03% at 440±30 nm).

Other solid solution samples including CaZrO<sub>3</sub>–CaTaO<sub>2</sub>N,<sup>255</sup> SrTiO<sub>3</sub>–LaTiO<sub>2</sub>N,<sup>256</sup> La<sub>0.8</sub>Ba<sub>0.2</sub>Fe<sub>0.9</sub>Mn<sub>0.1</sub>O<sub>3-x</sub>,<sup>257</sup> Na<sub>1-x</sub>La<sub>x</sub>Fe<sub>1-x</sub>Ta<sub>x</sub>O<sub>3</sub>,<sup>258</sup> Na<sub>0.5</sub>La<sub>0.5</sub>TiO<sub>3</sub>–LaCrO<sub>3</sub>,<sup>259</sup> Cu–(Sr<sub>1-y</sub>Na<sub>y</sub>)(Ti<sub>1-x</sub>Mo<sub>x</sub>)O<sub>3</sub>,<sup>260</sup> Na<sub>1-x</sub>La<sub>x</sub>Ta<sub>1-x</sub>Cr<sub>x</sub>O<sub>3</sub>,<sup>261</sup> BiFeO<sub>3</sub>–(Na<sub>0.5</sub>Bi<sub>0.5</sub>)TiO<sub>3</sub>,<sup>262</sup> Sr<sub>1-x</sub>Bi<sub>x</sub>Ti<sub>1-x</sub>Cr<sub>x</sub>O<sub>3</sub><sup>263</sup> have been reported as visible light photocatalysts for water splitting in a sacrificial system and degradation of organics.

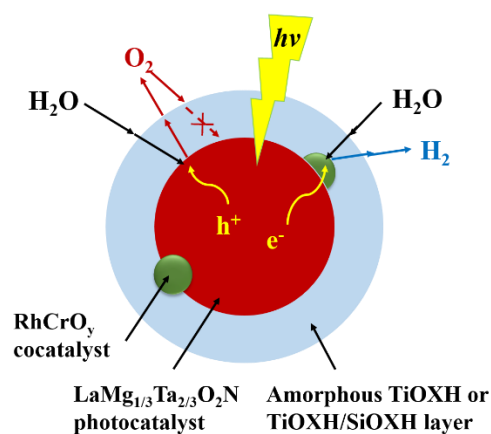


**Fig. 8** Reaction mechanism for water splitting on a surface coated LaMg<sub>x</sub>Ta<sub>1-x</sub>O<sub>1+3x</sub>N<sub>2-3x</sub> photocatalyst. Reprinted with permission from ref. 254. Copyright © 2015, Wiley-VCH Verlag GmbH & Co. KGaA, Weinheim.

In brief, with good hopes of increasing the visible light harvesting, charge separation and transfer, and surface photocatalytic

efficiency, research on the ABO<sub>3</sub> type and modified ABO<sub>3</sub> type perovskite photocatalysts has been heavily focused on nanostructuring, morphology control, band-gap engineering by doping of metal and non-metal dopants and forming solid solution. Among these ABO<sub>3</sub>-related photocatalysts, La and Rh co-doped SrTiO<sub>3</sub> has been demonstrated to be the so far best candidate for hydrogen evolution under visible light irradiation as demonstrated by Domen *et al.*<sup>112</sup> On the other hand, ABO<sub>2</sub>N and its solid solution compounds have been recorded with “benchmark” performance as extending the threshold of excitation wavelength near to 700 nm for water splitting.<sup>247</sup> However, the solar energy conversion efficiency and the stability of these nitridized perovskites need to be further improved. Although great progress on the ABO<sub>3</sub> perovskites photocatalysts has been achieved during the recent decades, considerable research is needed to develop new perovskite-based photocatalysts or design more efficient composites based on the reported materials.

#### 4. Layered perovskite materials for photocatalysis

In addition to the “ideal” ABO<sub>3</sub> and the modified ABO<sub>3</sub> materials discussed above, a number of layered perovskite photocatalysts are also reported. According to their structural characteristics, the reported layered perovskite photocatalysts are classified and discussed along with the summarization as shown in Table 4.

##### 4.1 Ruddlesden Popper (RP) phase

In the general formula of RP phase, A<sub>n-1</sub>A′<sub>2</sub>B<sub>n</sub>X<sub>3n+1</sub>, A and A′ represent alkali, alkaline earth, or rare earth metals while B refers to transition metals. The A cations are located in the perovskite layer and have a 12-fold cuboctahedral coordination to the anions. The A′ cations have a coordination number of nine and are located at the perovskites boundary with an intermediate block layer. The B cations are located inside the anionic octahedral, pyramids and squares. A series of RP-type layered tantalates, A′<sub>2</sub>ATa<sub>2</sub>O<sub>7</sub> (A′ = H, Li, K and Rb; A = La<sub>2/3</sub>, Ca and Sr) as well as their hydrated products were presented as UV-light photocatalysts for water splitting.<sup>264-268</sup> The band gaps of these RP-type compounds are about 3.9–4.1 eV. The first example of RP-type layered tantalates with hydrated interlayer, A<sub>2</sub>SrTa<sub>2</sub>O<sub>7</sub>·nH<sub>2</sub>O (A = H, Li, K and Rb), was prepared by conventional solid state reaction and cation exchange methods.<sup>264</sup> Overall water splitting was achieved on H<sub>2</sub>SrTa<sub>2</sub>O<sub>7</sub>·nH<sub>2</sub>O and K<sub>2</sub>SrTa<sub>2</sub>O<sub>7</sub>·nH<sub>2</sub>O. The hydrated catalysts showed higher H<sub>2</sub> and O<sub>2</sub> evolution rates than anhydrous Li<sub>2</sub>SrTa<sub>2</sub>O<sub>7</sub> and KTaO<sub>3</sub>. From the study of photoluminescence, they concluded that the recombination of photogenerated electrons and holes in hydrated tantalates was less. Thus, the photogenerated charges can be more effectively reacted with water to generate H<sub>2</sub> and O<sub>2</sub>. In addition, they further substituted Sr in A<sub>2</sub>SrTa<sub>2</sub>O<sub>7</sub> with La, and the hydrated A<sub>2</sub>La<sub>2/3</sub>TaO<sub>7</sub> exhibited higher activity than anhydrous perovskites (KTaO<sub>3</sub> and La<sub>1/3</sub>TaO<sub>3</sub>).<sup>265</sup> Incorporation of Ni(II) species into the interlayer space, as the effective sites for H<sub>2</sub> evolution, was found to enhance the

photocatalytic water splitting activity. Other tantalates such as  $K_2Sr_{1.5}Ta_3O_{10}$ ,<sup>266</sup> N-alkyl chains grafted  $H_2CaTa_2O_7$ ,<sup>267</sup>  $Li_2CaTa_2O_7$ ,<sup>268</sup>  $H_{1.81}Sr_{0.81}Bi_{0.19}Ta_2O_7$ ,<sup>269</sup> were studied as UV-light photocatalysts for degradation of dyes.

$A_2La_2Ti_3O_{10}$  (A = K, Rb and Cs) and doped  $A_2La_2Ti_3O_{10}$  comprise another family of RP-type layered titanates. Domen *et al.* firstly reported the ion-exchangeable layered perovskites with a general formula of  $A_{2-x}La_2Ti_{3-x}Nb_xO_{10}$  (A = K, Rb, Cs; x = 0, 0.5, 1) for water splitting.<sup>270</sup> As shown in Fig. 9, the  $Rb_2La_2Ti_3O_{10}$  showed the highest activity (869 and 430  $\mu\text{mol/g/h}$  for  $H_2$  and  $O_2$ , respectively) with 4% Ni loading under UV-light irradiation among all of these compositions. A partial substitution of  $Ti^{4+}$  by  $Nb^{5+}$  reduced the number of alkaline metals cations located to keep charge balance at the interlayer space. As a result, the hydration of the interlayer in  $Nb^{5+}$  substituted layered perovskites was inhibited, which reduced the photocatalytic activity consequently. Furthermore,  $K_2La_2Ti_3O_{10}$  sample was also prepared by polymerized complex and hydrothermal methods.<sup>271,272</sup> The polymerized complex synthesis helps to reduce the calcination time and enhance the purity of sample. The optimized Ni/ $KaLa_2Ti_3O_{10}$  prepared by this method was more photoactive than conventional Ni/ $K_2La_2Ti_3O_{10}$  for water splitting, even though they have similar surface areas and band gaps. Later on, a series of Sn, Cr, Zn, V, Fe, Ni, W and N-doped  $K_2La_2Ti_3O_{10}$  samples were prepared to reduce the band gap of  $K_2La_2Ti_3O_{10}$  for performing photocatalysis tests under UV and visible light irradiation.<sup>273-278</sup> However, only Sn-doping effectively reduced the band gap of  $K_2La_2Ti_3O_{10}$  from ca. 3.6 eV to 2.7 eV. The band gap of N-doped  $K_2La_2Ti_3O_{10}$  was estimated about 3.4 eV. Other RP-type titanates such as  $Sr_3Ti_2O_7$ ,<sup>279</sup>  $Sr_4Ti_3O_{10}$ ,<sup>280</sup>  $Sr_2SnO_4$ ,<sup>281</sup> Cr-doped  $Sr_2TiO_4$ ,<sup>282</sup> Rh and Ln-doped  $Ca_3Ti_2O_7$ <sup>283</sup> and  $Na_2Ca_2Nb_4O_{13}$ <sup>284</sup> have also been investigated.

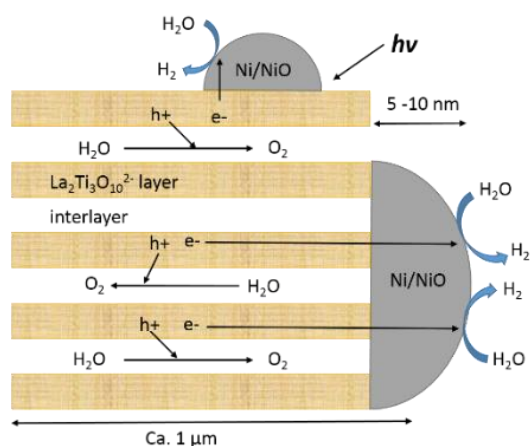


**Fig. 9** Proposed reaction mechanism of water splitting on layered  $A_2La_2Ti_3O_{10}$  catalyst. Reprinted with permission from ref. 270. Copyright © 1997, American Chemical Society.

#### 4.2 Aurivillius phase (AL)

Aurivillius phase is a form of perovskite represented by the general formula of  $(Bi_2O_2)^{2+}(A_{n-1}B_nO_{3n+1})^{2-}$ , where A represents the 12-fold

coordinated cation with low valence in the perovskite sub-lattice, B denotes the octahedral site occupied by ions with high valence, and n is the number of perovskite layers between the  $[Bi_2O_2]^{2+}$  layers.  $Bi_2MO_6$  (M = W and Mo), composed of perovskite-like  $[MO_4]^{2-}$  layers sandwiched between bismuth oxide  $[Bi_2O_2]^{2+}$  layers, are the simplest members of the Aurivillius family and the most studied samples in this family. They were firstly reported by Kudo and co-workers for photocatalytic water splitting under visible light irradiation.<sup>285-288</sup> The  $Bi_2WO_6$  (2.8 eV) exhibits higher  $O_2$  evolution efficiency than the  $Bi_2MoO_6$  (3.0 eV) from aqueous  $AgNO_3$  solution under visible light irradiation. Due to the suitable band gap energy, relatively high photocatalytic activity and good stability, the  $Bi_2MO_6$  compounds have been intensively studied as the AL-type visible light photocatalysts. More than one hundred papers related to the  $Bi_2WO_6$  and  $Bi_2MoO_6$  photocatalysts have been reported so far. Most of the studies in the literature are focused on the preparation of various nanostructured  $Bi_2WO_6$  and  $Bi_2MoO_6$  including nanosheets, nanofibers, hierarchical architectures, ordered arrays, nanoplates, inverse opals, hollow spheres and films etc., by different preparation methods such as hydrothermal, solvothermal, molten salt, electrospinning, microwave and thermal evaporation deposition methods. The hydrothermal synthetic route has been mostly employed to control the morphologies and shapes of the particles. The photocatalytic activities of these nanostructured materials are mainly evaluated by degradation of organic pollutants and selective organic transformations. In addition to the studies on the bare  $Bi_2WO_6$  and  $Bi_2MoO_6$ , doping of Zn, Mo, F, Er, N, Zr, Gd and W etc. into  $Bi_2WO_6$  and  $Bi_2MoO_6$  was investigated for improving the photocatalytic behaviour under visible light. The summarization of these  $Bi_2MO_6$  photocatalysts is not given here, since more detailed discussions can be found in several specific reviews.<sup>289-292</sup>

$ABi_2Nb_2O_9$  (A = Ca, Sr, Ba and Pb) is another member of the AL-type layered perovskite with n = 2. <sup>293-299</sup>  $PbBi_2Nb_2O_9$  with a band gap of 2.88 eV was firstly reported as an undoped, single-phase oxide photocatalyst working under visible light.<sup>293</sup> Under visible light irradiation, Pt/ $PbBi_2Nb_2O_9$  gave a QE of 0.95% for  $H_2$  evolution from aqueous methanol solution, and a QE of 29% for  $O_2$  evolution from  $AgNO_3$  solution. However, the other niobates like  $ABi_2Nb_2O_9$  (A = Ca, Sr, Ba) have the larger band gaps about 3.3-3.5 eV.<sup>296-299</sup> Under UV-light irradiation, Ag/ $ALa_4Ti_4O_{15}$  (A = Ca, Sr and Ba) photocatalysts with ca. 3.8 eV of band gaps can reduce  $CO_2$  to CO and HCOOH by bubbling  $CO_2$  gas into the aqueous suspension of the photocatalyst powder without any sacrificial reagents.<sup>300</sup> Among these perovskites, Ag/ $BaLa_4Ti_4O_{15}$  is the most active photocatalyst. Under specific loading of Ag co-catalyst on the edge of  $BaLa_4Ti_4O_{15}$ , the main reduction product from Ag/ $BaLa_4Ti_4O_{15}$  suspension was CO rather than  $H_2$ . As shown in Fig. 10, it was proposed that the edge and the basal plane of  $BaLa_4Ti_4O_{15}$  were the reduction and water oxidation sites, respectively. Loading fine Ag particles (10-20 nm) onto  $BaLa_4Ti_4O_{15}$  by impregnation and  $H_2$  reduction or liquid phase reduction method,  $CO_2$  reduction to CO and HCOOH predominated over water reduction to form  $H_2$ . The stoichiometric ratio of reduction and oxidation products ( $H_2 + CO : O_2 = 2:1$ ) suggested that water was consumed as an electron donor for the  $CO_2$  production.

In addition to the unique magnetoelectric property, nanostructured four-layered  $\text{Bi}_5\text{FeTi}_3\text{O}_{15}$  perovskite with a band gap of *ca.* 2.1 eV also exhibits visible light photocatalytic activities.<sup>301,302</sup> The hydrothermal synthesis can produce nanoplates-based, flower-like hierarchical morphology, and the detailed growth process, from nanonets to nanoplates-built microflowers was revealed. The photocatalytic activity of the as-prepared  $\text{Bi}_5\text{FeTi}_3\text{O}_{15}$  was evaluated by photodegradation of acetaldehyde and rhodamine B under visible light irradiation.<sup>301</sup> By degradation of rhodamine B under solar-light irradiation, the photocatalytic performance of La substituted  $\text{Bi}_{5-x}\text{La}_x\text{Ti}_3\text{FeO}_{15}$  ( $x = 1, 2$ ) with band gaps of 2.0-2.7 eV was also evaluated.<sup>303</sup> Other AL-type compounds such as  $\text{K}_{0.5}\text{La}_{0.5}\text{Bi}_2\text{M}_2\text{O}_9$  ( $M = \text{Ta}, \text{Nb}$ ),<sup>304</sup>  $\text{Bi}_4\text{Ti}_3\text{O}_{12}$ ,<sup>285</sup>  $\text{BaBi}_4\text{Ti}_4\text{O}_{15}$ ,<sup>285</sup>  $\text{Bi}_3\text{TiNbO}_9$ ,<sup>285</sup> Cr-doped  $\text{Bi}_4\text{Ti}_3\text{O}_{12}$ ,<sup>305</sup>  $\text{Bi}_2\text{ASrTi}_2\text{TaO}_{12}$  ( $A = \text{Bi}, \text{La}$ ),<sup>306</sup> have been studied as UV light photocatalysts for water splitting.

Among AL-type perovskites, only  $\text{Bi}_2\text{MO}_6$  ( $M = \text{W}$  or  $\text{Mo}$ ),  $\text{PbBi}_2\text{Nb}_2\text{O}_9$  and  $\text{Bi}_5\text{Ti}_3\text{FeO}_{15}$  are active under visible light. Considering the band edge positions, these perovskites are more useful for water oxidation and pollutants degradation owing to the deep valence band positions, whereas their activities for  $\text{H}_2$  production are much lower even loading with Pt co-catalyst.  $\text{PbBi}_2\text{Nb}_2\text{O}_9$  is a unique AL-type perovskite that shows a QE of 29% for  $\text{O}_2$  evolution in 0.05 M  $\text{AgNO}_3$  solution,<sup>293</sup> yet the presence of toxic lead in the compounds is still a concern from the environmental view of point.

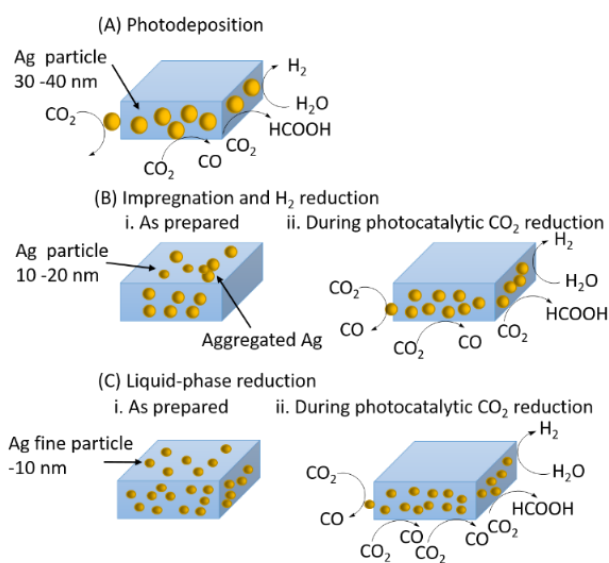


**Fig. 10** Mechanism of photocatalytic  $\text{CO}_2$  reduction over  $\text{BaLa}_4\text{Ti}_4\text{O}_{15}$  with Ag co-catalyst loaded by several methods. Reprinted with permission from ref. 300. Copyright © 2011, American Chemical Society.

### 4.3 Dion-Jacobsen (DJ) phase

A series of layered lanthanide tantalates and their ion-exchanged compounds with general formula of  $\text{A}(\text{Ln}_{n-1}\text{Ta}_n\text{O}_{3n+1})$  ( $A = \text{K}, \text{Rb}, \text{Cs}, \text{Ag}$  and  $\text{H}$ ;  $\text{Ln} = \text{La}, \text{Pr}, \text{Nd}, \text{Sm}$ ;  $n = 2$  and  $3$ , respectively) were studied as DJ-type photocatalysts.<sup>307-309</sup> The band gaps of these tantalates

are 3.8-4.3 eV. Upon UV-light irradiation,  $\text{RbNdTa}_2\text{O}_7$  was firstly demonstrated by Machida *et al.* for efficient evolution of stoichiometric  $\text{H}_2/\text{O}_2$  even without loading metal catalysts.<sup>307</sup> Later on, they further investigated the  $\text{H}_2$  and  $\text{O}_2$  evolution from  $\text{MLnTa}_2\text{O}_7$  tantalates ( $M = \text{H}, \text{Na}, \text{Rb}$  and  $\text{Cs}$ ;  $\text{Ln} = \text{La}, \text{Pr}, \text{Nd}$  and  $\text{Sm}$ ). In the case of  $M = \text{Rb}$ , the activity follows in the order of  $\text{Ln}: \text{Nd} > \text{Sm} > \text{La} > \text{Pr}$ .<sup>308</sup> The effect of  $\text{Ln}$  was explained from the aspects of energy level of the  $\text{Ln } 4f$  bands and degree of  $\text{Ln-O-Ta}$  hybridization in band structure dominated by  $\text{Ta } 5d$  and  $\text{O } 2p$  orbitals. Furthermore, they evaluated the effect of ion exchange of interlayer cations ( $M = \text{H}, \text{Na}$  and  $\text{Rb}$ ) on the photocatalytic activities of  $\text{MLnTa}_2\text{O}_7$ .<sup>309</sup> The photocatalytic activity of hydrated  $\text{HLnTa}_2\text{O}_7$  was very low regardless of the unchanged band gap energy. The hydrated interlayer would lead to a considerable modification of valence band structure and formation of structural defects as evident from the XRD study, which was suggested as the possible reason for the reduced activity. Unlike the hydrated forms of layered perovskites such as  $\text{K}_4\text{Nb}_6\text{O}_{17}$  and  $\text{K}_2\text{La}_2\text{Ti}_3\text{O}_{10}$ , which are highly active for overall water splitting, the hydration of  $\text{MLnTa}_2\text{O}_7$  may not allow successive photooxidation reactions inside the interlayer. To further elucidate the effect of interlayer hydration, another group of DJ-type tantalates ( $\text{MCa}_2\text{Ta}_3\text{O}_{10}$ ,  $M = \text{Cs}, \text{Na}, \text{H}$  and  $\text{C}_6\text{H}_{13}\text{NH}_3$ ) with triple-layer structure was synthesized.<sup>310,311</sup> In the presence of 0.5 wt%  $\text{NiO}_x$ , the hydrated Na-exchanged phase exhibited an order of magnitude higher activity compared to the anhydrous Cs phase and the hydrous H phase for overall water splitting. While the organic  $\text{C}_6\text{H}_{13}\text{NH}_3$ -intercalated phase was not stable in the photooxidation reactions. The hydrated interlayer was found as the active sites for water splitting by  $\text{H}_2\text{O}/\text{D}_2\text{O}$  isotopic experiment. Thus, the effect of hydration, associated with the mobility of water molecule inside the interlayer space, is different among the DJ-type layered perovskites. On the other hand, N-doped  $\text{CsCa}_2\text{Ta}_3\text{O}_{10}$  with a band gap of 2.0 eV was reported as the first example on the utilization of N-doped ion-exchangeable layered perovskite photocatalysts for water oxidation under visible light.<sup>312</sup>

In the case of layered niobates with DJ phase,  $\text{APb}_2\text{Nb}_3\text{O}_{10}$  ( $A = \text{K}, \text{Rb}, \text{Cs}$  and  $\text{H}$ ) was initially studied for  $\text{H}_2$  evolution from an aqueous alcohol solution.<sup>313</sup> The band gaps of most of the layered niobates are wide, however,  $\text{RbPb}_2\text{Nb}_3\text{O}_{10}$  sheets have an absorption band in visible light region up to *ca.* 500 nm with a broad band tail absorption, which may be due to the existence of defects in niobate sheets. The  $\text{RbPb}_2\text{Nb}_3\text{O}_{10}$  was not efficient for  $\text{H}_2$  evolution under visible light, even loading with Pt co-catalyst. However, when  $\text{Rb}^+$  ions were exchanged by  $\text{H}^+$  ion, the hydrated  $\text{HPb}_2\text{Nb}_3\text{O}_{10}$  exhibits remarkable enhancement of  $\text{H}_2$  evolution activity. This enhancement was suggested due to the fast migration of reactants ( $\text{H}_2\text{O}$  and  $\text{CH}_3\text{OH}$ ) into the interlayer space of  $\text{HPb}_2\text{Nb}_3\text{O}_{10}$ . Another series of layered  $\text{AB}_2\text{Nb}_3\text{O}_{10}$  ( $A = \text{H}, \text{Li}, \text{Na}$  and  $\text{K}$ ;  $B = \text{Ca}$  and  $\text{Sr}$ ) based materials have relative larger band gaps.<sup>314-322</sup> The colloidal  $\text{KCa}_2\text{Nb}_3\text{O}_{10}$  nanosheets suspension was immediately flocculated when added to an aqueous alkali hydroxide solution. The delaminated nanosheets were restacked together with accommodating alkali metal ions and water molecules between the nanosheets. Such exfoliation/restacking process generated porous aggregates with

high surface area and enhanced photocatalytic activity for hydrogen evolution from an aqueous methanol solution under UV-light irradiation.<sup>315</sup> Furthermore, by incorporation of RuO<sub>x</sub> into the exfoliated/restacked material as active sites for water oxidation, overall water splitting with stoichiometric ratio was achieved upon UV-light illumination.<sup>316</sup> Mallouk's group found that the photocatalytic activity of restacked triple-layered nanosheets (HSr<sub>2</sub>Nb<sub>3</sub>O<sub>10</sub>) was an order of magnitude higher than that of the double-layered HLaNb<sub>2</sub>O<sub>7</sub> nanosheets, even though that there was little difference in the physicochemical characteristics.<sup>320</sup> In addition, they constructed visible light H<sub>2</sub> production system from HCa<sub>2</sub>Nb<sub>3</sub>O<sub>10</sub> nanosheets utilizing Ru-bipyridine dye as sensitizer.<sup>321,322</sup> Recently, Pt nanoclusters with a diameter smaller than 1 nm were deposited on interlayer nanospace of KCa<sub>2</sub>Nb<sub>3</sub>O<sub>10</sub>. The Pt incorporated material exhibited eight-fold greater photocatalytic activity for water splitting than the previous RuO<sub>2</sub> loaded sample.<sup>317</sup>

The interlayer cation effect was also studied by silver-exchange of A-site cations in RbLaNb<sub>2</sub>O<sub>7</sub> and RbA<sub>2</sub>Nb<sub>3</sub>O<sub>10</sub> (A: Ca and Sr).<sup>323,324</sup> Substitution of silver cation into the interlayer spacing of these layered compounds is able to reduce the band gap by about 0.5-1.0 eV. The Ag-exchanged products exhibited significantly improved activity by an order of magnitude than those prior to Ag-exchange for H<sub>2</sub> production under UV-light irradiation. The Ag-exchanged RbCa<sub>2</sub>Nb<sub>3</sub>O<sub>10</sub> with loading 1.0 wt% Pt co-catalyst exhibited the highest photocatalytic H<sub>2</sub> production rate (ca. 13616 μmol/g/h) from 20% methanol solution under UV-light irradiation, but it was not active under visible light irradiation. The Ag<sup>+</sup> at the particle surfaces was reduced to Ag particle during prolonged UV-light irradiation, which was one of the reasons for enhanced activities. In addition, hydrated HLaNb<sub>2</sub>O<sub>7</sub> and H<sub>1-x</sub>LaNb<sub>2-x</sub>Mo<sub>x</sub>O<sub>7</sub> were also studied for H<sub>2</sub> production from methanol solution under UV-light irradiation.<sup>325,326</sup>

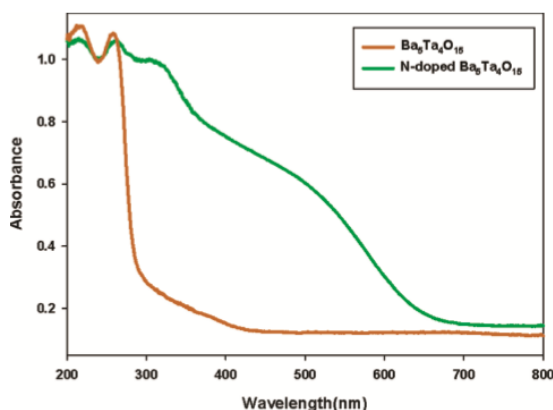


**Fig. 11** UV-Visible absorbance spectra of Ba<sub>5</sub>Ta<sub>4</sub>O<sub>15</sub> and N-doped Ba<sub>5</sub>Ta<sub>4</sub>O<sub>15</sub>. Reprinted with permission from ref. 331. Copyright © 2011, American Chemical Society.

#### 4.4 {111} layered perovskites

Layered perovskite A<sub>5</sub>B<sub>4</sub>O<sub>15</sub> (A = Ba and Sr, B = Nb and Ta) with a plane in parallel with {111} was investigated as a series of UV-light photocatalysts. Ba<sub>5</sub>Nb<sub>4</sub>O<sub>15</sub> photocatalyst was firstly prepared by conventional solid-state reaction and polymer-complex methods for

water splitting under UV-light irradiation.<sup>327</sup> By loading a suitable amount of NiO co-catalyst, the Ba<sub>5</sub>Nb<sub>4</sub>O<sub>15</sub> exhibited remarkably enhanced H<sub>2</sub> and O<sub>2</sub> evolution rates of 4.8 and 2.4 mmol/h/g, respectively. At a similar time, Zhu *et al.* synthesized monomolecular-layered Ba<sub>5</sub>Ta<sub>4</sub>O<sub>15</sub> nanosheets with hexagonal structure by a hydrothermal method.<sup>328</sup> The thickness of the nanosheets is ca. 1.1 nm, which corresponds to a monolayer of Ba<sub>5</sub>Ta<sub>4</sub>O<sub>15</sub>. The monolayered structure of Ba<sub>5</sub>Ta<sub>4</sub>O<sub>15</sub> facilitates the migration of electron-hole pairs to the sample surface, as demonstrated by degradation of rhodamine B and gaseous formaldehyde. H<sub>2</sub> evolution on the Rh-loaded Ba<sub>5</sub>Ta<sub>4</sub>O<sub>15</sub> from an aqueous methanol solution was also reported with a rate of 1600 μmol/g/h under UV-light irradiation.<sup>329</sup> After that, the photophysical and photocatalytic properties of Sr<sub>5</sub>Nb<sub>4</sub>O<sub>15</sub> and Ba<sub>5</sub>Nb<sub>4</sub>O<sub>15</sub> were compared with La<sub>4</sub>Ti<sub>3</sub>O<sub>12</sub> and AlLa<sub>4</sub>Ti<sub>4</sub>O<sub>15</sub> (A = Ca, Sr and Ba) layered perovskites.<sup>330</sup> Their band gaps are ca. 3.7-4.1 eV. The NiO<sub>x</sub> loaded BaLa<sub>4</sub>Ti<sub>4</sub>O<sub>15</sub> and NiO<sub>x</sub>/Ba<sub>5</sub>Nb<sub>4</sub>O<sub>15</sub> are the most active photocatalysts for water splitting among the tested titanates and niobates.

Recently, N-doped layered Ba<sub>5</sub>Ta<sub>4</sub>O<sub>15</sub> and Sr<sub>5</sub>Ta<sub>4</sub>O<sub>15</sub> were studied for water splitting under visible light irradiation.<sup>331,332</sup> N-doping markedly reduced the band gaps from ca. 4.0 eV to 1.78 eV for the doped Ba<sub>5</sub>Ta<sub>4</sub>O<sub>15</sub> and 2.2 eV for the doped Sr<sub>5</sub>Ta<sub>4</sub>O<sub>15</sub>, respectively. The strong absorption of visible light for the N-doped Ba<sub>5</sub>Ta<sub>4</sub>O<sub>15</sub> was also demonstrated by the red-shift of band absorption in UV-Vis absorption spectrum as shown in Fig. 11.<sup>331</sup> For the doped Sr<sub>5</sub>Ta<sub>4</sub>O<sub>15</sub>, both conduction and valence band edges of Sr<sub>5</sub>Ta<sub>4</sub>O<sub>15-x</sub>N<sub>x</sub> estimated from Mott-Schottky measurement possess sufficient potentials for the respective water reduction and oxidation. This is the first example of nitrogen-doped tantalum-based layered oxide that is able to achieve both the two half reactions of water splitting under visible light illumination.

#### 4.5 {110} layered perovskites

{110} layered perovskite materials have a general composition of A<sub>n</sub>B<sub>n</sub>O<sub>3n+2</sub> (A = Sr, La; B = Ta, Nb, Ti; n = 4, 5). For example, Sr<sub>2</sub>M<sub>2</sub>O<sub>7</sub> (B = Ta and Nb) with the perovskite slabs parallel to {110} face were studied as UV-light photocatalysts.<sup>333-337</sup> Lee's group firstly reported Sr<sub>2</sub>Nb<sub>2</sub>O<sub>7</sub> and La<sub>2</sub>Ti<sub>2</sub>O<sub>7</sub>, La<sub>4</sub>CaTi<sub>5</sub>O<sub>17</sub> photocatalysts for overall water splitting with a maximum quantum yields at 23% for Sr<sub>2</sub>Nb<sub>2</sub>O<sub>7</sub> in the presence of Ni co-catalyst under UV-light irradiation.<sup>333</sup> The band gaps of these materials are estimated in the range of 3.2-4.3 eV. Among these tested materials, La<sub>4</sub>CaTi<sub>5</sub>O<sub>17</sub> exhibited the highest H<sub>2</sub> evolution rate of 499 μmol/h/g with 1.0 wt% Ni deposition. Kudo's group examined Sr<sub>2</sub>Ta<sub>2</sub>O<sub>7</sub> and Sr<sub>2</sub>Nb<sub>2</sub>O<sub>7</sub> photocatalysts for water splitting and investigated the factors influencing the photocatalytic activity between the tantalates and niobates.<sup>337</sup> The Sr<sub>2</sub>Ta<sub>2</sub>O<sub>7</sub> has a wider band gap (4.6 eV) and much higher conduction band level than that of Sr<sub>2</sub>Nb<sub>2</sub>O<sub>7</sub> (3.9 eV). In the presence of NiO co-catalyst, conduction band electrons from Sr<sub>2</sub>Ta<sub>2</sub>O<sub>7</sub> can easily transfer to the NiO co-catalyst due to the higher conduction band level. Whereas this electron transfer process seems to be hard for Sr<sub>2</sub>Nb<sub>2</sub>O<sub>7</sub>, leading to the significant lower activity for NiO/Sr<sub>2</sub>Nb<sub>2</sub>O<sub>7</sub>. On the other hand, from the concerning of delocalization of electron-hole pairs, the

bond angle of O-Ta-O in  $\text{Sr}_2\text{Ta}_2\text{O}_7$  is close to  $180^\circ$  in contrast to the twisted  $\text{Sr}_2\text{Nb}_2\text{O}_7$ , which promotes the movement of photogenerated electron-hole pairs in  $\text{Sr}_2\text{Ta}_2\text{O}_7$ . The solid solutions of  $\text{Sr}_2\text{Ta}_{2-x}\text{Nb}_x\text{O}_7$  ( $x = 0 - 2$ ) were also prepared by different methods and evaluated for their photocatalytic activities.<sup>335,336</sup> N-doped  $\text{Sr}_2\text{Ta}_2\text{O}_7$  coupled with graphene sheets has been shown to give increased photocatalytic hydrogen production under visible light.<sup>338</sup> By specifically loading Pt co-catalyst onto graphene support as a solid-state electron mediator, a ca. 80% increase in hydrogen production and a quantum efficiency of 6.45% were achieved.

$\text{La}_2\text{Ti}_2\text{O}_7$  family is another group of {110} layered perovskites, that has wide band gaps of ca. 3.8 eV.<sup>333,339-345</sup> The  $\text{La}_2\text{Ti}_2\text{O}_7$  exhibited a QE up to 12% for water splitting with NiO co-catalyst.<sup>333</sup> By doping of different metals such as Ba, Sr, Ca, Cr, Fe and Rh, the band gap of  $\text{La}_2\text{Ti}_2\text{O}_7$  can be reduced and the photocatalytic activities were further improved under UV or visible light irradiation.<sup>346-349</sup> Ba-doping gave the largest enhancement on the rate of  $\text{H}_2$  formation, with a QE = 50% on NiO/Ba- $\text{La}_2\text{Ti}_2\text{O}_7$  in the presence of NaOH suspension, which is slightly lower than the best catalyst, La-doped  $\text{NaTaO}_3$  (56%) in the presence of NaOH.<sup>346</sup> Only Cr, Fe and Rh doping can induce intense absorption of visible light, and produce  $\text{H}_2$  from a methanol solution under visible light irradiation. The origin of visible light activity was found as the electrons transition from the partially filled  $3d$  bands of  $\text{Cr}^{3+}$  and  $\text{Fe}^{3+}$  to the conduction band of  $\text{La}_2\text{Ti}_2\text{O}_7$ .<sup>347,348</sup> Recently, Rh-doped  $\text{La}_2\text{Ti}_2\text{O}_7$  prepared by molten salt synthesis was active under visible light irradiation up to 540 nm.<sup>350</sup> Rh<sup>3+</sup> doping into the Ti sites of  $\text{La}_2\text{Ti}_2\text{O}_7$  generated electron donor levels within the band gap in analogy with Rh-doped  $\text{SrTiO}_3$ . The visible light activity was originated from the electrons transition from these Rh<sup>3+</sup> donor states to the conduction band, and the oxidized Rh<sup>4+</sup> species returned back to their original states via oxidization of  $\text{CH}_3\text{OH}$ .

In a summary, the layered perovskites are usually prepared by solid-state reaction, and the protonated form could be obtained by acid-exchange method, which have been summarized in Table 4. The layered perovskites are easily transformed into nanosheets structure via exfoliation process using tetra (n-butyl) ammonium hydroxide. The exfoliation/restacking process could enhance the surface area of the perovskite materials. The layered perovskites reported so far possess wide band gaps as the common characteristics, which therefore requires the band-gap engineering to improve their performance under visible light irradiation. For example, Wang *et al.* have demonstrated N-doping of the layered perovskites such as  $\text{CsCa}_2\text{Ta}_3\text{O}_{10}$ ,<sup>312</sup>  $\text{Ba}_5\text{Ta}_4\text{O}_{15}$ <sup>331</sup> and  $\text{Sr}_2\text{Ta}_2\text{O}_7$ <sup>338</sup> successfully reduced their band-gaps to ca. 2.0 eV, however the photocatalytic water splitting performance still need to be improved. Exceptionally,  $\text{Bi}_2\text{WO}_6$  and  $\text{Bi}_2\text{MoO}_6$  are the simplest and the most studied visible light photocatalysts in Aurivillius phases.<sup>285-288</sup> Many research papers refer to the preparation of novel nanostructures for the applications of water splitting and pollutants degradation. Another key feature of these layered perovskites, especially for the RP-type and DJ-type niobates, tantalates and titanates, is possessing the ion-exchangeable and hydratable capabilities owing to the presence of structural channels in the crystal interlayers. The hydrated photocatalysts generally show better photocatalytic water splitting

performance. These interlayer spaces could be utilized for loading co-catalyst as to enhance the distribution of co-catalyst onto photocatalyst. By this approach, the water splitting reaction would occur not only on the surface of a photocatalyst, but also possibly in the inner region of a photocatalyst. In addition, compared to the {100} layered perovskites, there are few research examples on the {110} and {111} layered perovskites. Among them, NiO/Ba- $\text{La}_2\text{Ti}_2\text{O}_7$  is one of the most active photocatalysts with a QE = 50%, which is slightly lower than the best La-doped  $\text{NaTaO}_3$  sample under strong UV-light irradiation.<sup>346</sup>

## 5. Theoretical modelling and calculation of perovskite photocatalysts

Compared to binary metal oxides, perovskite and perovskite-related structures with three or more compositions provide a very wide platform to tailor the properties of materials by controlling both the compositions and stoichiometry as demonstrated in the above sections. To rationally design and synthesize perovskite photocatalysts, it is highly necessary to understand the underlying relationships between the composition, structure and performance of materials. Although many modern powerful experimental characterizations can provide some insight into the dependence of the physicochemical properties and performance on the compositions and crystal structure of materials, there is still a large gap between them to be bridged by theoretical modelling and calculations. Increasing efforts in this aspect have mainly focused on theoretical electronic band structures of perovskite materials, which intrinsically control the light absorption, band edges and transport properties of charge carriers and thus reactivity and stability. This consequently deepens the understanding of such dependence at electronic structure level. The progress of theoretical studies can be roughly divided into two parts. These include the electronic band structures of unmodified and modified perovskite materials and representative results are summarized below.

Band structure of a crystalline material with defined compositions and stoichiometry is sensitive to its phase. A most famous case in photocatalysis area is anatase and rutile  $\text{TiO}_2$  showing a band gap difference of around 0.2 eV and remarkably different photocatalytic activity as a result of different crystal structures. Similar phenomenon also exists in perovskite materials.  $\text{NaTaO}_3$ , a very active photocatalyst for overall water splitting under UV irradiation, usually has two different crystal structures of monoclinic  $P2/m$  and orthorhombic  $Pm\bar{c}n$ .<sup>50,351,352</sup> The band structure and density of states calculated on the basis of the density functional theory (DFT) in Fig. 12 show that both phases have their conduction and valence bands with major Ta  $5d$  and O  $2p$  states, respectively, and the monoclinic phase with an indirect bandgap has a slightly larger bandgap than the orthorhombic phase with a direct band gap.<sup>351</sup> A couple of favorable electronic features of the monoclinic phase for photocatalysis include a larger number of effective states available for the photo-induced electrons and holes and a much smaller recombination rate for the photo-induced electron-hole pairs due to the involvement of

phonons in the gap transition.<sup>50</sup> On the other hand, the nearly linear bond angle of Ta–O–Ta for the monoclinic phase favors the delocalization of the excited energy in tantalate crystals. As a consequence of these favorable electronic and crystal structures together with its large surface area, the monoclinic NaTaO<sub>3</sub> crystals prepared by a sol-gel route gave a much higher photocatalytic activity in overall water splitting than the orthorhombic NaTaO<sub>3</sub> crystals prepared by a solid-state reaction. Besides these two phases, the third phase of NaTaO<sub>3</sub> is cubic. Theoretical electronic structures show that, similar to the monoclinic phase, the cubic phase has an indirect band gap.<sup>353</sup> However, its band gap is the smallest among three phases and smaller by about 0.4 eV than that of the orthorhombic phase. Considering the low recombination probability of the photo-induced charge carriers and wide absorption range enabled by a small indirect band gap, the cubic NaTaO<sub>3</sub> could be a competitive candidate for photocatalytic water splitting and deserves more experimental attention.

NaNbO<sub>3</sub> crystal is another typical ternary perovskite photocatalyst and also gives an obvious phase dependent electronic structure and photocatalytic activity. Both the cubic and orthorhombic phases experimentally and theoretically have indirect band gaps and the cubic phase has a smaller band gap.<sup>354</sup> Besides a narrower band gap of cubic NaNbO<sub>3</sub>, two other electronic structure features favouring photocatalysis were theoretically revealed. These are 1) the more dispersive conduction band gives a smaller electron effective mass and thus favors electron migration; 2) the delocalized orbital at the bottom of conduction band enables the isotropic transfer of photogenerated electrons along the x, y and z directions. These advantageous features were proposed to be responsible for the higher photocatalytic hydrogen generation of the cubic phase from the mixture of water and methanol than the orthorhombic phase.

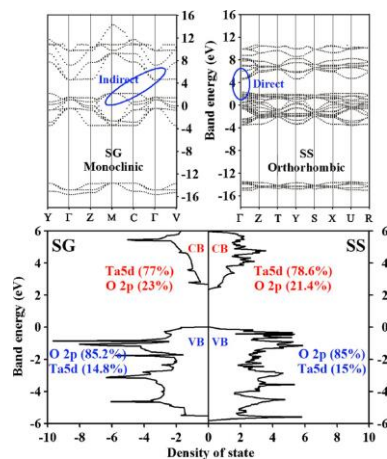


**Fig. 12** Calculated band structure (top) and density of states (bottom) for the sol-gel and solid-state NaTaO<sub>3</sub> from first-principles methods. Reprinted with permission from ref. 351. Copyright © 2006, AIP Publishing LLC.

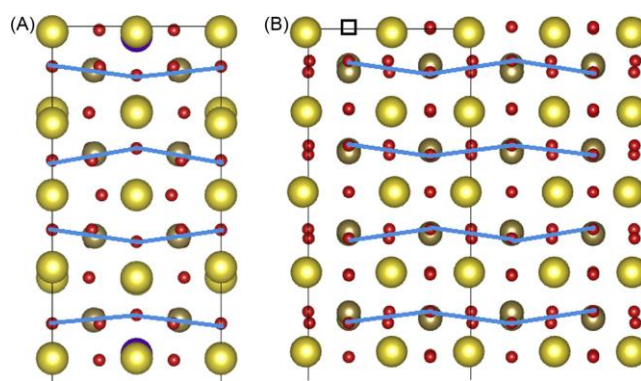


**Fig. 13** Structural distortion of a La-doped surface without O vacancy (A) and non-doped surface with O vacancy (B). Blue lines indicate the zig-zag distorted alignment of O atoms in the defective surfaces. Reprinted with permission from ref. 355.

Surface structure/morphology of a photocatalyst plays an equally important role in controlling photocatalysis efficiency by modulating surface charge transfer processes between reactant molecules/ions and photocatalyst. Taking NaTaO<sub>3</sub> as an example, the stepped-surface structure formed in both La doped and oxygen deficient NaTaO<sub>3</sub> was considered to be a key factor of enhancing photocatalytic activity.<sup>50,59</sup> The edge and groove of the nanosteps was identified to spatially separate reductive and oxidative sites, respectively. To illuminate the origin of forming such important surface steps, Liu *et al.* theoretically investigated the influence of oxygen vacancies and La doping on surface structure of cubic NaTaO<sub>3</sub> (the cubic structure was used in order to save computational expense in this study).<sup>355</sup> It was found that the La doping at Na sites and oxygen vacancies can result in a similar zig-zag distortion of the original regular flat atom layers in the modified surfaces seen in non-defective surfaces (Fig. 13). The shrinkage and expansion of the lattice parameters in the region neighbouring the La dopant and oxygen vacancies, caused by such zig-zag distortion, was proposed to induce the formation of stepped-surface structures observed in the La-doped NaTaO<sub>3</sub> particles and high-T treated non-doped NaTaO<sub>3</sub> particles. These findings provide some implications for constructing desired surface structure at nanoscale of photocatalyst by introducing intrinsic defects or heteroatoms.

Compared to the phase dependent photocatalytic activity illuminated above, the trend of the activity change with the compositions of perovskites is much more complex. Many early theoretical studies<sup>82,179,182,186,299,356-364</sup> attempted to reveal the underlying relationships between the photocatalytic activity and the compositions of (cubic & distorted) ternary ABO<sub>3</sub> perovskites and ordered double A<sub>2</sub>BB'O<sub>6</sub> perovskites in terms of the band gap, mobility of charge carriers and band edges. Eng *et al.* systematically investigated the electronic structure of *d*<sup>0</sup> (Ti<sup>4+</sup>; Nb<sup>5+</sup>; Ta<sup>5+</sup>; Mo<sup>6+</sup>; and W<sup>6+</sup>) transition metal oxides belonging to the perovskite family.<sup>356</sup> It was revealed that the band gaps of *d*<sup>0</sup> transition metal oxide perovskites is dependent on the effective electronegativity of the transition metal ion, the connectivity of the octahedra, and the deviation from linearity of the B–O–B bonds. The band gap sensitively increases as the effective electronegativity of transition



metal ion decreases (the electronegativity follows the order of  $\text{Mo}^{6+} > \text{W}^{6+} > \text{Nb}^{5+} \sim \text{Ti}^{4+} > \text{Ta}^{5+}$ ). The transition from the three-dimensional connectivity of the ternary perovskite structure to the isolated electronic structure of the ordered double perovskite increases the band gap by 0.8–1.5 eV as a result of the decreased conduction band width. Distorting the linear B–O–B bonds allows for an increased band gap by up to 0.5 eV due to the conduction band width narrowing. In contrast, reducing the dimensionality of the structure from the 3-D connectivity of the ternary perovskite structure to the 2-D and pseudo 2-D connectivity of the layered perovskite phases has a minimal influence on the band gap if the size and shape of  $\text{BO}_6$  octahedra is kept. In addition, the identity and concentration of inert A ions (A: alkali, alkaline-earth, or rare-earth ions) also has a minimal influence on the band gaps, as also demonstrated in  $\text{ABi}_2\text{Nb}_2\text{O}_9$  (A = Ca, Sr, Ba).<sup>299</sup> However, the replacement of these common A ions with  $\text{Ag}^+$  leads to a great decrease in band gap of  $\text{ABO}_3$  due to the formation of a more negative valence band of hybrid Ag 4d and O 2p orbitals than the valence band of dominant O 2p orbitals (for example,  $\text{AgTaO}_3$  and  $\text{AgNbO}_3$  has a smaller band gap by 0.6 eV than  $\text{NaTaO}_3$  and  $\text{NaNbO}_3$ , respectively).<sup>82</sup> Similar changes were also observed in layered Dion–Jacobson phases  $\text{RbLaNb}_2\text{O}_7$  and  $\text{RbA}_2\text{Nb}_3\text{O}_{10}$  (A = Ca, Sr) and the Ruddlesden–Popper phase  $\text{Rb}_2\text{La}_2\text{Ti}_3\text{O}_{10}$  by using silver ions to exchange ions in the interlayers.<sup>325</sup> The knowledge obtained could provide important guidelines for tailoring the band gaps of perovskites by rationally choosing appropriate transition metal ions and controlling stoichiometry.<sup>310,365–370</sup>

Besides the band gap which controls the light absorption range, the position of band edges, dispersion of band structures and band width are also crucial factors affecting photocatalytic activity. Their roles were theoretically investigated together with experimental results in different systems.<sup>179,186</sup> For  $\text{MSnO}_3$  ( $\text{M}^{2+} = \text{Ca}^{2+}, \text{Sr}^{2+}, \text{Ba}^{2+}$ ),<sup>179</sup> photocatalytic reactions for  $\text{H}_2$  and  $\text{O}_2$  evolution in the presence of sacrificial reagents follows the orders of  $\text{CaSnO}_3 > \text{SrSnO}_3 > \text{BaSnO}_3$ , and  $\text{CaSnO}_3 < \text{SrSnO}_3 < \text{BaSnO}_3$ , respectively. The order of  $\text{H}_2$  generation was consistent with not only that of the conduction-band edges but also with that of the transferred excitation energy, while that of  $\text{O}_2$  generation was consistent with that of the angle of the Sn–O–Sn bonds as well as the delocalization of excited energy, revealed by theoretical results. Similarly, the activity of photocatalytic degradation of methyl orange with  $\text{MSnO}_3$  follows the order of  $\text{CaSnO}_3 > \text{SrSnO}_3 > \text{BaSnO}_3$  as a consequence of the dipole moments from the octahedral tilting distortion, widened band gap and increased surface area.<sup>371</sup> Yuan *et al.* proposed that the largely dispersed conduction band,  $180^\circ$  Zr–O–Zr bond angle, and highly negative flat-band potential are responsible for the high photocatalytic activity of  $\text{BaZrO}_3$  for water splitting.<sup>179</sup>

Many promising perovskite oxides with a  $d^0$  electronic configuration have a large band gap so as to have the ability of splitting water to produce hydrogen and oxygen under UV irradiation only. Attempts containing theoretical studies to address this issue include doping,<sup>120,207,214,263,282,305,348,372–390</sup> forming oxynitrides and oxysulfide,<sup>359,391–396</sup> introducing intrinsic defects,<sup>100,145,146,397–399</sup> and forming solid-solutions.<sup>249,258,259,400,401</sup> Early studies mainly focused

on doping cations in B site of  $\text{ABO}_3$  and derived complex perovskites.  $\text{ACo}_{1/3}\text{Nb}_{2/3}\text{O}_3$  (A = Ca, Sr, and Ba) with a random distribution of  $\text{Co}^{2+}$  and  $\text{Nb}^{5+}$  in M site in a manner of charge-balanced manner showed a visible light absorption band.<sup>207</sup> The origin of the visible light absorption revealed by DFT calculations is the strong hybridization of  $\text{Co}^{2+}$  states with O 2p states to form a more negative valence band. Cr or Fe doping in layered  $\text{La}_2\text{Ti}_2\text{O}_7$  introduced an additional visible light absorption band without changing its intrinsic absorption edge as a result of forming partially filled 3d band in the band gap.<sup>348</sup> Similar results were also observed in Cr doped  $\text{Sr}_2\text{TiO}_4$ .<sup>282</sup> Importantly, the substitutional Sc doping for Ti atoms in  $\text{Sr}_2\text{TiO}_4$  not only reduced the band gap but also enhanced the dispersion of conduction and valence bands (partially contributed from generation of O vacancies).<sup>382</sup> The DFT calculations of  $\text{SrTi}_x\text{M}_{1-x}\text{O}_3$  (M = Ru, Rh, Ir and Pt) implied that the highest visible light photocatalytic activity of  $\text{SrTi}_x\text{Rh}_{1-x}\text{O}_3$  was due to its suitable band energetics, and the induced hybridized Ti/Rh orbitals in the band gap of  $\text{SrTiO}_3$ .<sup>214</sup>

Anion doping provides a flexible way of modifying valence band or introducing intermediate band/localized states above valence band as does in the widely studied anion doped  $\text{TiO}_2$ .<sup>402</sup> Among all anion doping, nitrogen doping is the most widely used to increase visible light absorption of perovskites. One advantage is the capability of narrowing the band gap to around 2 eV, an ideal value for fully harvesting visible light part of solar spectrum, due to the more negative energy level of N 2p states than O 2p states. The second is the close ionic radii of  $\text{O}^{2-}$  and  $\text{N}^{3-}$  (1.35 Å vs. 1.46 Å) to enable a minimal lattice distortion caused by the substitutional doping of N for O. The third is the experimental feasibility of introducing N into perovskites by heating materials in easily available gaseous ammonia atmospheres. Experimental results indeed demonstrated the effectiveness of nitrogen doping in increasing visible light absorption of wide-bandgap perovskites such as  $\text{Sr}_2\text{Nb}_2\text{O}_7$ ,  $\text{La}_2\text{Ti}_2\text{O}_7$ ,  $\text{SrTiO}_3$ ,  $\text{NaTaO}_3$  and  $\text{Ba}_5\text{Ta}_4\text{O}_{15}$ .<sup>102,109,273,331,349,372,403–409</sup> Theoretical studies were conducted to understand the mechanism of anion doping in increasing visible light absorption. The mixing of N 2p and O 2p orbitals to elevate valence band edge was theoretically found to contribute to the band gap narrowing of N doped layered perovskite  $\text{Ba}_5\text{Ta}_4\text{O}_{15}$ .<sup>331</sup> The effect of different doping states of nitrogen in  $\text{La}_2\text{Ti}_2\text{O}_7$ , a layered monoclinic perovskite, on electronic structure modification was studied.<sup>387,389</sup> Only localized states are formed in the band gap when N substitutes O or the substitutional N for O is coupled with interstitial Ti. While the complex of two substitutional N with oxygen vacancies creates a continuum energy band just above the valence band maximum, which is considered to be account for the band gap narrowing of N doped  $\text{La}_2\text{Ti}_2\text{O}_7$  obtained experimentally without increasing additional electron-hole recombination centers. On the other hand, by surveying more than 40 models with different ionic states of dopants, distance between dopants, doping concentrations and formation of oxygen vacancy, the model with three dispersed substitutional N atoms at O sites and one oxygen vacancy in 87-atom supercell was identified to explain both the shift-up of the valence bands and the narrowed band gap of N-doped  $\text{La}_2\text{Ti}_2\text{O}_7$  observed experimentally.<sup>387</sup>

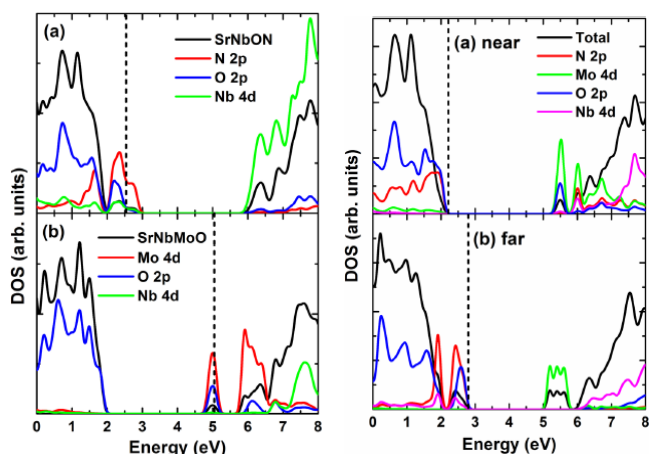


**Fig. 14** The left panel: The calculated (using HSE06 functional) total and partial density of states of mono doping of (a) nitrogen and (b) molybdenum in  $\text{Sr}_2\text{Nb}_2\text{O}_7$ . The right panel: The calculated (using HSE06 functional) total and partial density of states of (N, Mo) co-doped  $\text{Sr}_2\text{Nb}_2\text{O}_7$  with (a) near and (b) far configuration. The vertical lines indicate the Fermi levels. Reprinted with permission from ref. 376. Copyright © 2012, AIP Publishing LLC.

Although N doping can effectively extend visible light absorption range of doped perovskites, two major challenges associated with N doping in oxides include a low solubility of nitrogen in doped materials and charge imbalance between  $\text{N}^{3-}$  and  $\text{O}^{2-}$ . They cause a not full hybridization of N 2p orbitals with O 2p orbitals, and increased recombination centers of photogenerated electrons and holes, respectively. Co-doping of cation-anion or anion-anion in perovskites was actively pursued and their unique advantages have been demonstrated by synergistically addressing these challenges.<sup>376,377,379-381</sup> Nisar *et al.* showed that, although a respective mono-doping of N and Mo in  $\text{Sr}_2\text{Nb}_2\text{O}_7$  can increase visible light absorption by introducing partially unoccupied states/bands above valence band or below conduction band (the left panel of Fig. 14), these states/bands act as the recombination centers of photogenerated electrons and holes.<sup>376</sup> Co-doping of N and Mo with a “far” configuration can significantly reduce the band gap by negatively shifting valence band edge with the newly formed occupied states (the right panel of Fig. 14) as a result of charge compensation effect between N and Mo. The valence band edge consists of the hybrid N 2p, O 2p, and Nb 4d orbitals and the bottom of the conduction band edge dominantly consists of Mo 4d orbitals. Moreover, the band edges of co-doped  $\text{Sr}_2\text{Nb}_2\text{O}_7$  with narrowed band gap are still suitable for overall water splitting. The role of cation-anion mediated charge compensation in realizing band gap narrowing by removing localized states of dopants in the band gap was also validated in (V, Nb, Ta)/(N) co-doped  $\text{La}_2\text{Ti}_2\text{O}_7$ .<sup>380</sup> Furthermore, the stability of the co-doping system is improved due to the coulomb interactions and charge compensations effect.

Greatly improved concentration of nitrogen dopant in oxide perovskites can lead to the formation of corresponding oxynitride perovskites with much narrowed band gaps. Theoretical studies were conducted to understand the mechanism of band gap narrowing in oxynitride perovskites.<sup>372,393,396</sup> Ji *et al.* compared electronic structures of nitrogen doped  $\text{Sr}_2\text{Nb}_2\text{O}_7$  ( $\text{Sr}_2\text{Nb}_2\text{O}_5\text{N}_2$ ) and

$\text{SrNbO}_2\text{N}$ .<sup>372</sup> As a result of a higher concentration of N in  $\text{SrNbO}_2\text{N}$ ,  $\text{SrNbO}_2\text{N}$  has a much smaller theoretical band gap than  $\text{Sr}_2\text{Nb}_2\text{O}_5\text{N}_2$  (0.2 eV vs 2.23 eV). The Ti–(O, N) covalent bonding and existence of N atoms are responsible for the reduced band gap of  $\text{LaTiO}_2\text{N}$  photocatalyst.<sup>393</sup> The valence band edge in oxynitrides is dominantly composed of N 2p states, which have a more negative level than O 2p states. On the other hand, thanks to the rapid increase of computational powers, it is possible to make computational screening of a huge number of perovskites affordable.<sup>358,359,410-414</sup> This definitely promotes the discovery of new unknown visible light photocatalysts. By screening 19000 cubic perovskites obtained by combining 52 different metals with oxygen, nitrogen, sulfur and fluorine as anions, 20 and 12 materials with potential interest for one- and two-photon water splitting were suggested by considering efficient light absorption, suitable band edges for water splitting, appropriate electron/hole mobility.<sup>411</sup> Most of these materials are oxides and oxynitrides. However, further theory calculations of the intermediate energetics for hydrogen evolution and oxygen evolution, conducted by Montoya *et al.*,<sup>414</sup> suggest that none of the materials proposed above has the satisfactory surface chemical properties that should allow for total water splitting in a single material. Therefore, co-catalysts are still necessary to overcome the kinetic limitations for water splitting. Although the surveyed oxysulfides have the same order of magnitude as the oxynitrides as a result of the close electronegativity of sulfur to nitrogen, they show low stability due to a large difference in atomic radius between sulfur and oxygen.

Forming solid solutions, which can be considered as a kind of cation-cation co-doping with specific molar ratio of two cation dopants, represents an alternative of tuning electronic band structures of perovskites in a wide range by changing both conduction and valence bands. Many solid solution perovskites such as  $(\text{AgNbO}_3)_{1-x}(\text{SrTiO}_3)_x$ ,<sup>248,249</sup>  $\text{NaTaO}_3\text{-LaFeO}_3$ ,<sup>258</sup> and  $\text{Na}_{0.5}\text{La}_{0.5}\text{TiO}_3\text{-LaCrO}_3$ <sup>259</sup> show increased visible light absorption due to the band gap narrowing. The band gap of a solid solution is usually located between the band gaps of its two pristine components by simultaneously lowering conduction band edge and elevating valence band edge. For example, the band structures of  $\text{AgNbO}_3$ ,  $\text{SrTiO}_3$  and solid solution samples are shown in Fig. 15 based on the experimental and theoretical calculation results.<sup>248,249</sup> The Ag 4d orbitals move up the valence band edge composed by O 2p orbitals, while the conduction band edge composed by Nb 4d orbitals is more negative than that composed by Ti 3d orbitals. For  $(\text{AgNbO}_3)_{0.75}(\text{SrTiO}_3)_{0.25}$  with optimum performance, both the band gap energy and band edge potentials are in the middle of the parent  $\text{AgNbO}_3$  and  $\text{SrTiO}_3$ , due to the hybridization of (Ag 4d + O 2p) orbitals and (Ti 3d + Nb 4d) orbitals, respectively. However, it should be pointed out that doping introduces trap states in the gap and so can effectively reduce band gap, which is suggested as an alternative model. The modulated band structure takes advantage of the more negative conduction band edge of  $\text{SrTiO}_3$  and the less positive valence band edge of  $\text{AgNbO}_3$ . As a result, it gave rise to a significantly enhanced photocatalytic activity for  $\text{O}_2$  evolution and  $\text{CH}_3\text{CHO}$  decomposition.

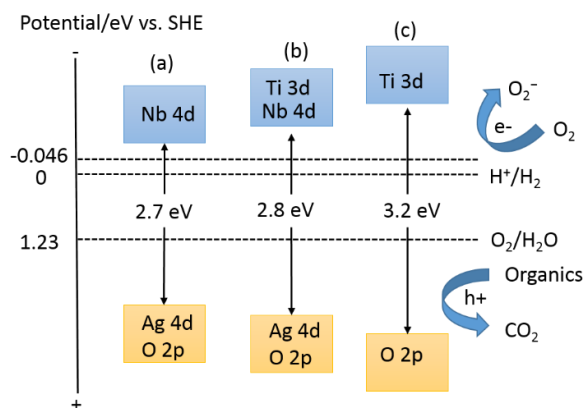


**Fig. 15** Schematic band structures of (a)  $\text{AgNbO}_3$ , (b)  $(\text{Ag}_{0.75}\text{Sr}_{0.25})(\text{Nb}_{0.75}\text{Ti}_{0.25})\text{O}_3$  and (c)  $\text{SrTiO}_3$ . Reprinted with permission from ref. 248. Copyright © 2008, American Chemical Society.

Tailoring intrinsic defects or structures<sup>100,397-399</sup> can also modify electronic structure of perovskites to extend light absorption range. N-type  $\text{SrTiO}_3$  with intrinsic oxygen vacancies is a promising photocatalyst for overall water splitting. Different from point defects of oxygen vacancies usually formed in metal oxides, line defects associated with oxygen vacancies along {100} and {001} directions were proposed and created in  $\text{SrTiO}_3$  with a high concentration of oxygen vacancies (i.e.,  $\text{SrTiO}_{2.75}$ ).<sup>100</sup> Theoretical results imply that such a line defect creates a fully filled new band composed of Ti *d*-Ti *d* bonding states across the vacancy sites in the band gap because of the formation of Ti-Ti bonds in the framework of  $\text{SrTiO}_3$  with heavy loss of oxygen. The excitation of electrons in the newly formed band to conduction bands is responsible for the additional visible light absorption band. On the other hand, Fu *et al.* showed that the electronic states induced by the combination of oxygen and strontium atoms on the surface of SrO-terminated nanowires lead to a shift in the conduction band toward the valence band and thus narrow the band gap.<sup>397</sup> Similar phenomenon was also observed in CaO-terminated  $\text{CaTiO}_3$  nanowires.<sup>398</sup> It is interesting that the creation of vacancies in A site can significantly change electronic band structure of  $\text{SrNbO}_3$  for a wide absorption range up to 700 nm.<sup>145</sup> On the basis of DFT calculations, the origin of the strong visible light absorption band of the metallic  $\text{Sr}_{1-x}\text{NbO}_3$  obtained was proposed to stem from the optical transitions of electrons in the partially occupied band to the unoccupied one above. A systematic theoretical investigation of electronic structure and optical transition of three typical *d*<sup>1</sup> metallic oxides  $\text{SrNbO}_3$ ,  $\text{SrVO}_3$ , and  $\text{CaVO}_3$  by Zhu *et al.* indicated that electron direct transition in the visible light region can only occur in  $\text{SrNbO}_3$  due to the different parity of band edge wave functions as a result of the mixing of Sr *d* states with Nb *e<sub>g</sub>* states.<sup>399</sup> Moreover, the large bandwidth of unoccupied band of  $\text{SrNbO}_3$  accounts for a smaller effective masses of photogenerated carriers and thus favors the transport of the carriers to surface reactive sites. These features were considered to be the key of realizing visible light photocatalytic activity in such a metallic material.

## 6. Potential Applications

Since the discovery of photoelectrochemical water splitting phenomenon in 1972, great effort has been devoted to this promising fields with the hopes of developing new generation and sustainable solar conversion systems that can address the energy and environmental challenges. Fundamentally, how to make better use of the redox power from photo-generated charge carriers (electrons and holes) is the key towards feasible application of semiconductor photocatalysis. The reduction capability of the photo-generated electrons has been heavily used for water splitting to produce hydrogen and  $\text{CO}_2$  reduction, while the oxidation power provided by the photo-generated holes or secondary radicals are important for many reactions involving organic decomposition and disinfection processes. Over the past a few decades, a vast amount of literature has been accumulated in the research and development sectors towards possible commercialization of the semiconductor photocatalysis technologies, including water splitting for solar hydrogen, organic pollutant degradation in air/water, and solar driven  $\text{CO}_2$  conversion. Among these demonstrated photocatalysis applications, over half are based on  $\text{TiO}_2$  photocatalysts.

Compared with  $\text{TiO}_2$  materials, perovskite photocatalysts have their unique features in terms of tuneable compositions, crystalline and electronic/energy band structures, which in some cases lead to more effective photo-induced reduction and oxidation efficiencies. To date, perovskite photocatalysts have been demonstrated to be active in both environmental remediation and solar fuel generation fields. The examples of water splitting for hydrogen fuel generation have been intensively discussed in above sections and in also the attached photocatalyst Table list 1-4. It is important to note that due to the lack of measurement standard, the comparison of solar hydrogen and oxygen yields (Tables 1-4) from one material system to another is not appropriate in many cases. The photocatalyst itself including the amount and form of the sample, the loading of co-catalysts, and reaction conditions such as reactor design and configuration, light sources and reaction solvents (for sacrificial systems) are all playing important roles in determining the photocatalytic water splitting performance. One reasonable way to screen the photocatalyst materials is to use quantum yield (QE). Encouragingly, to date the water splitting QE record is held by a member of the perovskite family,  $\text{NaTaO}_3$  (56%, under strong UV irradiation), which has also subsequently inspired great research efforts in exploring other perovskite family members with the purpose of improving QE and better use of visible light, as indicated in the Tables 1-4. It is clear that there is still much room for our researchers to work on, if we are set to solve the 10% STH efficiency target in the years ahead. Another even more challenging topic is to use perovskite photocatalysts for  $\text{CO}_2$  reduction to produce some valuable chemicals but the examples in this field have been quite limited so far.

In the environmental remediation sector, the use of photocatalysts has more diverse options depending on the application purposes. The chemicals in various water sources represent a large group of pollutants which could be potentially

decomposed by photocatalytic process. As listed in Tables 1-4, a number of organic compounds including colourful dyes (MO, MB, RhB, etc), phenol and its derivatives, pesticides, and acetaldehyde have been used to testify the photocatalytic performance of the various perovskite photocatalysts, and some of the systems are working quite effectively. However, for any practically feasible photocatalytic water treatment process, one has to consider not only photocatalyst itself, but also reaction kinetics of the organic mineralization, and reactor engineering. The immobilization of particulate photocatalysts in thin films can overcome the challenging photocatalyst recovery issue, while at the cost of reduced surface areas for efficient photocatalytic process to happen. In the air pollutant removal or self-cleaning coatings sector, predominated work have been done on TiO<sub>2</sub> based system while quite rare examples were demonstrated in perovskite photocatalyst system.

## 7. Conclusions and perspectives

Photocatalysis on semiconductor nanomaterials represents a potential strategy to utilize abundant solar energy to tackle the challenging energy and environmental issues that we are facing. Thanks to the continued research efforts for a few decades, the semiconductor photocatalysis has seen accelerated development in recent years with an impressive number of > 5000 research publications in 2015. Among these, one of the most exciting latest progresses is the perovskite based composite photocatalyst SrTiO<sub>3</sub>:La,Rh/Au/BiVO<sub>4</sub>:Mo developed by Domen *et al.*, which exhibited remarkable solar-to-hydrogen conversion efficiency of over 1%, as briefly discussed above. However, considering the targeted STH efficiency of 10% for practical application of solar fuels, we still have a relatively long journey to realize our ambition. Likewise, the use of photocatalysis in environmental remediation also has the same challenges, and photocatalytic CO<sub>2</sub> reduction, or in other words, artificial photosynthesis, is even more challenging with very low selectivity and conversion efficiency. However, we should bear in mind that our mother Nature has evolved for millions of years to realize the < 2% photosynthesis efficiency, and should have the every confidence to achieve commercially feasible solar to fuel conversion efficiency in the years ahead.

From the viewpoint of practical applications, a semiconductor photocatalyst should at least have the merits of high photocatalytic activity, low cost, scalability and long term stability. In this regard, the selection, design and development of new types of photocatalysts hold the key for sustainable photocatalytic solar energy utilization. Some of the perovskite photocatalysts have demonstrated their potentials for efficient photocatalysis, yet the vast option of material systems represents a huge task for our researchers to conquer. In addition to the conventional "trial and error" approach which has been used by many researchers in photocatalyst development, theoretical prediction and high throughput material genome should provide very powerful tools to guide us for rationally designing better photocatalysts with efficient light harvesting, facilitated charge separation/transfer and appropriate redox powers to drive the redox reactions. These new

approaches could be particularly suitable to the multi-compositional perovskite material systems. From the economic concern, it should be avoided to use rare metal elements. Considering that ~90% elements in the periodic table could be included into the generic inorganic perovskite structure, it is recommended to use the alkali or alkaline earth metal elements in A-site and first-row transitional metal elements in B-site to compose the perovskite matrix. Another strategy is to develop new types of double perovskites or triple perovskites photocatalysts as demonstrated from the reported literature. Facet control, surface decorations, conceptual Z-scheme design, band structure alignment and interfacial engineering on the perovskite photocatalysts can also be critically important towards efficient photocatalysis, which are worth further investigating.

In addition to the material development discussed in this article, other aspects in the whole photocatalysis processes are equally important. This includes the fundamental understanding of the photocatalysis process and products by using advanced in-situ characterizations, the design of photoreactors which can allow better sunlight utilization, efficient mass transfer for the reactants to adsorb/desorb on the surface of photocatalysts, and recovery/regeneration of the photocatalysts for long cycle life. Despite decades of intensive research efforts, the standardization of semiconductor photocatalysis measurement and evaluation is still not available to date. While the photocatalysis society will need to work collaboratively to achieve this goal, for our individuals, the use of simulated sunlight, and evaluation of quantum yield in our reported photocatalytic systems will be valuable for our peer researchers to better understand, to compare and to improve the photocatalysis systems, thus facilitating the knowledge sharing and accelerated progresses of this challenging yet highly promising field.

Under the current global climate of having huge demand for developing sustainable energy supply and environmental solutions, the utilization of solar energy through photocatalysis process has a bright future for simultaneously addressing energy crisis and environmental challenges. It is important for our research community to work together not only in the fundamental understanding of better photocatalyst design, but also in the engineering of whole low-cost and scalable photocatalysis process to achieve sustainable solar utilization systems.

## Acknowledgements

We acknowledge funding from the Engineering and Physical Research Council for research award EP/K036769/1 and Platform Grant EP/K015540/1. The financial support from the Major Basic Research Program, Ministry of Science and Technology of China (2014CB239401) and NSFC (51422210, 51629201) is acknowledged. We also acknowledge support from The Royal Society Newton Fellowship, NA140077 and The Royal Society Wolfson Merit Award, WRM 2012/R2.

## Notes and references

- 1 X. Chen and S. S. Mao, *Chem. Rev.*, 2007, **107**, 2891.

- 2 X. Lang, W. Ma, C. Chen, H. Ji and J. Zhao, *Acc. Chem. Res.*, 2014, **47**, 355.
- 3 H. Park, H. -i. Kim, G. -h. Moon and W. Choi, *Energy Environ. Sci.*, 2016, **9**, 411.
- 4 A. J. Bard and M. A. Fox, *Acc. Chem. Res.*, 1995, **28**, 141.
- 5 H. Zhou, X. F. Li, T. X. Fan, F. E. Osterloh, J. Ding, E. M. Sabio, D. Zhang and Q. X. Guo, *Adv. Mater.*, 2010, **22**, 951.
- 6 G. Zhang, W. Choi, S. H. Kim and S. B. Hong, *J. Hazard. Mater.*, 2011, **188**, 198.
- 7 W. Wang and Y. Ku, *J. Photochem. Photobio. A*, 2003, **159**, 47.
- 8 R. Vinu and G. Madras, *Environ. Sci. Technol.*, 2008, **42**, 913.
- 9 D. Zhao, C. Chen, C. Yu, W. Ma and J. Zhao, *J. Phys. Chem. C*, 2009, **113**, 13160.
- 10 B. Sun, E. P. Reddy and P. G. Smirniotis, *Environ. Sci. Technol.*, 2005, **39**, 6251.
- 11 C. Hu, Y. Lan, J. Qu, X. Hu and A. Wang, *J. Phys. Chem. B*, 2006, **110**, 4066.
- 12 L. S. Zhang, K. H. Wong, H. Y. Yip, C. Hu, J. C. Yu, C. Y. Chan and P. K. Wong, *Environ. Sci. Technol.*, 2010, **44**, 1392.
- 13 Y. Hou, X. Li, Q. Zhao, G. Chen and C. L. Raston, *Environ. Sci. Technol.* 2012, **46**, 4042.
- 14 Z. Zou, J. Ye, K. Sayama and H. Arakawa, *Nature*, 2001, **414**, 625.
- 15 K. Maeda, K. Teramura, D. Lu, T. Takata, N. Saito, Y. Inoue and K. Domen, *Nature*, 2006, **440**, 295.
- 16 J. Tang, Z. Zou and J. Ye, *Angew. Chem. Int. Ed.*, 2004, **43**, 4463.
- 17 P. Wang, B. Huang, X. Qin, X. Zhang, Y. Dai, J. Wie and M-H. Whangbo, *Angew. Chem. Int. Ed.*, 2008, **47**, 7931.
- 18 Z. Yi, J. Ye, N. Kikugawa, T. Kato, S. Ouyang, H. Stuart-Williams, H. Yang, J. Cao, W. Luo, Z. Li, Y. Liu and R. L. Withers, *Nature Mater.*, 2010, **9**, 559.
- 19 X. Chen, L. Liu, P. Y. Yu and S. S. Mao, *Science*, 2011, **331**, 746.
- 20 Wang, K. Maeda, A. Thomas, K. Takanabe, G. Xin, J. M. Carlsson, K. Domen and M. Antonietti, *Nature Mater.*, 2009, **8**, 76.
- 21 J. Liu, S. Wen, Y. Hou, F. Zuo, G. J. O. Beran and P. Feng, *Angew. Chem. Int. Ed.*, 2013, **52**, 3241.
- 22 G. Liu, P. Niu, L. Yin and H. Cheng, *J. Am. Chem. Soc.*, 2012, **134**, 9070.
- 23 G. Liu, L. Yin, P. Niu, W. Jiao and H. Cheng, *Angew. Chem. Int. Ed.*, 2013, **52**, 6362.
- 24 M. Latorre-Sanchez, A. Primo and H. Garcia, *Angew. Chem. Int. Ed.*, 2013, **52**, 11813.
- 25 L. F. Velasco, J. C. Lima and C. Ania, *Angew. Chem. Int. Ed.*, 2014, **53**, 4146.
- 26 J. Liu, Y. Liu, N. Liu, Y. Han, X. Zhang, H. Huang, Y. Lifshitz, S-T. Lee, J. Zhong and Z. Kang, *Science*, 2015, **347**, 970.
- 27 S. Ghosh, N. A. Kouame, L. Ramos, S. Remita, A. Dazzi, A. Deniset-Besseau, P. Beaunier, F. Goubard, P. Aubert and H. Remita, *Nature Mater.*, 2015, **14**, 505.
- 28 R. S. Sprick, J-X. Jiang, B. Bonillo, S. Ren, T. Ratvijitvech, P. Guiglion, M. A. Zwijnenburg, D. J. Adams and A. I. Cooper, *J. Am. Chem. Soc.*, 2015, **137**, 3265.
- 29 G. Zhang, C. Ni, L. Liu, G. Zhao, F. Fina and J. T.S. Irvine, *J. Mater. Chem. A*, 2015, **3**, 15413.
- 30 A. J. Nozik, *Appl. Phys. Lett.*, 1977, **30**, 567.
- 31 A. J. Nozik, *Annu. Rev. Phys. Chem.*, 1978, **29**, 189.
- 32 O. Khaselev and J. A. Turner, *Science*, 1998, **280**, 425.
- 33 J. Gu, Y. Yan, J. L. Young, K. X. Steirer, N. R. Neale and J. A. Turner, *Nature Mater.*, 2016, **15**, 456.
- 34 K. Maeda, *ACS Catal.*, 2013, **3**, 1486.
- 35 K. Maeda, A. Xiong, T. Yoshinaga, T. Ikeda, N. Sakamoto, T. Hisatomi, M. Takashima, D. Lu, M. Kanehara, T. Setoyama, T. Teranishi and K. Domen, *Angew. Chem. Int. Ed.*, 2010, **49**, 4096.
- 36 B. A. Pinaud, J. D. Benck, L. C. Seitz, A. J. Forman, Z. Chen, T. G. Deutsch, B. D. James, K. N. Baum, G. N. Baum, S. Ardo, H. Wang, E. Miller and T. F. Jaramillo, *Energy Environ. Sci.*, 2013, **6**, 1983.
- 37 M. A. Pena and J. L. G. Fierro, *Chem. Rev.*, 2001, **101**, 1981.
- 38 F. E. Osterloh, *Chem. Mater.*, 2008, **20**, 35.
- 39 A. Kudo and Y. Miseki, *Chem. Soc. Rev.*, 2009, **38**, 253.
- 40 X. Chen, S. Shen, L. Guo and S. S. Mao, *Chem. Rev.*, 2010, **110**, 6503.
- 41 A. Kubacka, M. Fernandez-Garcia and G. Colon, *Chem. Rev.*, 2012, **112**, 1555.
- 42 J. Shi and L. Guo, *Prog. Nat. Sci.*, 2012, **22**, 592.
- 43 P. Kanhere and Z. Chen, *Molecules*, 2014, **19**, 19995.
- 44 W. Wang, M. O. Tade and Z. Shao, *Chem. Soc. Rev.*, 2015, **44**, 5371.
- 45 C. Li, X. G. Lu, W. Z. Ding, L. M. Feng, Y. H. Gao and Z. M. Guo, *Acta Cryst.*, 2008, **64**, 702.
- 46 H. Kato and A. Kudo, *Catal. Lett.*, 1999, **58**, 153.
- 47 H. Kato and A. Kudo, *J. Phys. Chem. B*, 2001, **105**, 4285.
- 48 H. Kato and A. Kudo, *Catal. Today*, 2003, **78**, 561.
- 49 J. W. Liu, G. Chen, Z. H. Li and Z. G. Zhang, *Int. J. Hydrogen Energy*, 2007, **32**, 2269.
- 50 C-C. Hu and H. Teng, *Appl. Catal. A: General*, 2007, **331**, 44.
- 51 C-C. Hu, C-C Tsai and H. Teng, *J. Am. Ceram. Soc.*, 2009, **92**, 460.
- 52 X. Li and J. Zang, *J. Phys. Chem. C*, 2009, **113**, 19411.
- 53 X. Fu, X. Wang, D. Y.C. Leung, W. Xue, Z. Ding, H. Huang and X. Fu, *Catal. Commun.*, 2010, **12**, 184.
- 54 T. Yokoi, J. Sakuma, K. Maeda, K. Domen, T. Tatsumi and J. N. Kondo, *Phys. Chem. Chem. Phys.*, 2011, **13**, 2563.
- 55 J. Shi, G. Liu, N. Wang and C. Li, *J. Mater. Chem.*, 2012, **22**, 18808.
- 56 T. Meyer, J. B. Priebe, R. O. Silva, T. Peppel, H. Junge, M. Beller, A. Bruckner and S. Wohlrab, *Chem. Mater.*, 2014, **26**, 4705.
- 57 Y. Li, H. Gou, J. Lu and C. Wang, *Int. J. Hydrogen Energy*, 2014, **39**, 13481.
- 58 A. Kudo and H. Kato, *Chem. Phys. Lett.*, 2000, **331**, 373.
- 59 H. Kato, K. Asakura and A. Kudo, *J. Am. Chem. Soc.*, 2003, **125**, 3082.
- 60 D. G. Porob and P. A. Muggard, *J. Solid State Chem.*, 2006, **179**, 1727.
- 61 S. C. Yan, Z. Q. Wang, Z. S. Li and Z. G. Zou, *Solid State Ionics*, 2009, **180**, 1539.
- 62 L. M. Torres-Martinez, A. Cruz-Lopez, I. Juarez-Ramirez and M. M. L. Rosa, *J. Hazard. Mater.*, 2009, **165**, 774.
- 63 L. M. Torres-Martinez, R. Gomez, O. Vazquez-Cuchillo, I. Juarez-Ramirez, A. Cruz-Lopez and F. J. Alejandro-Sandoval, *Catal. Commun.*, 2010, **12**, 268.

- 64 H. Husin, H-M. Chen, W-N Su, C-J. Pan, W-T, Chuang, H-S. Sheu and B-J. Hwang, *Appl. Catal. B: Environ.*, 2011, **102**, 343.
- 65 X. Li and J. Zang, *Catal. Commun.*, 2011, **12**, 1380.
- 66 A. Iwase, H. Kato and A. Kudo, *Appl. Catal. B: Environ.*, 2013, **136-137**, 89.
- 67 A. Iwase, H. Kato and A. Kudo, *ChemSusChem*, 2009, **2**, 873.
- 68 J. Wang, S. Su, B. Liu, M. Cao and C. Hu, *Chem. Commun.*, 2013, **49**, 7830.
- 69 Y. Su, S. Wang, Y. Meng, H. Han and X. Wang, *RSC Advances*, 2012, **2**, 12932.
- 70 Y. Su, L. Peng, J. Guo, S. Huang, L. Lv and X. Wang, *J. Phys. Chem. C*, 2014, **118**, 10728.
- 71 P. D. Kanhere, J. Zheng and Z. Chen, *J. Phys. Chem. C*, 2011, **115**, 11846.
- 72 P. Kanhere, J. Zheng and Z. Chen, *Int. J. Hydrogen Energy*, 2012, **37**, 4889.
- 73 Z. Li, Y. Wang, J. Liu, G. Chen, Y. Li and C. Zhou, *Int. J. Hydrogen Energy*, 2009, **34**, 147.
- 74 X. Zhou, J. Shi and C. Li, *J. Phys. Chem. C*, 2011, **115**, 8305.
- 75 D-R. Liu, C-D. Wei, B. Xue, X-G. Zhang and Y-S. Jiang, *J. Hazard. Mater.*, 2010, **182**, 50.
- 76 X. Wu, S. Yin, Q. Dong and T. Sato, *Phys. Chem. Chem. Phys.*, 2013, **15**, 20633.
- 77 H. W. Kang, S. N. Lim, S. B. Park and A. A. Park, *Int. J. Hydrogen Energy*, 2013, **38**, 6323.
- 78 M. Yang, X. Huang, S. Yan, Z. Li, T. Yu and Z. Zou, *Mater. Chem. Phys.*, 2010, **121**, 506.
- 79 Z. Zhao, R. Li, Z. Li and Z. Zou, *J. Phys. D: Appl. Phys.*, 2011, **44**, 165401.
- 80 W. Yang, G. Tan, H. Ren, A. Xia, Y. Luo and L. Yin, *J. Mater. Sci: Mater. Electron.*, 2014, **25**, 3807.
- 81 T. Ishihara, H. Nishiguchi, K. Fukamachi and Y. Takita, *J. Phys. Chem. B*, 1999, **103**, 1.
- 82 H. Kato, H. Kobayashi and A. Kudo, *J. Phys. Chem. B*, 2002, **106**, 12441.
- 83 F. T. Wagner and G. A. Somorjai, *Nature*, 1980, **285**, 559.
- 84 F. T. Wagner and G. A. Somorjai, *J. Am. Chem. Soc.*, 1980, **102**, 5494.
- 85 K. Domen, S. Naito, M. Soma, T. Onishi and K. Tamaru, *J. C. S. Chem. Comm.*, 1980, 543.
- 86 K. Domen, S. Naito, T. Onishi, K. Tamaru and M. Soma, *J. Phys. Chem.*, 1982, **86**, 3657.
- 87 K. Domen, A. Kudo, T. Onishi, N. Kosugi and H. Kuroda, *J. Phys. Chem.*, 1986, **90**, 292.
- 88 X. Wie, G. Xu, Z. Ren, C. Xu, G. Shen and G. Han, *J. Am. Ceram. Soc.*, 2008, **91**, 3795.
- 89 X. Wei, G. Xu, Z. Ren, C. Xu, W. Wenig, G. Shen and G. Han, *J. Am. Ceram. Soc.*, 2010, **93**, 1297.
- 90 Q. Kuang and S. Yang, *ACS Appl. Mater. Inter.*, 2013, **5**, 3683.
- 91 L. F. da Silva, W. Avansi Jr, J. Andres, C. Ribeiro, M. L. Moreira, E. Longo and V. R. Mastelaro, *Phys. Chem. Chem. Phys.*, 2013, **15**, 12386.
- 92 T. Puangpetch, T. Sreethawong, S. Yoshikawa and S. Chavadej, *J. Mol. Catal. A: Chem.*, 2009, **312**, 97.
- 93 T. K. Townsend, N. D. Browning and F. E. Osterloh, *ACS Nano*, 2012, **6**, 7420.
- 94 J. W. Liu, G. Chen, Z. H. Li and Z. G. Zhang, *J. Solid State Chem.*, 2006, **179**, 3704.
- 95 H. Yu, S. Ouyang, S. Yan, Z. Li, T. Yu and Z. Zou, *J. Mater. Chem.*, 2011, **21**, 11347.
- 96 T-H. Xie, X. Sun and J. Lin, *J. Phys. Chem. C*, 2008, **112**, 9753.
- 97 R. Konta, T. Ishii, H. Kato and A. Kudo, *J. Phys. Chem. B*, 2004, **108**, 8992.
- 98 J. Shi, J. Ye, L. Ma, S. Ouyang, D. Jing and L. Guo, *Chem. Eur. J.*, 2012, **18**, 7543.
- 99 J-P. Zou, L-Z. Zhang, S-L. Luo, L-H. Leng, X-B. Luo, M-J. Zhang, Y. Luo and G-C. Guo, *Int. J. Hydrogen Energy*, 2012, **37**, 17068.
- 100 K. Xie, N. Umezawa, N. Zhang, P. Reunchan, Y. Zhang and J. Ye, *Energy Environ. Sci.*, 2011, **4**, 211.
- 101 H. Tan, Z. Zhao, W-B. Zhu, E. N. Coker, B. Li, M. Zheng, W. Yu, H. Fan and Z. Sun, *ACS Appl. Mater. Inter.*, 2014, **6**, 19184.
- 102 F. Zou, Z. Jiang, X. Qin, Y. Zhao, L. Jiang, J. Zhi, T. Xiao and P. P. Edwards, *Chem. Commun.*, 2012, **48**, 8514.
- 103 J. Wang, S. Yin, Q. Zhang, F. Saito and T. Sato, *J. Mater. Chem.*, 2003, **13**, 2348.
- 104 H. Kato and A. Kudo, *J. Phys. Chem. B*, 2002, **106**, 5029.
- 105 H. Yu, S. Yan, Z. Li, T. Yu and Z. Zou, *Int. J. Hydrogen Energy*, 2012, **37**, 12120.
- 106 T. Ishii, H. Kato and A. Kudo, *J. Photochem. Photobio. A: Chem.*, 2004, **163**, 181.
- 107 S. Ouyang, H. Tong, N. Umezawa, J. Cao, P. Li, Y. Bi, Y. Zhang and J. Ye, *J. Am. Chem. Soc.*, 2012, **134**, 1974.
- 108 A. Jia, X. Liang, Z. Su, T. Zhu and S. Liu, *J. Hazard. Mater.*, 2010, **178**, 233.
- 109 T. Ohno, T. Tsubota, Y. Nakamura and K. Sayama, *Appl. Catal. A: General*, 2005, **288**, 74.
- 110 M. Miyauchi, M. Takashio and H. Tobimatsu, *Langmuir*, 2004, **20**, 232.
- 111 R. Niishiro, H. Kato and A. Kudo, *Phys. Chem. Chem. Phys.*, 2005, **7**, 2241.
- 112 Q. Wang, T. Hisatomi, Q. Jia, H. Tokudome, M. Zhong, C. Wang, Z. Pan, T. Takata, M. Nakabayashi, N. Shibata, Y. Li, L. D. Sharp, A. Kudo, T. Yamada and K. Domen, *Nature Mater.*, 2016, **15**, 611.
- 113 L. Gomathi Devi and G. Krishnamurthy, *J. Hazard. Mater.*, 2009, **162**, 899.
- 114 L. Gomathi Devi and G. Krishnamurthy, *J. Phys. Chem. A*, 2011, **115**, 460.
- 115 J. Liu, Y. Sun and Z. Li, *CrystEngComm*, 2012, **14**, 1473.
- 116 K. Maeda, *ACS Appl. Mater. Inter.*, 2014, **6**, 2167.
- 117 S. Upadhyay, J. Shrivastava, A. Solanki, S. Choudhary, V. Sharma, P. Kumar, N. Singh, V. R. Satsangi, R. Shrivastav, U. V. Waghmare and S. Dass, *J. Phys. Chem. C*, 2011, **115**, 24373.
- 118 H. Mizoguchi, K. Ueda, M. Orita, S-C Moon, K. Kajihara, M. Hirano and H. Hosono, *Mater. Res. Bull.*, 2002, **37**, 2401.
- 119 K. Shimura and H. Yoshida, *Energy Environ. Sci.*, 2010, **3**, 615.
- 120 H. Zhang, G. Chen, Y. Li and Y. Teng, *Int. J. Hydrogen Energy*, 2010, **35**, 2713.
- 121 S. Nishimoto, M. Matsuda and M. Miyake, *Chem. Lett.*, 2006, **35**, 308.
- 122 H. Zhang, G. Chen, X. He and J. Xu, *J. Alloys Compd.*, 2012, **516**, 91.

- 123 D. Arney, T. Watkins and P. A. Maggard, *J. Am. Ceram. Soc.*, 2011, **94**, 1483.
- 124 C. Zhen, J. C. Yu, G. Liu and H-M. Cheng, *Chem. Commun.*, 2014, **50**, 10416.
- 125 K. Iwashina and A. Kudo, *J. Am. Chem. Soc.*, 2011, **133**, 13272.
- 126 H. Hayashi, Y. Hakuta and Y. Kurata, *J. Mater. Chem.*, 2004, **14**, 2046.
- 127 Q-P. Ding, Y-P. Yuan, X. Xiong, R-P. Li, H-B. Huang, Z-S. Li, T. Yu, Z-G. Zou and S-G. Yang, *J. Phys. Chem. C*, 2008, **112**, 18846.
- 128 J. Lan, X. Zhou, G. Liu, J. Yu, J. Zhang, L. Zhi and G. Nie, *Nanoscale*, 2011, **3**, 5161.
- 129 T. Zhang, K. Zhao, J. Yu, J. Jin, Y. Qi, H. Li, X. Hou and G. Liu, *Nanoscale*, 2013, **5**, 8375.
- 130 L. Yan, J. Zhang, X. Zhou, X. Wu, J. Lan, Y. Wang, G. Liu, J. Yu and L. Zhi, *Int. J. Hydrogen Energy*, 2013, **38**, 3554.
- 131 L. Jiang, Y. Qiu and Z. Yi, *J. Mater. Chem. A*, 2013, **1**, 2878.
- 132 L. Yan, T. Zhang, W. Lei, Q. Xu, X. Zhou, P. Xu, Y. Wang and G. Liu, *Catal. Today*, 2014, **224**, 140.
- 133 R. Wang, Y. Zhu, Y. Qiu, C-F. Leung, J. He, G. Liu and T-C Lau, *Chem. Eng. J.*, 2013, **226**, 123.
- 134 G. Li, Z. Yi, Y. Bai, W. Zhang and H. Zhang, *Dalton Trans.*, 2012, **41**, 10194.
- 135 X. Li, Z. Zhuang, W. li and Q. Li, *Catal. Lett.*, 2012, **142**, 901.
- 136 K. Katsumata, C. E. J. Cordonier, T. Shichi and A. Fujishima, *J. Am. Chem. Soc.*, 2009, **131**, 3856.
- 137 H. Shi, G. Chen and Z. Zou, *Appl. Catal. B: Environ.*, 2014, **156-157**, 378.
- 138 H. Shi, X. Li, H. Iwai, Z. Zou and J. Ye, *J. Phys. Chem. Solids*, 2009, **70**, 931.
- 139 B. Paul and K-H. Choo, *Catal. Today*, 2014, **230**, 138.
- 140 H. Shu, J. Xie, H. Xu, H. Li, Z. Gu, G. Sun and Y. Xu, *J. Alloys Compnd.*, 2010, **496**, 633.
- 141 W. Wu, S. Liang, Y. Chen, L. Shen, R. Yuan and L. Wu, *Mater. Res. Bull.*, 2013, **48**, 1618.
- 142 G. Li, S. Yan, Z. Wang, X. Wang, Z. Li, J. Ye and Z. Zou, *Dalton Trans.*, 2009, **40**, 8519.
- 143 D. Arney, C. Hardy, B. Greve and P. A. Maggard, *J. Photochem. Photobio. A: Chem.*, 2010, **214**, 54.
- 144 G. Li, T. Kato, D. Wang, Z. Zou and J. Ye, *Dalton Trans.*, 2009, **13**, 2423.
- 145 X. Xu, C. Randorn, P. Efstathiou and J. T.S. Irvine, *Nature Mater.*, 2012, **11**, 595.
- 146 P. Efstathiou, X. Xu, H. Menard and J. T.S. Irvine, *Dalton Trans.*, 2013, **42**, 7880.
- 147 F. Gao, X. Chen, K. Yin, S. Dong, Z. Ren, F. Yuan, T. Yu, Z. Zou and J-M. Liu, *Adv. Mater.*, 2007, **19**, 2889.
- 148 Y. Huo, M. Miao, Y. Zhang, J. Zhu and H. Li, *Chem. Commun.*, 2011, **47**, 2089.
- 149 C. M. Cho, J. H. Noh, I-S. Cho, J-S. An and K. S. Hong, *J. Am. Ceram. Soc.*, 2008, **91**, 3753.
- 150 S. Li, Y-H. Lin, B-P. Zhang, Y. Wang and C-W. Nan, *J. Phys. Chem. C*, 2010, **114**, 2903.
- 151 X. Xu, Y-H. Lin, P. Li, L. Shu and C-W. Nan, *J. Am. Ceram. Soc.*, 2011, **94**, 2296.
- 152 W. Ji, K. Yao, Y-F. Lim, Y. C. Liang and A. Suwardi, *Appl. Phys. Lett.*, 2013, **103**, 062901.
- 153 X. Y. Chen, T. Yu, F. Gao, H. T. Zhang, L. F. Liu, Y. M. Wang, Z. S. Li, Z. G. Zou and J. M. Liu, *Appl. Phys. Lett.*, 2007, **91**, 022114.
- 154 S. Li, J. Zhang, M. G. Kibria, Z. Mi, M. Chaker, D. Ma, R. Nechache and F. Rosei, *Chem. Commun.*, 2013, **49**, 5856.
- 155 Y. Huo, Y. Jin and Y. Zhang, *J. Mol. Catal. A: Chem.*, 2010, **331**, 15.
- 156 A. M. Schultz, Y. Zhang, P. A. Salvador and G. S. Rohrer, *ACS Appl. Mater. Inter.*, 2011, **3**, 1562.
- 157 Y-N. Feng, H-C. Wang, Y. Shen, Y-H. Lin and C-W. Nan, *Int. J. Appl. Ceram. Technol.*, 2014, **11**, 676.
- 158 Y-N. Feng, H-C. Wang, Y-D. Luo, Y. Shen and Y-H. Lin, *J. Appl. Phys.*, 2013, **113**, 146101.
- 159 H-C. Wang, Y-H. Lin, Y-N. Feng and Y. Shen, *J. Electroceram.*, 2013, **31**, 271.
- 160 Y-L. Pei and C. Zhang, *J. Alloys Compnd.*, 2013, **570**, 57.
- 161 R. Guo, L. Fang, W. Dong, F. Zheng and M. Shen, *J. Phys. Chem. C*, 2010, **114**, 21390.
- 162 F. Deganello, M. L. Tummino, C. Calabrese, M. L. Testa, P. Avetta, D. Fabbi, A. B. Prevot, E. Montoneri and G. Magnacca, *New J. Chem.*, 2015, **39**, 877.
- 163 L. Li, X. Wang and Y. Zhang, *Mater. Res. Bull.*, 2014, **50**, 18.
- 164 S. Thirumalairajan, K. Girija, V. R. Mastelaro and N. Ponpandian, *New J. Chem.*, 2014, **38**, 5480.
- 165 K. M. Parida, K. H. Reddy, S. Martha, D. P. Das and N. Biswal, *Int. J. Hydrogen Energy*, 2010, **35**, 12161.
- 166 S. N. Tijare, M. V. Joshi, P. S. Padole, P. A. Mangrulkar, S. S. Rayalu and N. K. Labhsetwar, *Int. J. Hydrogen Energy*, 2012, **37**, 10451.
- 167 S. Thirumalairajan, K. Girija, I. Ganesh, D. Mangalaraj, C. Viswanathan and A. Balamurugan, *Chem. Eng. J.*, 2012, **209**, 420.
- 168 R. Hu, C. Li, X. Wang, Y. Sun, H. Jia, H. Su and Y. Zhang, *Catal. Commun.*, 2012, **29**, 35.
- 169 S. Thirumalairajan, K. Girija, N. Y. Hebalkar, D. Mangalaraj, C. Viswanathan and N. Ponpandian, *RSC Advances*, 2013, **3**, 7549.
- 170 F-T. Li, Y. Liu, R-H. Liu, Z-M. Sun, D-S. Zhao and C-G. Kou, *Mater. Lett.*, 2010, **64**, 223.
- 171 L. Li, M. Zhang, P. Tian, W. Gu and X. Wang, *Ceram. Inter.*, 2014, **40**, 13813.
- 172 L. Jia, T. Ding, Q. Li and Y. Tang, *Catal. Commun.*, 2007, **8**, 963.
- 173 M. Ghaffari, P. Y. Tan, M. E. Oruc, O. K. Tan, M. S. Tse and M. Shannon, *Catal. Today*, 2011, **161**, 70.
- 174 P. Dhanasekaran and N. M. Gupta, *Int. J. Hydrogen Energy*, 2012, **37**, 4897.
- 175 T. Choi, S. Lee, Y. Kiryukhin and S. W. Cheong, *Science*, 2009, **324**, 63.
- 176 M. Alexe and D. Hesse, *Nature Commun.*, 2011, **2**, 256.
- 177 T-N Ye, M. Xu, W. Fu, Y-Y. Cai, X. Wei, K-X. Wang, Y-N. Zhao, X-H. Li and J-S. Chen, *Chem. Commun.*, 2014, **50**, 3021.
- 178 N. Prastomo, N. H. B. Zakaria, G. Kawamura, H. Muto, M. Sakai and A. Matsuda, *J. Eur. Ceram. Soc.*, 2011, **31**, 2699.
- 179 Y. Yuan, X. Zhang, L. Liu, X. Jiang, J. Lv, Z. Li and Z. Zou, *Int. J. Hydrogen Energy*, 2008, **33**, 5941.
- 180 X. Ma, J. Zhang, H. Li, B. Duan, L. Guo, M. Que and Y. Wang, *J. Alloys Compnd.*, 2013, **580**, 564.

- 181 Z. Khan and M. Qureshi, *Catal. Commun.*, 2012, **28**, 82.
- 182 W. F. Zhang, J. Tang and J. Ye, *Chem. Phys. Lett.*, 2006, **418**, 174.
- 183 D. Chen and J. Ye, *Chem. Mater.*, 2007, **19**, 4585.
- 184 C. W. Lee, D. W. Kim, I. S. Cho, S. Park, S. S. Shin, S. W. Seo and K. S. Hong, *Int. J. Hydrogen Energy*, 2012, **37**, 10557.
- 185 W. Wang, S. Liang, K. Ding, J. Bi, J. C. Yu, P. K. Wong and L. Wu, *J. Mater. Sci.*, 2014, **49**, 1893.
- 186 W. Zhang, J. Tang and J. Ye, *J. Mater. Res.*, 2007, **22**, 1859.
- 187 Y. Yuan, J. Zheng, X. Zhang, Z. Li, T. Yu, J. Ye and Z. Zou, *Solid State Ionics*, 2008, **178**, 1711.
- 188 W. Y. Jung and S-S. Hong, *J. Ind. Eng. Chem.*, 2013, **19**, 157.
- 189 B. Dong, Z. Li, Z. Li, X. Xu, M. Song, W. Zheng, C. Wang, S. S. Al-Deyab and M. El-Newehy, *J. Am. Ceram. Soc.*, 2010, **93**, 3587.
- 190 S. Fu, H. Niu, Z. Tao, J. Song, C. Mao, S. Zhang, C. Chen and D. Wang, *J. Alloys Compnd.*, 2013, **576**, 5.
- 191 L. Jia, J. Li, W. Fang, H. Song, Q. Li and Y. Tang, *Catal. Commun.*, 2009, **10**, 1230.
- 192 L. Jia, J. Li and W. Fang, *Catal. Commun.*, 2009, **11**, 87.
- 193 Y. Li, S. Yao, W. Wen, L. Xue and Y. Yan, *J. Alloys Compnd.*, 2010, **491**, 560.
- 194 L. Jia, J. Li and W. Fang, *J. Alloys Compnd.*, 2010, **489**, L13.
- 195 J. Li, G. Wang, H. Wang, C. Tang, Y. Wang, C. Liang, W. Cai and L. Zhang, *J. Mater. Chem.*, 2009, **19**, 2253.
- 196 L. Wang and W. Wang, *Int. J. Hydrogen Energy*, 2012, **37**, 3041.
- 197 Z. Ai, G. Lu and S. Lee, *J. Alloys Compnd.*, 2014, **613**, 260.
- 198 C-C. Hu, Y-L. Lee and H. Teng, *J. Mater. Chem.*, 2011, **21**, 3824.
- 199 M. Ghiasi and A. M. Malekzadeh, *Sep. Purif. Technol.*, 2014, **134**, 12.
- 200 M. Yazdanbakhsh, H. Tavakkoli and S. M. Hosseini, *Desalination*, 2011, **281**, 388.
- 201 H. Tavakkoli, D. Beiknejad and T. Tabari, *Desalination and water treatment*, 2014, **52**, 7377.
- 202 H. B. Sales, V. Bouquet, S. Deputier, S. Ollivier, F. Gouttefangeas, M. Guilloux-Viry, V. Dorcet, I. T. Weber, A. G. de Souza and I. M. G. dos Santos, *Solid State Sci.*, 2014, **28**, 67.
- 203 T. Ishihara, H. Nishiguchi, K. Fukamachi and Y. Takita, *J. Phys. Chem. B*, 1999, **103**, 1.
- 204 H. Hagiwara, N. Ono, T. Inoue, H. Matsumoto and T. Ishihara, *Angew. Chem. Int. Ed.*, 2006, **45**, 1420.
- 205 H. Hagiwara, T. Inoue, K. Kaneko and T. Ishihara, *Chem. Eur. J.*, 2009, **15**, 12862.
- 206 H. Hagiwara, T. Inoue, S. Ida and T. Ishihara, *Phys. Chem. Chem. Phys.*, 2011, **13**, 18031.
- 207 J. Yin, Z. Zou and J. Ye, *J. Phys. Chem. B*, 2003, **107**, 4936.
- 208 J. Yin, Z. Zou and J. Ye, *J. Phys. Chem. B*, 2003, **107**, 61.
- 209 J. Yin, Z. Zou and J. Ye, *J. Phys. Chem. B*, 2004, **108**, 8888.
- 210 J. Yin, Z. Zou and J. Ye, *J. Phys. Chem. B*, 2004, **108**, 12790.
- 211 C-H. Lu, C-Y. Hu and C-H. Wu, *Mater. Lett.*, 2007, **61**, 3959.
- 212 S. G. Hur, T. W. Kim, S-J. Hwang, H. Park, W. Choi, S. J. Kim and J-H. Choy, *J. Phys. Chem. B*, 2005, **109**, 15001.
- 213 S. G. Hur, T. W. Kim, S-J. Hwang and J-H. Choy, *J. Photochem. Photobiol. A: Chem.*, 2006, **183**, 176.
- 214 S. W. Bae, P. H. Borse and J. S. Lee, *Appl. Phys. Lett.*, 2008, **92**, 104107.
- 215 M. Ghaffari, H. Huang, P. Y. Tan and O. K. Tan, *Powder Tech.*, 2012, **225**, 221.
- 216 H-X. Chen, Z-X. Wei, Y. Wang, W-W. Zeng and C-M. Xiao, *Mater. Chem. Phys.*, 2011, **130**, 1387.
- 217 C. Li, F. F. Liu, J. Qiao, C. Li and X. H. Huang, *Adv. Mater. Res.*, 2014, **968**, 58.
- 218 E. D. Jeong, S. M. Yu, J. Y. Yoon, J. S. Bae, C. R. Cho, K. T. Lim, R. Dom, P. H. Borse and H. G. Kim, *J. Ceram. Process Res.*, 2012, **13**, 305.
- 219 J. Li, L. Jia, W. Fang and J. Zeng, *Int. J. Hydrogen Energy*, 2010, **35**, 5270.
- 220 J. Li, J. Zeng, L. Jia and W. Fang, *Int. J. Hydrogen Energy*, 2010, **35**, 12733.
- 221 R. Hu, C. Li, X. Wang, Y. Sun, H. Jia, H. Su and Y. Zhang, *Catal. Commun.*, 2012, **29**, 35.
- 222 Y. Yuan, Z. Zhao, J. Zheng, M. Yang, L. Qiu, Z. Li and Z. Zou, *J. Mater. Chem.*, 2010, **20**, 6772.
- 223 W. Sun, S. Zhang, C. Wang, Z. Liu and Z. Mao, *Catal. Lett.*, 2001, **44**, 2203.
- 224 W. Zhang, J. Chen, X. An, Q. Wang, L. Fan, F. Wang, J. Deng, R. Yu and X. Xing, *Dalton Trans.*, 2014, **43**, 9255.
- 225 H. W. Kang, S. N. Lim and S. B. Park, *Int. J. Hydrogen Energy*, 2012, **37**, 4026.
- 226 L. Xu, C. Li, W. Shi, J. Guan and Z. Sun, *J. Mol. Catal. A: Chem.*, 2012, **360**, 42.
- 227 L. Ni, M. Tanabe and H. Irie, *Chem. Commun.*, 2013, **49**, 10094.
- 228 F. Zhang, A. Yamakata, K. Maeda, Y. Moriya, T. Takata, J. Kubota, K. Teshima, S. Oishi and K. Domen, *J. Am. Chem. Soc.*, 2012, **134**, 8348.
- 229 A. Kasahara, K. Nukumizu, T. Takata, J. N. Kondo, M. Hara, H. Kobayashi and K. Domen, *J. Phys. Chem. B*, 2003, **107**, 791.
- 230 A. Kasahara, K. Nukumizu, G. Hitoki, T. Takata, J. N. Kondo, M. Hara, H. Kobayashi and K. Domen, *J. Phys. Chem. A*, 2002, **106**, 6750.
- 231 A. E. Maegli, S. Pokrant, T. Hisatomi, M. Trottmann and K. Domen, A. Weidenkaff, *J. Phys. Chem. C*, 2014, **118**, 16344.
- 232 A. Yamakata, M. Kawaguchi, N. Nishimura, T. Minegishi, J. Kubota and K. Domen, *J. Phys. Chem. C*, 2014, **118**, 23897.
- 233 M. Matsukawa, R. Ishikawa, T. Hisatomi, Y. Moriya, N. Shibata, J. Kubota, Y. Ikuhara and K. Domen, *Nano Lett.*, 2014, **14**, 1038.
- 234 R. Aguiar, A. Kalytta, A. Reller, A. Weidenkaff and S. G. Ebbinghaus, *J. Mater. Chem.*, 2008, **18**, 4260.
- 235 C. L. Paven-Thivet, A. Ishikawa, A. Ziani, L. L. Gendre, M. Yoshida, J. Kubota, F. Tessier and K. Domen, *J. Phys. Chem. C*, 2009, **113**, 6156.
- 236 C. M. Leroy, A. E. Maegli, K. Sivula, T. Hisatomi, N. Xanthopoulos, E. H. Ota, S. Yoon, A. Weidenkaff, R. Sanjines and M. Gratzel, *Chem. Commun.*, 2012, **48**, 820.
- 237 T. Minegishi, N. Nishimura, J. Kubota and K. Domen, *Chem. Sci.*, 2013, **4**, 1120.
- 238 C. Izawa and T. Watanabe, *Chem. Lett.*, 2014, **43**, 1441.
- 239 J. Feng, W. Luo, T. Fang, H. Lv, Z. Wang, J. Gao, W. Liu, T. Yu, Z. Li and Z. Zou, *Adv. Funct. Mater.*, 2014, **24**, 3535.



- 240 N. Nishimura, B. Raphael, K. Maeda, L. L. Gendre, R. Abe, J. Kubota and K. Domen, *Thin Solid Films*, 2010, **518**, 5855.
- 241 D. Yamasita, T. Takata, M. Hara, J. N. Kondo and K. Domen, *Solid State Ionics*, 2004, **172**, 591.
- 242 M. Higashi, R. Abe, K. Teramura, T. Takata, B. Ohtani and K. Domen, *Chem. Phys. Lett.*, 2008, **452**, 120.
- 243 M. Higashi, R. Abe, T. Takata and K. Domen, *Chem. Mater.*, 2009, **21**, 1543.
- 244 K. Maeda, D. Lu and K. Domen, *Angew. Chem. Int. Ed.*, 2013, **52**, 6488.
- 245 M. Higashi, K. Domen and R. Abe, *J. Am. Chem. Soc.*, 2013, **135**, 10238.
- 246 B. Siritanaratkul, K. Maeda, T. Hisatomi and K. Domen, *ChemSusChem*, 2011, **4**, 74.
- 247 K. Maeda, M. Higashi, B. Siritanaratkul, R. Abe and K. Domen, *J. Am. Chem. Soc.*, 2011, **133**, 12334.
- 248 D. Wang, T. Kato and J. Ye, *J. Am. Chem. Soc.*, 2008, **130**, 2724.
- 249 D. Wang, T. Kako and J. Ye, *J. Phys. Chem. C*, 2009, **113**, 3785.
- 250 T. Matoba, K. Maeda and K. Domen, *Chem. Eur. J.*, 2011, **17**, 14731.
- 251 K. Maeda, D. Lu and K. Domen, *ACS Catal.*, 2013, **3**, 1026.
- 252 K. Maeda and K. Domen, *Angew. Chem.*, 2012, **124**, 10003.
- 253 K. Maeda and K. Domen, *J. Catal.*, 2014, **310**, 67.
- 254 C. Pan, T. Takata, M. Nakabayashi, T. Matsumoto, N. Shibata, Y. Ikuhara and K. Domen, *Angew. Chem. Int. Ed.*, 2015, **54**, 2955.
- 255 P. Wu, J. Shi, Z. Zhou, W. Tang and L. Guo, *Int. J. Hydrogen Energy*, 2012, **37**, 13704.
- 256 W. Luo, Z. Li, X. Jiang, T. Yu, L. Liu, X. Chen, J. Ye and Z. Zou, *Phys. Chem. Chem. Phys.*, 2008, **10**, 6717.
- 257 Z-X. Wei, C-M. Xiao, W-W. Zeng and J-P. Liu, *J. Mol. Catal. A: Chem.*, 2013, **370**, 35.
- 258 P. Kanhere, J. Nisar, Y. Tang, B. Pathak, R. Ahuja, J. Zheng and Z. Chen, *J. Phys. Chem. C*, 2012, **116**, 22767.
- 259 J. Shi, J. Ye, Z. Zhou, M. Li and L. Guo, *Chem. Eur. J.*, 2011, **17**, 7858.
- 260 X. Qiu, M. Miyauchi, H. Yu, H. Irie and K. Hashimoto, *J. Am. Chem. Soc.*, 2010, **132**, 15259.
- 261 Z. G. Yi and J. H. Ye, *J. Appl. Phys.*, 2009, **106**, 074910.
- 262 H. Liu, Y. Guo, B. Guo, W. Dong and D. Zhang, *J. Eur. Ceram. Soc.*, 2012, **32**, 4335.
- 263 M. Lv, Y. Xie, Y. Wang, X. Sun, F. Wu, H. Chen, S. Wang, C. Shen, Z. Chen, S. Ni, G. Liu and X. Xu, *Phys. Chem. Chem. Phys.*, 2015, **17**, 26320.
- 264 K-i. Shimizu, Y. Tsuji, T. Hatamachi, K. Toda, T. Kodama, M. Sato and Y. Kitayama, *Phys. Chem. Chem. Phys.*, 2004, **6**, 1064.
- 265 K-i. Shimizu, S. Itoh, T. Hatamachi, T. Kodama, M. Sato and K. Toda, *Chem. Mater.*, 2005, **17**, 5161.
- 266 W. Yao and J. Ye, *Chem. Phys. Lett.*, 2007, **435**, 96.
- 267 Y. Wang, C. Wang, L. Wang, Q. Hao, X. Zhu, X. Chen and K. Tang, *RSC Adv.*, 2014, **4**, 4047.
- 268 Z. Liang, K. Tang, Q. Shao, G. Li, S. Zeng and H. Zheng, *J. Solid State Chem.*, 2008, **181**, 964.
- 269 Y. Li, G. Chen, C. Zhou and Z. Li, *Catal. Lett.*, 2008, **123**, 80.
- 270 T. Takata, Y. Furumi, K. Shinohara, A. Tanaka, M. Hara, J. N. Kondo and K. Domen, *Chem. Mater.*, 1997, **9**, 1063.
- 271 S. Ikeda, M. Hara, J. N. Kondo and K. Domen, *Chem. Mater.*, 1998, **10**, 72.
- 272 Y. Huang, J. Wu, Y. Wie, J. Lin and M. Huang, *J. Alloys Compnd.*, 2008, **456**, 364.
- 273 V. Kumar and G. S. Uma, *J. Hazard. Mater.*, 2011, **189**, 502.
- 274 C. T. K. Thaminimulla, T. Takata, M. Hara, J. N. Knodo and K. Domen, *J. Catal.*, 2000, **196**, 362.
- 275 Y-H. Yang, Q-Y. Chen, Z-L. Yin and J. Li, *Appl. Sur. Sci.*, 2009, **255**, 8419.
- 276 Y. Yang, Q. Chen, Z. Yin and J. Li, *J. Alloys Compnd.*, 2009, **488**, 364.
- 277 Y. Huang, Y. Wei, S. Cheng, L. Fan, Y. Li, J. Lin and J. Wu, *Sol. Energy Mater. Sol. Cells*, 2010, **94**, 761.
- 278 B. Wang, C. Li, D. Hirabayashi and K. Suzuki, *Int. J. Hydrogen Energy*, 2010, **35**, 3306.
- 279 H. Jeong, T. Kim, D. Kim and K. Kim, *Int. J. Hydrogen Energy*, 2006, **31**, 1142.
- 280 Y-G. Ko and W-Y. Lee, *Catal. Lett.*, 2002, **83**, 157.
- 281 J. Sato, N. Saito, H. Nishiyama and Y. Inoue, *J. Phys. Chem. B*, 2001, **105**, 6061.
- 282 X. Sun, Y. Xie, F. Wu, H. Chen, M. Lv, S. Ni, G. Liu and X. Xu, *Inorg. Chem.*, 2015, **54**, 7445.
- 283 S. Nishimoto, Y. Okazaki, M. Matsuda and M. Miyake, *J. Ceram. Soc. Jpn.*, 2009, **117**, 1175.
- 284 D. Arney, L. Fuoco, J. Boltersdorf and P. A. Maggard, *J. Am. Ceram. Soc.*, 2012, **96**, 1158.
- 285 A. Kudo and S. Hijii, *Chem. Lett.*, 1999, 1103.
- 286 J. Tang, Z. Zou and J. Ye, *Cata. Lett.*, 2004, **92**, 53.
- 287 J. Yu and A. Kudo, *Chem. Lett.*, 2005, **34**, 1528.
- 288 Y. Shimodaira, H. Kato, H. Kobayashi and A. Kudo, *J. Phys. Chem. B*, 2006, **110**, 17790.
- 289 L. Zhang, H. Wang, Z. Chen, P. K. Wong and J. Liu, *Appl. Catal. B*, 2011, **106**, 1.
- 290 L. Zhang and Y. Zhu, *Catal. Sci. Technol.*, 2012, **2**, 694.
- 291 Y. Feng, Q. Wu, G. Zhang and Y. Sun, *Prog. Chem.*, 2012, **24**, 2124.
- 292 N. Zhang, R. Ciriminna, M. Ragliaro and Y-J. Xu, *Chem. Soc. Rev.*, 2014, **43**, 5276.
- 293 H. G. Kim, D. W. Hwang and J. S. Lee, *J. Am. Chem. Soc.*, 2004, **126**, 8912.
- 294 H. G. Kim, O. S. Becker, J. S. Jang, S. M. Ji, P. H. Borse and J. S. Lee, *J. Solid State Chem.*, 2006, **179**, 1214.
- 295 H. G. Kim, P. H. Borse, J. S. Jang, E. D. Jeong, J. S. Lee, *Mater. Lett.*, 2008, **62**, 1427.
- 296 W. Wu, S. Liang, Y. Chen, L. Shen, H. Zheng and L. Wu, *Catal. Commun.*, 2012, **17**, 39.
- 297 J-H. Kim, K-T. Hwang, U-S. Kim and Y-M. Kang, *Ceram. Int.*, 2012, **38**, 3901.
- 298 W. Wu, S. Liang, X. Wang, J. Bi, P. Liu and L. Wu, *J. Solid State Chem.*, 2011, **184**, 81.
- 299 Y. Li, G. Chen, H. Zhang and Z. Lv, *Int. J. Hydrogen Energy*, 2010, **35**, 2652.
- 300 K. Iizuka, T. Wato, Y. Miseki, K. Saito and A. Kudo, *J. Am. Chem. Soc.*, 2011, **133**, 20863.
- 301 S. Sun, W. Wang, H. Xu, L. Zhou, M. Shang and L. Zhang, *J. Phys. Chem. C*, 2008, **112**, 17835.
- 302 J. S. Jang, S. S. Yoon, P. H. Borse, K. T. Lim, T. E. Hong, E. D. Jeong, O-S. Jung, Y. B. Shim and H. G. Kim, *J. Ceram. Soc. Jpn.*, 2009, **117**, 1268.
- 303 G. Naresh and T. K. Mandal, *ACS Appl. Mater. Inter.*, 2014, **6**, 21000.
- 304 W. Chen, C. Li, H. Gao, J. Yuan, W. Shangguan, J. Su and Y. Sun, *Int. J. Hydrogen Energy*, 2012, **37**, 12846.
- 305 H. Zhang, G. Chen and X. Li, *Solid State Ionics*, 2009, **180**, 1599.

- 306 D. Wang, K. Tang, Z. Liang and H. Zheng, *J. Solid State Chem.*, 2010, **183**, 361.
- 307 M. Machida, J-i. Yabunaka and T. Kijima, *Chem. Commun.*, 1999, 1939.
- 308 M. Machida, J-i. Yabunaka and T. Kijima, *Chem. Mater.*, 2000, **12**, 812.
- 309 M. Machida, K. Miyazaki, S. Matsushima and M. Arai, *J. Mater. Chem.*, 2003, **13**, 1433.
- 310 M. Machida, T. Mitsuyama, K. Ikeue, S. Matsushima and M. Arai, *J. Phys. Chem. B*, 2005, **109**, 7801.
- 311 T. Mitsuyama, A. Tsutsumi, T. Hata, K. Ikeue and M. Machida, *Bull. Chem. Soc. Jpn.*, 2008, **81**, 401.
- 312 X. Zong, C. Sun, Z. Chen, A. Mukherji, H. Wu, J. Zou, S. C. Smith, G. Q. Lu and L. Wang, *Chem. Commun.*, 2011, **47**, 6293.
- 313 J. Yoshimura, Y. Ebina, J. Kondo, K. Domen and A. Tanaka, *J. Phys. Chem.*, 1993, **97**, 1970.
- 314 Y. Ebina, A. Tanaka, J. N. Kondo and K. Domen, *Chem. Mater.*, 1996, **8**, 2534.
- 315 Y. Ebina, T. Sakaki, M. Harada and M. Watanabe, *Chem. Mater.*, 2002, **14**, 4390.
- 316 Y. Ebina, N. Sakai and T. Sasaki, *J. Phys. Chem. B*, 2005, **109**, 17212.
- 317 T. Oshima, D. Lu, O. Ishitani and K. Maeda, *Angew. Chem. Int. Ed.*, 2015, **54**, 2698.
- 318 Y. Huang, Y. Li, Y. Wie, M. Huang and J. Wu, *Sol. Energy Mater. Sol. Cells*, 2011, **95**, 1019.
- 319 Y. Wei, X. Zhang, J. Xu, J. Wang, Y. Huang, L. Fan and J. Wu, *Appl. Catal. B: Environ.*, 2014, **147**, 920.
- 320 K. Maeda and T. E. Mallouk, *J. Mater. Chem.*, 2009, **19**, 4813.
- 321 K. Maeda, M. Eguchi, W. Justin Youngblood and T. E. Mallouk, *Chem. Mater.*, 2009, **21**, 3611.
- 322 K. Maeda, M. Eguchi, S-H. A. Lee, W. Justin Youngblood, H. Hata and T. E. Mallouk, *J. Phys. Chem. C*, 2009, **113**, 7962.
- 323 D. Arney and P. A. Muggard, *ACS Catal.*, 2012, **2**, 1711.
- 324 J. Boltersdorf and P. A. Muggard, *ACS Catal.*, 2013, **3**, 2547.
- 325 Y. Huang, Y. Wei, L. Fan, M. Huang, J. Lin and J. Wu, *Int. J. Hydrogen Energy*, 2009, **34**, 5318.
- 326 Y. Huang, J. Li, Y. Wie, Y. Li, J. Lin and J. Wu, *J. Hazard. Mater.*, 2009, **166**, 103.
- 327 Y. Miseki, H. Kato and A. Kudo, *Chem. Lett.*, 2006, **35**, 1052.
- 328 T-G. Xu, C. Zhang, X. Shao, K. Wu and Y-F. Zhu, *Adv. Funct. Mater.*, 2006, **16**, 1599.
- 329 R. Marschall, J. Soldat and M. Wark, *Photochem. Photobiol. Sci.*, 2013, **12**, 671.
- 330 Y. Miseki, H. Kato and A. Kudo, *Energy. Environ. Sci.*, 2009, **2**, 306.
- 331 A. Mukherji, C. Sun, S. C. Smith, G. Q. Lu and L. Wang, *J. Phys. Chem. C*, 2011, **115**, 15674.
- 332 S. Chen, J. Yang, C. Ding, R. Li, S. Jin, D. Wang, H. Han, F. Zhang and C. Li, *J. Mater. Chem. A*, 2013, **1**, 5651.
- 333 H. G. Kim, D. W. Hwang, J. Kim, Y. G. Kim and J. S. Lee, *Chem. Commun.*, 1999, 1077.
- 334 D. Chen and J. Ye, *Chem. Mater.*, 2009, **21**, 2327.
- 335 H. Kato and A. Kudo, *J. Photochem. Photobio. A: Chem.*, 2001, **145**, 129.
- 336 M. Yoshino, M. Kakihana, W. S. Cho, H. Kato and A. Kudo, *Chem. Mater.*, 2002, **14**, 3369.
- 337 A. Kudo, H. Kato and S. Nakagawa, *J. Phys. Chem. B*, 2000, **104**, 571.
- 338 A. Mukherji, B. Seger, G. Q. Lu, L. Wang, *ACS Nano*, 2011, **5**, 3483.
- 339 H. G. Kim, D. W. Hwang, S. W. Bae, J. H. Jung and J. S. Lee, *Catal. Lett.*, 2003, **91**, 193.
- 340 S. M. Ji, H. Jun, J. S. Jang, H. C. Son, P. H. Borse and J. S. Lee, *J. Photochem. Photobio. A: Chem.*, 2007, **189**, 141.
- 341 D. Arney, B. Porter, B. Greve and P. A. Muggard, *J. Photochem. Photobio. A: Chem.*, 2008, **199**, 230.
- 342 H. Song, T. Peng, P. Cai, H. Yi and C. Yan, *Catal. Lett.*, 2007, **113**, 54.
- 343 K. W. Li, Y. Wang, H. Wang, M. Zhu and H. Yan, *Nanotechnology*, 2006, **17**, 4863.
- 344 J. Kim, D. W. Hwang, H-G. Kim, S. W. Bae, S. M. Ji and J. S. Lee, *Chem. Commun.*, 2002, 2488.
- 345 D. W. Hwang, J. S. Lee, W. Li and S. H. Oh, *J. Phys. Chem. B*, 2003, **107**, 4963.
- 346 J. Kim, D. W. Hwang, H-G. Kim, S. W. Bae, J. S. Lee, W. Li and S. H. Oh, *Top. Catal.*, 2005, **35**, 295.
- 347 D. W. Hwang, H. G. Kim, J. S. Lee, J. Kim, W. Li and S. H. Oh, *J. Phys. Chem. B*, 2005, **109**, 2093.
- 348 D. W. Hwang, H. G. Kim, J. S. Jang, S. W. Bae, S. M. Ji and J. S. Lee, *Catal. Today*, 2004, **93-95**, 845.
- 349 F. Meng, Z. Hong, J. Arndt, M. Li, M. Zhi, F. Yang and N. Wu, *Nano Res.*, 2012, **5**, 213.
- 350 Q. Wang, T. Hisatomi, Y. Moriya, K. Maeda and K. Domen, *Catal. Sci. Technol.*, 2013, **3**, 2098.
- 351 W. Lin, C. Cheng, C. Hu and H. Teng, *Appl. Phys. Lett.*, 2006, **89**, 211904.
- 352 K. S. Knight and B. J. Kennedy, *Solid State Sci.*, 2015, **43**, 15.
- 353 Z. Li, G. Chen and J. Liu, *Solid State Commun.*, 2007, **143**, 295.
- 354 P. Li, S. Ouyang, G. Xi, T. Kako and J. Ye, *J. Phy. Chem. C*, 2012, **116**, 7621.
- 355 X. Liu and K. Sohlberg, *Comput. Mater. Sci.*, 2015, **103**, 1.
- 356 H. W. Eng, P. W. Barnes, B. M. Auer and P. M. Woodward, *J. Solid State Chem.*, 2003, **175**, 94.
- 357 M. Yashima and S. Matsuyama, *J. Phys. Chem. C*, 2012, **116**, 24902.
- 358 I. E. Castelli, J. M. Garcia-Lastra, F. Huser, K. S. Thygesen and K. W. Jacobsen, *New J. Phys.*, 2013, **15**, 690.
- 359 W. Li, E. Ionescu, R. Riedel and A. Gurlo, *J. Mater. Chem. A*, 2013, **1**, 12239.
- 360 A. Sayede, R. Khenata, A. Chahed and O. Benhelal, *J. Appl. Phys.*, 2013, **113**, 88.
- 361 A. V. Bandura, R. A. Evarestov and Y. F. Zhukovskii, *RSC Adv.*, 2015, **5**, 24115.
- 362 M. Machida, J. Yabunaka, T. Kijima, S. Matsushima and M. Arai, *Int. J. Inorg. Mater.*, 2001, **3**, 545.
- 363 D. Li, J. Zheng and Z. Zou, *J. Phys. Chem. Solids*, 2006, **67**, 801.
- 364 T. Hatakeyama, S. Takeda, F. Ishikawa, A. Ohmura, A. Nakayama, Y. Yamada, A. Matsushita and J. Ye, *J. Ceram. Soc. Jpn.*, 2010, **118**, 91.
- 365 J. M. Ramirez-de-Arellano, S. Ruiz-Chavarria, H. Valencia-Sanchez, G. Tavizon and P. de la Mora, *Comput. Mater. Sci.*, 2014, **93**, 160.
- 366 Y. Li, G. Chen, H. Zhang, Z. Li and J. Sun, *J. Solid. State Chem.*, 2008, **181**, 2653.
- 367 B. Xu, W. Zhang, X. Liu, J. Yin and Z. Liu, *J. Mater. Res.*, 2007, **22**, 2185.
- 368 K. G. Kanade, J. O. Baeg, K. J. Kong, B. B. Kale, S. M. Lee, S. J. Moon, C. W. Lee and S. Yoon, *Int. Hydrogen Energy*, 2008, **33**, 6904.
- 369 Y. Li, G. Chen, H. Zhang and Z. Li, *J. Phys. Chem. Solids*, 2009, **70**, 536.
- 370 C. Tablero, *J. Alloy Compd.*, 2015, **639**, 203.
- 371 W. Wang, S. Liang, K. Ding, J. Bi, J. Yu, P. Wong and L. Wu, *J. Mater. Sci.*, 2014, **49**, 1893.

- 372 S. Ji, P. H. Borse, H. G. Kim, D. W. Hwang, J. S. Jang, S. W. Bae and J. S. Lee, *Phys. Chem. Chem. Phys.*, 2005, **7**, 1315.
- 373 Y. Huang, Y. Wei, S. Cheng, L. Fan, Y. Li, J. Lin and J. Wu, *Sol. Energy Mater. Sol. Cells*, 2010, **94**, 761.
- 374 T. Onishi, *Top. Catal.*, 2010, **53**, 566.
- 375 N. Li and K. Yao, *Aip Adv.*, 2012, **2**, 47803.
- 376 J. Nisar, B. Pathak and R. Ahuja, *Appl. Phys. Lett.*, 2012, **100**, 181903.
- 377 J. Nisar, B. Pathak, B. C. Wang, T. W. Kang and R. Ahuja, *Phys. Chem. Chem. Phys.*, 2012, **14**, 4891.
- 378 M. R. Pai, J. Majeed, A. M. Banerjee, A. Arya, S. Bhattacharya, R. Rao and S. R. Bharadwaj, *J. Phys. Chem. C*, 2012, **116**, 1458.
- 379 P. Liu, J. Nisar, R. Ahuja and B. Pathak, *J. Phys. Chem. C*, 2013, **117**, 5043.
- 380 P. Liu, J. Nisar, B. Pathak and R. Ahuja, *Phys. Chem. Chem. Phys.*, 2013, **15**, 17150.
- 381 P. Liu, J. Nisar, B. S. Sa, B. Pathak and R. Ahuja, *J. Phys. Chem. C*, 2013, **117**, 13845.
- 382 J. Yun, Z. Zhang, J. Yan and W. Zhao, *Thin Solid Films*, 2013, **542**, 276.
- 383 H. Chen and N. Umezawa, *Int. J. Photoenergy*, 2014, **2014**, 20964.
- 384 Z. Guo, B. S. Sa, B. Pathak, J. Zhou, R. Ahuja and Z. Sun, *Int. J. Hydrogen Energy*, 2014, **39**, 2042.
- 385 S. Hu, L. Jia, B. Chi, J. Pu and L. Jian, *J. Power Sources*, 2014, **266**, 304.
- 386 M. Al-Hadidi, J. P. Goss, P. R. Briddon, R. Al-Hamadany, M. Ahmed and M. J. Rayson, *Model. Simul. Mater. Sc.*, 2015, **23**, 1.
- 387 Z. Ma, K. Wu, R. Sa, Q. Li, C. He and Z. Yi, *Int. J. Hydrogen Energy*, 2015, **40**, 980.
- 388 A. Slassi, *Mat. Sci. Semicon. Pro.*, 2015, **32**, 100.
- 389 J. Zhang, W. Dang, Z. Ao, S. K. Cushing and N. Wu, *Phys. Chem. Chem. Phys.*, 2015, **17**, 8994.
- 390 F. Wu, M. Lv, X. Sun, Y. Xie, H. Chen, S. Ni, G. Liu and X. Xu, *Chemcatchem*, 2016, **8**, 615.
- 391 A. Ishikawa, T. Takata, T. Matsumura, J. N. Kondo, M. Hara, H. Kobayashi and K. Domen, *J. Phys. Chem. B*, 2004, **108**, 2637.
- 392 S. G. Ebbinghaus, H. P. Abicht, R. Dronskowski, T. Muller, A. Reller and A. Weidenkaff, *Prog. Solid State Ch.*, 2009, **37**, 173.
- 393 M. Yashima, M. Saito, H. Nakano, T. Takata, K. Ogisu and K. Domen, *Chem. Commun.*, 2010, **46**, 4704.
- 394 S. Balaz, S. H. Porter, P. M. Woodward and L. J. Brinson, *Chem. Mater.*, 2013, **25**, 3337.
- 395 M. Yashima, U. Fumi, H. Nakano, K. Omoto and J. R. Hester, *J. Phys. Chem. C*, 2013, **117**, 18529.
- 396 A. Fuertes, *Mater. Horiz.*, 2015, **2**, 453.
- 397 Q. Fu, T. He, J. Li and G. Yang, *J. Appl. Phys.*, 2012, **112**, 104322.
- 398 Q. Fu, J. Li, T. He and G. Yang, *J. Appl. Phys.*, 2013, **113**, 104303.
- 399 Y. Zhu, Y. Dai, K. Lai, Z. Li and B. Huang, *J. Phys. Chem. C*, 2013, **117**, 5593.
- 400 Z. Shao, S. Saitzek, J. F. Blach, A. Sayede, P. Roussel and R. Desfeux, *Eur. J. Inorg. Chem.*, 2011, **42**, 3569.
- 401 Y. Wu and G. Ceder, *J. Phys. Chem. C*, 2013, **117**, 24710.
- 402 R. Asahi, T. Morikawa, H. Irie and T. Ohwaki, *Chem. Rev.*, 2014, **114**, 9824.
- 403 Y. Mi, S. Wang, J. Chai, J. Pan, C. H. A. Huan, Y. Feng and C. K. Ong, *Appl. Phys. Lett.*, 2006, **89**, 231922.
- 404 Y. Mi, Z. Yu, S. Wang, X. Gao, A. T. S. Wee, C. K. Ong and C. H. A. Huan, *J. Appl. Phys.*, 2007, **101**, 063708.
- 405 U. Sulaeman, S. Yin and T. Sato, *J. Nanomater.*, 2010, **2010**, 629727.
- 406 D. Liu, Y. Jiang and G. Gao, *Chemosphere*, 2011, **83**, 1546.
- 407 S. Ida, Y. Okamoto, M. Matsuka, H. Hagiwara and T. Ishihara, *J. Am. Chem. Soc.*, 2012, **134**, 15773.
- 408 L. Qi and X. Li, *J. Sol-Gel Sci. Techn.*, 2014, **69**, 625.
- 409 V. Jeyalakshmi, R. Mahalakshmy, K. Ramesh, P. V. C. Rao, N. V. Choudary, G. S. Ganesh, K. Thirunavukkarasu, K. R. Krishnamurthy and B. Viswanathan, *RSC Adv.*, 2015, **5**, 5958.
- 410 R. F. Berger and J. B. Neaton, *Phys. Rev. B*, 2012, **86**, 165211.
- 411 I. E. Castelli, D. D. Landis, K. S. Thygesen, S. Dahl, I. Chorkendorff, T. F. Jaramillo and K. W. Jacobsen, *Energy Environ. Sci.*, 2012, **5**, 9034.
- 412 I. E. Castelli, T. Olsen, S. Datta, D. D. Landis, S. Dahl, K. S. Thygesen and K. W. Jacobsen, *Energy Environ. Sci.*, 2012, **5**, 5814.
- 413 I. E. Castelli, K. S. Thygesen and K. W. Jacobsen, *Top. Catal.*, 2014, **57**, 265.
- 414 J. H. Montoya, M. Garcia-Mota, J. K. Nørskov and A. Vojvodic, *Phys. Chem. Chem. Phys.*, 2015, **17**, 2634.